

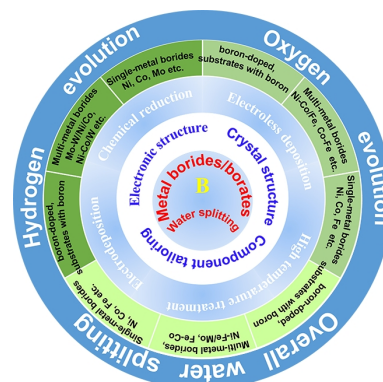
Transition Metal Boride-Based Materials for Electrocatalytic Water Splitting

Feng-Ge Wang¹, Xin Liu¹, Qian-Xi Lv¹, Bin Liu^{1*}, Yong-Ming Chai¹ and Bin Dong^{1*}

¹State Key Laboratory of Heavy Oil Processing, College of Chemistry and Chemical Engineering, China University of Petroleum (East China), Qingdao 266580, China

ABSTRACT Electrocatalytic water splitting to produce hydrogen is an eco-friendly way to achieve sustainable utilization of renewable energy. The industrial application of water electrolysis, which is severely limited by slow kinetic reactions on electrode surfaces, requires the development of highly reactive, low-cost and stable electrocatalytic materials. Transition metal borides/borates have recently emerged as promising electrocatalytic materials for catalyzing hydrogen/oxygen evolution reactions (HER/OER) in inexpensive electrolyzers. However, so far, there has been little comprehensive summary of transition metal borides/borates. Here, this review provides the latest research progress on transition metal borides/borates for electrocatalytic water splitting. The structural characteristics of transition metal borides/borates and their synthesis methods in recent years are discussed. Then, the theoretical and experimental progress of transition metal borides including single-metal borides, multi-metal borides, borate derived and other nanocomposites containing boron (boron-doped nanocomposites/substrate with boron) in electrocatalytic reaction and the role of boron in regulating electrocatalytic performance are further emphasized. Finally, the potential challenges and future prospects of transition metal borides/borates in electrocatalysis are presented.

Keywords: transition metal borides/borates, electrocatalysts, hydrogen evolution reaction (HER), oxygen evolution reaction (OER), overall water splitting



1 INTRODUCTION

To solve the global energy supply and environmental problems, it is urgent to develop an advanced, green technology to achieve sustainable use of renewable energy. At present, hydrogen energy is considered as a clean energy substitute for traditional fossil fuel because of its high energy density and no pollution.^[1-3] Compared with other hydrogen production processes, electrocatalytic water splitting (EWS) can sustainably, steadily and cleanly produce hydrogen by making full use of intermittent renewable energy sources such as solar and wind.^[4-6] The EWS is composed of oxygen evolution reaction (OER) at the anode and hydrogen evolution reaction (HER) at the cathode.^[7] Although the EWS to produce hydrogen is a promising technology, to achieve industrial scale, it is necessary to reduce or even overcome the high overpotential caused by the slowly kinetic reaction on the electrode surface. The slow kinetics of electrode surface can be improved effectively by using high efficiency electrocatalyst, thus improving energy conversion efficiency.^[8] To date, although Pt-based materials and oxides of Ru/Ir are considered advanced HER and OER electrocatalysts respectively, high cost and low content limit their large-scale applications in electrocatalysis.^[9,10] Therefore, to achieve large-scale industrial electrocatalytic hydrogen production, a lot of efforts have been made in the development of transition metal-based materials with low cost, high activity and good stability, which can replace noble metal based electrocatalysts. Among all kinds of transition metal-based electrocatalysts, sulfides,^[11,12] selenides,^[13,14] phosphides,^[15,16] carbides,^[17,18] and nitrides^[19,20] are effective electrocatalysts for

hydrogen evolution reaction, while transition metal oxides,^[21,22] hydroxides/oxyhydroxides^[23,24] and perovskites^[25-27] are widely studied for oxygen evolution reaction catalysts. At the same time, some of these HER/OER materials also exhibit bifunctional catalytic properties,^[28,29] and these bifunctional electrocatalytic materials have an advantage in improving the overall electrolysis efficiency of water.

With increasing attention to energy-related electrocatalysis, the great potential of transition metal borides/borates is gradually being developed. A large number of transition metal borides/borates have attracted attention, some of which are considered to be highly active and stable electrocatalysts for HER/OER. In this paper, borates are mainly oxoanions that are stably generated via oxidation during the preparation, storage and electrochemical reaction of borides. Compared to other transition metal-based materials, the unique physical/chemical structure of boron provides borides/borates with some special properties for electrolysis of water (Figure 1). Firstly, unlike phosphating and sulphuration, which involve the production of large amounts of toxic gases, boride synthesis methods are often environmentally friendly and generally not harmful to human health. Secondly, because boron is a metalloid element with electronegativity (2.04 in the Pauling scale) between metals and non-metals, there are a variety of bond types in borides, including metallic bonds M-M/M-B, ionic bonds M-B and covalent bonds B-B. Another characteristic of boron is that it has fewer valence electrons than valence orbitals. This electron-deficient property causes boron atoms to exhibit abundant covalent bonds in different boride lattices. These properties cause borides to

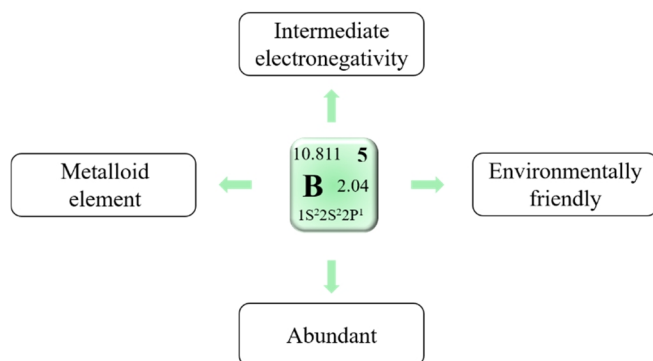


Figure 1. A schematic of properties of boron.

contain a wide variety of chemical bonds, unlike metallic sulfides, oxides, and nitrides, which contain only non-metallic bonds to metals.^[30] In many transition metal borides/borates, boron can be found to adjust the electronic structure of metal sites and promote electrochemical reactions.^[31,32] Furthermore, transition metal boride surfaces tend to inevitably oxidize to borates, boron oxides and transition metal oxides/(oxy)hydroxides.^[33] These oxide species are often favorable for oxygen evolution, but not necessary for hydrogen evolution. The diversity of borides composition and structure, as well as the unique chemistry of boron, offers great opportunities for many new discoveries. In bulk properties, early in the 1950s, the superconducting properties of borides, such as MgB_2 , were investigated.^[34,35] Moreover, borides also show outstanding performance in hardness, magnetism and

thermoelectric properties.^[36–38] Although electrocatalytic water-splitting applications of transition metal borides have been studied for decades, they are not considered as potential substitutes for noble metal-based catalysts. Until recently, a number of excellent transition metal borides/borates have been developed using various strategies, opening up new possibilities for the search for non-noble metal electrocatalysts. Although single-metal borides, multi-metal borides and their composites have been widely studied for HER, OER and overall water splitting applications in recent years, there is still a lack of comprehensive review and summary of these research progress, which is of great significance for future research on electrochemical water-splitting.^[39–41]

To this end, this review summarizes the research contents of various transition metal boride/borate nanomaterials for electrocatalytic water-splitting applications. Firstly, the structure characteristics, including component, crystal and electronic structure, and various preparation methods (Table 1) of transition metal borides/borates, are listed. Secondly, the research progress of transition metal boride/borate-based electrocatalysts is discussed and enlisted in Table 2 and Table 3 from the perspectives of HER, OER and overall water splitting. In detail, transition metal boride/borate based electrocatalysts, such as single-metal borides, multi-metal borides, and boron-doped nanocomposites/substrates with boron, are shown. Finally, the challenges and prospects of transition metal boride/borate based electrocatalysts are presented.

n STRUCTURAL CHARACTERISTIC

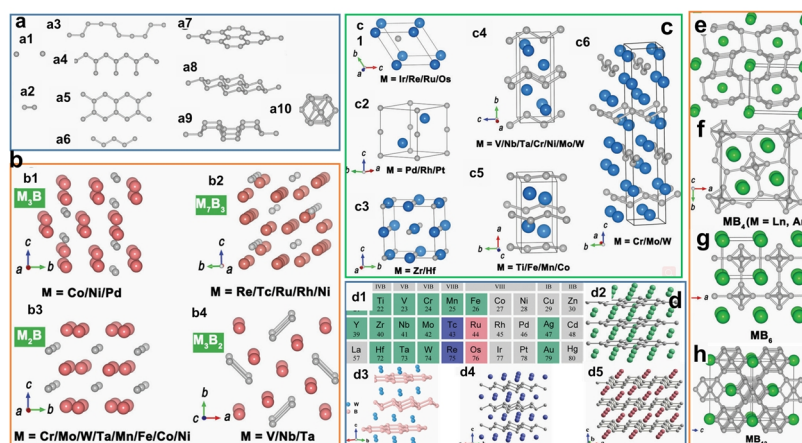


Figure 2. (a) Possible types of covalent linkage patterns of boron atoms in different crystal lattices: **a1**) Isolated boron atoms (e.g., Ni_3B), **a2**) paired boron atoms (e.g., V_3B_2), **a3**) puckered boron chains (e.g., Ni_4B_3), **a4**) branched boron chains (e.g., Ru_{11}B_8), **a5**) double boron chains (e.g., V_3B_4), **a6**) zig-zag boron chains (e.g., NiB), **a7**) graphene-like flat boron layers (e.g., TiB_2), **a8**) puckered boron layers with "chair" configuration (e.g., ReB_2), **a9**) puckered boron layers with "boat" configuration (e.g., RuB_2) and **a10**) B_6 octahedron (e.g., YB_6). (b) Representative crystal structures of **b1**) M_3B , **b2**) M_7B_3 , **b3**) M_2B and **b4**) M_3B_2 (Metal atoms and boron atoms are in pink and grey, respectively). (c) Crystal structures of **c1**) WC-type monoboride, **c2**) anti-NiAs-type monoboride, **c3**) NaCl-type monoboride, **c4**) CrB-type monoboride, **c5**) TiB-type monoboride and **c6**) MoB-type monoboride (Metal atoms and boron atoms are in blue and grey, respectively). 30, Copyright 2020 American Chemical Society. (d) **d1**) Elements constructing metal diborides, Crystal structures of **d2**) AlB_2 -type diboride, **d3**) WB_2 -type diboride, **d4**) ReB_2 -type diboride and **d5**) RuB_2 -type diboride. (Boron is in grey, and metals used for constructing the AlB_2 -type, ReB_2 -type and RuB_2 -type diborides are in green, blue and red, respectively; WB_2 -type: The pink balls represent boron atoms, whereas blue balls represent the corresponding metal atoms.) 30, Copyright 2020 American Chemical Society. 42, Copyright 2019 Wiley-VCH. Crystal structures of (e) MB_4 ($\text{M} = \text{Cr}, \text{Fe}$). (f) MB_4 ($\text{M} = \text{Y}, \text{La}, \text{Ce}, \text{Pr}, \text{Nd}, \text{Sm}, \text{Gd}, \text{Tb}, \text{Dy}, \text{Ho}, \text{Er}, \text{Tm}, \text{Yb}, \text{Lu}, \text{Th}, \text{U}$ and Pu). (g) MB_6 ($\text{M} = \text{K}, \text{Ca}, \text{Sr}, \text{Ba}, \text{Y}, \text{La}, \text{Ce}, \text{Pr}, \text{Nd}, \text{Sm}, \text{Eu}, \text{Gd}, \text{Tb}, \text{Dy}, \text{Ho}, \text{Er}$ and Tm). (h) MB_{12} ($\text{M} = \text{Zr}, \text{Hf}, \text{Y}, \text{Gd}, \text{Tb}, \text{Dy}, \text{Ho}, \text{Er}, \text{Tm}, \text{Yb}, \text{Lu}, \text{Th}, \text{U}$ and Pu). Metal atoms and boron atoms are in green and grey, respectively. 30, Copyright 2020 American Chemical Society.

High efficiency of water electrolysis cannot be achieved without excellent electrocatalytic materials. For example, the conductivity of material can affect the charge transfer and reaction rate on the electrode surface in catalytic process, thus affecting the catalytic activity. In addition, the electronic structure of materials can affect the formation of catalytic active phase and regulate the adsorption and desorption energy of reactant intermediates. According to the structure-activity relationship, the crystal structure and electronic structure of transition metal boride/borate materials are summarized.

Crystal Structure

Crystalline Borides/Borates. There are too many types of borides known in crystalline phase to list them all. In this section we mainly discuss the crystalline binary borides and corresponding oxoanions formed by oxidation. Among them, the proportion of transition metal borides (M_xB_y) in binary borides family is the highest (about 55%). The vast majority of metallic borides (over 80%) have a metal-boron ratio between 3:1 (M_3B) and 1:12 (MB_{12}). With the increase of boron content in borides, the arrangement of boron atoms is transformed from boron atoms/pairs into one-dimensional boron chains, two-dimensional boron layers and three-dimensional boron skeletons (Figure 2a).^[30]

Metal-rich borides (M_xB , $x>1$) contain four structural types, namely M_3B , M_7B_3 , M_2B and M_3B_2 (Figure 2b). The metal atoms are bonded together to form a three-dimensional metal skeleton, while the boron atoms/pairs are dispersed in the metal skeleton by M-B bonds.^[30]

Mono-borides can be divided into WC-type, anti-NiAs-type, NaCl-type, CrB-type, TiB-type and MnB-type, according to metal species (Figure 2c).^[30] The metal atoms in these borides have an arrangement similar to that of the elemental metals, while the boron atoms are inserted into the gap causing some expansion of the lattice. In Figure 2c1-3, isolated boron atoms can be seen

in these structures. In the case of CrB-type, TiB-type and MoB-type mono-borides (Figure 2c4-6), boron atoms form zig-zag chains to exist in the crystalline phase structures.

Diborides, made of 3D metal frames and 2D boron layers, are highly conductive. As shown in Figure 2d, metal diborides can be divided into AlB_2 -type, WB_2 -type, ReB_2 -type and RuB_2 -type crystal phase structures, according to the differences of two-dimensional covalent boron layers subunits.^[30,42] The boron layer in AlB_2 is a graphene-like structure (Figure 2d2). In addition, WB_2 is composed of graphene-like and puckered-type boron sheet subunits (Figure 2d3),^[42] while in ReB_2 -type and RuB_2 -type diborides comprise puckered boron layers with "chair" and "boat" configurations, respectively (Figure 2d4-5). The boron layers in the crystal phase structure of transition metal diborides can greatly affect HER electrocatalytic activity, and borides with borophene subunits can show higher catalytic activity than their counterparts.^[43,44] For example, Park's research group studied Mo_2B_4 bulk material, which contains both graphene-like boron layers and puckered boron layers. According to Gibbs free energy calculations of hydrogen, the borophene layers are highly active for hydrogen evolution.^[45] Meanwhile, Park et al. further studied $b-WB_2$, $b-MoB_2$, $a-MoB_2$ and $a-Mo_{0.7}W_{0.3}B_2$.^[46] Among them, $b-WB_2$ and $b-MoB_2$ contain both graphene- and phosphorene-like B layers (Figure 3a). Meanwhile, the introduction of 30% W does not change $a-MoB_2$ which only contains flat boron layers. The electrochemical test results show that the activity of hydrogen evolution reaction is related to the configuration of two-dimensional boron layers, and the order of electrocatalytic performance is $a-Mo_{0.7}W_{0.3}B_2 > a-MoB_2 > b-WB_2 > b-MoB_2$ (Figure 3b). In addition to the presence of borophene layers, the synergistic effect between W and Mo also leads to the highest activity of $a-Mo_{0.7}W_{0.3}B_2$. In addition, according to the relevant DFT theoretical calculation, the Gibbs free energy of the flat boron layers is close to zero, suggesting that the flat B layers are

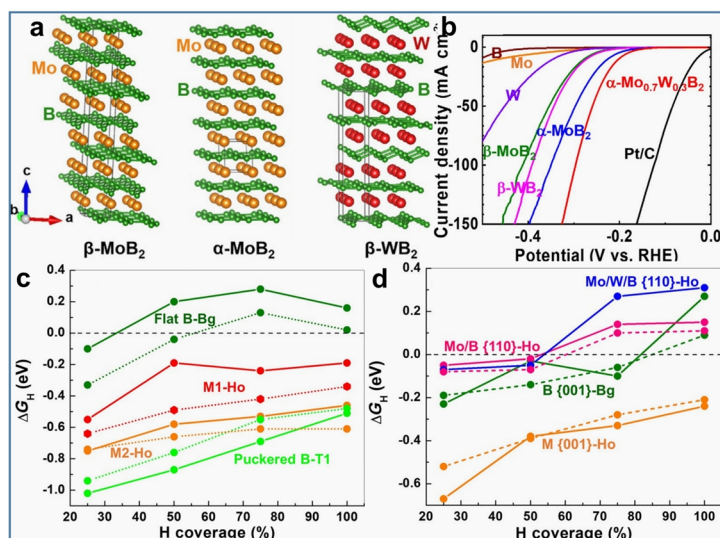


Figure 3. (a) Crystal structures of $b-MoB_2$ (left), $a-MoB_2$ (middle), and $b-WB_2$ (right) with unit cells represented in gray. (b) LSVs obtained in 0.5 M H_2SO_4 of all samples. (c) The ΔG_H for H adsorption on different sites of β - WB_2 (solid lines) and β - MoB_2 (dashed lines). (d) The ΔG_H for H adsorption on different sites of α - $Mo_{0.75}W_{0.25}B_2$ (solid lines) and α - MoB_2 (dashed lines). In (c) and (d) Bg presents the bridge sites; Ho represents the hollow sites. 46, Copyright 2019 Wiley-VCH.

active for HER (Figure 3c-d). Therefore, the presence of flat B layers in crystalline transition metal diborides plays a crucial role in HER activity. However, the configuration of the two-dimensional boron layers is inconclusive for OER.

In the boron rich system (MB_x , $x > 2$), boron cages/clusters as structural units formed by covalent bonds between boron atoms are further connected to generate a 3D boron skeleton. Meanwhile, metal atoms embedded in the void of the boron skeleton can provide additional valence electrons for the boron structural unit lacking electrons. In CrB_4 , FeB_4 and MnB_4 , the basic structural unit of boron is the boron cages (Figure 2e), while the MB_4 (M = lanthanide (Ln) and actinide (An) series) structural unit is the B_6 octahedron formed by the covalent bonding of boron atoms (Figure 2f). The structures of MB_6 and MB_{12} (transition metal elements are mainly lanthanides and actinides) are composed of 3D boron skeletons consisting of B_6 octahedron and B_{12} cubic octahedron, respectively (Figure 2g-h).^[30]

When exposed to air or water, the surface of transition metal borides inevitably oxidizes into the core-shell structure of oxygen bearing species.^[47-49] The oxygen-bearing species in oxide layer usually include transition metal oxides/(oxy)hydroxides and boron oxides/borates.^[50,51] Moreover, a large number of studies have shown that the presence of these species of oxide layer is critical for electrocatalytic reactions, which provides a reference for the design of efficient electrocatalysts.^[50-56] Wang's group recently have found that NiFe borides in-situ formed borate species leading to excellent OER catalytic activity.^[52] The formation of FeBO_3 and NiB_4O_7 was confirmed by theoretical calculation (Figure 4a-b) and in-situ synchrotron radiation X-ray diffraction (SRXRD) (Figure 4c). The atomic configurations of these two phases are shown in Figure 4d. In addition, DFT theoretical calculations show that NiB_4O_7 has a relatively low thermodynamic overpotential compared to NiOOH , NiFeOOH and FeBO_3 phases, suggesting that the NiB_4O_7 phase is the active phase in NiFe borides and contributes to excellent OER catalytic activity (Figure 4e). In addition, Masa reported in the literature that, in Ni-metal-

loid (B, Si, P, As, Te) alloys, under the potential required by the oxygen evolution reaction, Ni atoms are oxidized into nickel oxyhydroxide, the active phase of the catalyst, and at the same time, the surface metalloids are oxidized to the corresponding oxoanions which can affect the interface electrode/electrolyte properties and change the adsorption/desorption energy of the reaction intermediates for OER.^[50] Yuan et al. investigated the oxidation of nickel boride on three Ni-B-O@Ni_xB (x = 3, 2 and 0.5) surfaces.^[47] XPS characterization confirmed that the oxide layer is composed of nickel oxide/nickel hydroxide and boron-oxo species, and the surface of boron-rich Ni-B-O@NiB₂ was almost covered by oxides (Figure 4f-g). Therefore, it is inferred that the presence of boron species in borides can induce strain in the lattice structure of the metal and thus promote the oxidation of nickel by potentially reducing kinetic barriers. Electrochemical tests showed that boron rich Ni-B-O@NiB₂ achieved higher OER and lower HER activities, suggesting that the presence of oxide layer has a positive effect on not HER but OER activity. Therefore, more in-depth discussions and surface characterization are encouraged to explore the influence of boron-containing species on the evolution of TM species, as well as on OER activity. Another issue to be considered is the effect of oxidation on HER performance. Moreover, although oxidation on boride surface may not significantly affect the OER electrocatalytic activity, in situ oxides may reduce the electrical conductivity of the materials, potentially inhibiting HER activity and stability. The oxidability of metallic borides is similar to that of other nonmetallic oxides, although the degree of oxidation varies at room temperature. At present, surface doping of nonmetallic elements, as considered, can prevent surface oxidation and thus is an effective way to increase the stability of borides.

Amorphous Borides/Borates. A large number of transition metal borides are used in the field of electrocatalysis in amorphous form. Compared with their crystalline counterparts, the intrinsic disorder of amorphous phase and the presence of more coordination unsaturated active sites improve the reaction kinetic

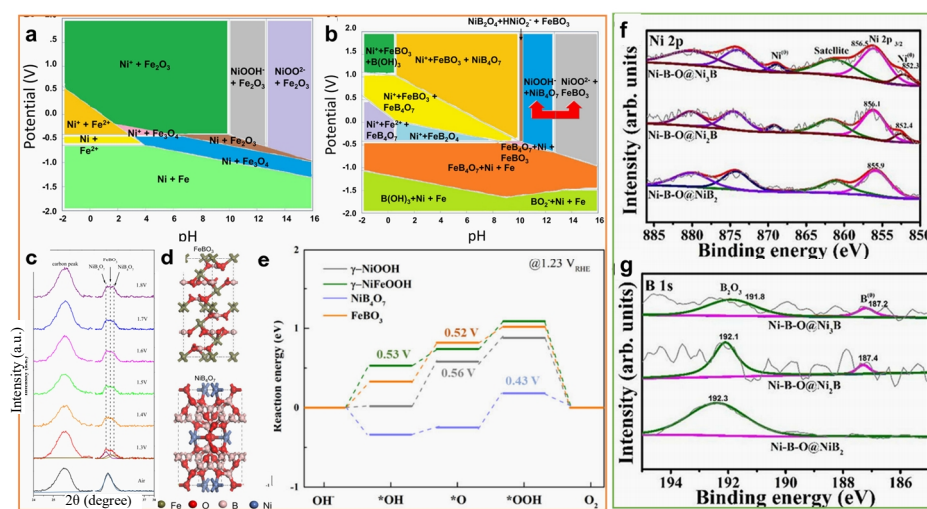


Figure 4. Results of DFT calculations for NiFe-boride catalysts. Pourbaix diagram of (a) NiFe and (b) NiFe-boride. (c) In-situ SRXRD patterns of the catalyst during the OER test in 1 M KOH electrolyte. (d) The cell configurations of NiB₄O₇ and FeB₃. (e) Predicted OER reaction energy diagram for NiB₄O₇, FeB₃, γ-NiOOH, and γ-NiFeOOH in the alkaline electrolyte at 1.23 V vs. RHE. (f) XPS spectra of the Ni 2p and (g) B 1s levels. 46, Copyright 2019 Wiley-VCH.

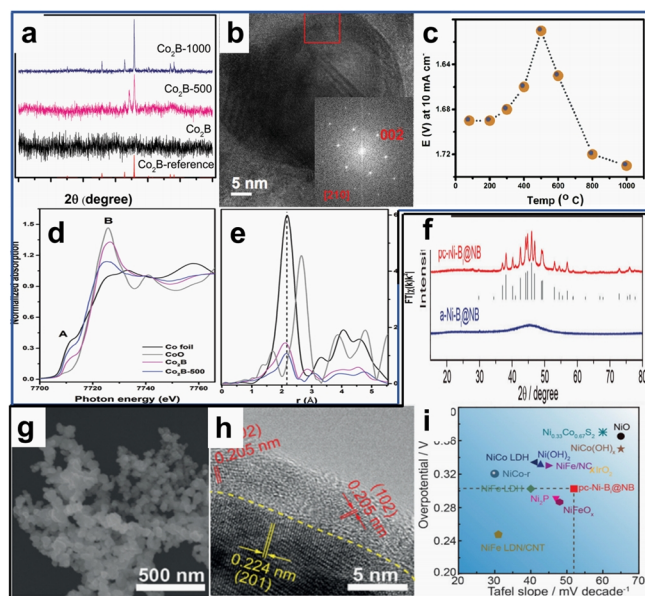


Figure 5. Effect of annealing temperature on the crystal structure of (a) Co_2B . (b) HRTEM image of Co_2B -500 with the inset showing the SAED pattern of the square marked region along the $[210]$ zone axis. (c) OER activity of Co_2B as a function of the annealing temperature under He for 2 h. (d) X-ray absorption near edge structure (XANES) and (e) extended X-ray absorption fine structure (EXAFS) spectra of Co_2B , Co_2B -500 and references of CoO and Co foils. 60, Copyright 2016 Wiley-VCH. (f) XRD patterns of a-Ni-Bi@NB and pc-Ni-Bi@NB. (g) SEM, and (h) HRTEM images of pc-Ni-Bi@NB. (i) Overpotential at 10 mA cm^{-2} and Tafel slope of the state-of-the-art OER electrocatalysts supported on glass carbon electrodes in 1 M KOH . 51, Copyright 2017, Wiley-VCH.

catalytic activity of electrocatalytic reactions.^[57] As a result, some amorphous transition metal borides exhibit excellent HER/OER activity.^[58,59] Although the atoms in amorphous material are disordered and the coordination unsaturated leads to abundant active sites, the poor electrical conductivity results in slow reaction kinetics. Although the conductivity and electronic structure can be adjusted by increasing the annealing temperature to improve the performance of amorphous materials, the performance of catalytic materials can decrease when the annealing temperature reaches a certain level.^[60-64] For example, Masa et al. studied $\text{Co}_2\text{B-X}$ obtained at different annealing temperatures ($X = 0, 500$ and 1000°C).^[60] According to XRD and HRTEM characterizations, with the increase of annealing temperature, the crystallinity of Co_2B is increased and Co_2B nanocrystalline phase appeared in the amorphous phase region when the annealing temperature reached 500°C (Figure 5a-b). Co_2B - 500°C exhibits the highest OER catalytic activity, but the performance decreases obviously when the annealing temperature increases further (Figure 5c). On one hand, according to the redox peaks on the LSV curves, with the increase of annealing temperature, the electrical conductivity of the material can be improved, which promoted the charge transfer and thus increased the OER activity. On the other hand, based on EXAFS characterizations, with the further increase of annealing temperature, the OER activity

clearly decreased due to the growth of particles and the decrease of surface area. More importantly, according to EXAFS characterization, the presence of boron induces the lattice strain of cobalt metal, which may potentially reduce the energy barrier required for cobalt oxidation, thus promoting the formation of reaction intermediates during OER (Figure 5d-e). In addition, Hu's group developed a nickel boride core-shell material ($\text{Ni-B}_i\text{@NiB}$) with a nickel borate layer whose crystallinity can adjust the OER activity.^[51] When annealed at different temperatures, $\text{Ni-B}_i\text{@NiB}$ exhibited different crystallinity and the OER activity was obviously dependent on the crystallinity of the nickel borate shell (Figure 5f-h). The author found that the partially crystallized $\text{Ni-B}_i\text{@NiB}$ catalyst (annealed at 350°C , pc- $\text{Ni-B}_i\text{@NB}$) exhibited higher OER catalytic activity than the amorphous phase (as-prepared sample, a- $\text{Ni-B}_i\text{@NB}$) and crystalline phase counterparts (annealed at 450°C) (Figure 5i). According to the quantitative analysis of turnover frequency (TOF), the increase of activity can be attributed to the relatively high intrinsic catalytic activity of partially crystallized $\text{Ni-B}_i\text{@NB}$. Therefore, both crystalline and amorphous phase materials can regulate the catalytic performance of transition metal boride/borate by adjusting the crystalline phase structure to affect the electrical conductivity and active sites.

Component Tailoring

In transition metal borides (MBs), the atomic ratio of B/TM can affect the activity of materials by changing morphology, particle size and structure. In the transition metal molybdenum boride, Park et al. found that HER activity is dependent on boron content under acidic conditions (i.e., $\text{MoB}_2 > \text{b-MoB} > \text{a-MoB} > \text{Mo}_2\text{B}$). Through BET and electrochemical active area (ECSA) measurements, it can be seen that boron-rich MoB_2 can expose more active sites per unit surface area.^[65] In addition, Li et al. studied the electrocatalytic activity of FeB_2 and Fe_2B in water electrolysis of alkaline electrolyte, finding boron-rich FeB_2 exhibited higher HER and OER electrocatalytic performance than iron-rich Fe_2B (Figure 6a-b).^[66] Theoretical calculation revealed that the surface with high boron content can affect the charge density distribution of iron boride, which is conducive to chemisorption and desorption of HER reaction intermediates (Figure 6c-d). In the OER process, on the one hand, FeB_2 can be reconstructed in situ to form amorphous FeOOH active phase. The inner FeB_2 nucleus, on the other hand, conducts electricity. These results suggest that evolving amorphous FeOOH and underlying conductive FeB_2 are critical for excellent OER performance. Furthermore, Zhang et al. reported that boron content can cause a great influence on the intrinsic HER activity of transition metal borides when studying nickel and cobalt boride for alkaline HER, in order $\text{NiB/Ni} > \text{NiB}_{0.25}/\text{Ni}$, $\text{CoB}_{0.71}/\text{Ni} > \text{CoB}_{0.37}/\text{Ni}$.^[67] Experimental results showed that the transition metal boride electrode with high boron content combined with high ECSA, low reaction resistance and high intrinsic HER activity together led to excellent HER activity. It is not a general rule to conclude that increasing boron content in transition metal borides improves electrocatalytic activity. For example, Ma group studied the crystal phase Co_xB ($x = 1-3$) and found that Co_2B exhibited the best OER activity in the

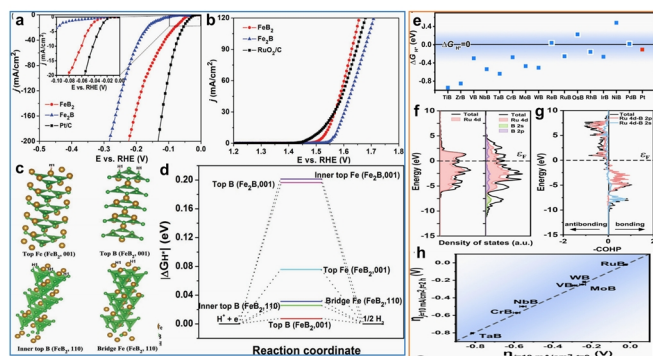


Figure 6. (a) Polarization curves of FeB₂, Fe₂B, and Pt/C for HER. (b) LSV polarization curves of FeB₂, Fe₂B, and RuO₂/C for OER. (c) Four typical H⁺ adsorption sites with relatively low ΔG_{H⁺} on the (110) and (001) surfaces of FeB₂. (d) Calculated free-energy diagram of HER over low-index (001) and high-index (110) surfaces of FeB₂ and Fe₂B. 48, Copyright 2017 Wiley-VCH. (e) Calculated DG_{H⁺} values of fifteen TMB intermetallics and Pt. (f) Calculated DOS and pDOS of Ru (0001) and RuB (001) surfaces. (g) COHP of the Ru-B bond in RuB. (h) The electrocatalytic activity and short-term stability of seven TMB intermetallics toward HER in acidic solution. The x- and y-axes represent the overpotentials required to reach the current density of 10 mA cm⁻² at time t = 0 and 2 h, respectively. The dashed line is the ideal response of a stable catalyst. 69, Copyright 2020 Wiley-VCH.

order of Co₂B > Co₃B > CoB.^[68] TOF results confirmed that Co₂B exhibited the highest intrinsic activity. In addition, according to ECSA and EIS test results, Co₂B has a higher active area and a smaller charge transfer resistance, then leading to high OER activity.

Electronic Structure

The electronic structure of transition metal borides depends largely on the constituent metals, crystal structure and stoichiometry. The electronic structure plays a decisive role in regulating the adsorption/desorption energy of reactive intermediates on the surface of materials and catalytic performance. Recently, several studies have shown that the HER catalytic performance of materials is strongly related to the d-band properties of metals (such as d-band center), which can change the Gibbs adsorption energy of intermediates on the catalytic surface.^[69-71] Among them, the d-band properties of metals are related to charge transfer between elements, orbital hybridization (that is, the ligand effect) and lattice structure (that is, the strain effect). For example, through theoretical calculations, Zou et al. found that the adsorption free energy of hydrogen atoms (DG_{H⁺}) on the metal-terminated surfaces of RuB exhibits appropriate DG_{H⁺} values (the optimized value is around near-zero) and therefore should be an effective HER catalyst (Figure 6e).^[69] As shown in Figure 6f-g, the density of states (DOS) and projected density of states (pDOS) of Ru and RuB are not zero at the Fermi level, which indicates that RuB is conductive. According to Bader charge analysis, there is only a small amount of charge transfer between the Ru and B atoms in RuB, and this slight change cannot be the

reason that affects the properties of d-band. In addition, compared with Ru, the d-bands of ruthenium-boron become broader and overlap with the sp-bands of B, suggesting a hybridization between Ru 4d and B 2sp (Figure 6f-g). The orbital hybridization between Ru and B atoms can lead to downshift of d-band center and the broadening of d-band (ligand effect), finally leading to weaker adsorption of hydrogen atoms and optimal adsorption energy. Electrochemical tests confirmed that the catalytic activity of RuB is the best for HER (Figure 6h). Boron possesses a unique electronic structure with an electronegativity value (2.04) between metal (M) and nonmetal. In addition, boron has fewer valence electrons than valence electron orbitals, giving it the characteristic of electron deficiency. In many amorphous TMB catalyzed hydrogen evolution reactions, there is a reverse electron transfer phenomenon. The transfer of boron electrons to the metal center results in the enrichment of electrons at the metal sites, which promotes the electrochemical reaction. By giving electrons, B acts as a sacrificial agent, preventing oxidation of metal sites and improving their stability. In addition, when used for OER catalysis, borides often undergo reconfiguration into the core-shell structure of amorphous oxide layer containing boron.^[53-55] Importantly, the formation mechanism of new phases derived in the OER process and the catalytic mechanism have not been determined. Take the multilayered oxygen-evolution electrode (MOEE) composed of oxidized NiFeBx alloy layer, NiFeBx alloy layer and nickel-iron alloy substrate as an example, Zou group found that an amorphous oxide layer with a thickness of about 2 nm was formed on the surface of NiFeBx during the electroactivation reaction.^[55] The stable presence of boron species in the oxide layer was confirmed in the form of metaborate, with the catalytic active phase to be g-NiOOH and iron as a dopant. As a result, the MOEE showed superior catalytic activity and stability by comparison to the NiFe substrate. Theoretical results from DFT calculations indicate that metaborate modified g-(Ni, Fe)OOH can achieve a relatively suitable adsorption energy for the intermediates compared with g-(Ni, Fe)OOH, resulting in a higher intrinsic activity. In addition, the bader charge analysis further confirmed that the electron density around the iron atoms was increased, while that around the nickel atoms was lower, which explained why the presence of metaborate can adjust the adsorption energy of surface oxygen. However, others believe that they have similar structure and function to reported Ni-B_i films, completely ignoring the effect of boron.^[72,73]

Based on the structural characteristics discussed above and the basic knowledge of electrochemistry, the following strategies should be followed in the design and synthesis of transition metal boride/borate-based catalysts. Firstly, the morphology of materials plays an exactly important role in catalytic activity. The specific surface area should be maximized and more active sites can be used for catalysis by synthesizing catalytic materials with certain nano morphology or amorphous/partially crystalline borides at low temperature in a certain aqueous solution to expose more available active sites. In addition, theoretical calculations and experimental tests also reveal the importance of planar B-layer to the HER process, because graphene B-layer has optimized adsorption energy. Therefore, the design and synthe-

sis of crystalline diborides with planar B layers are more beneficial to HER. Moreover, the change of elemental composition can significantly affect the morphology, electronic structure and crystal phase structure of electrocatalysts, and ultimately affect its electrochemical performance. However, it is impossible to accurately predict the electrochemical activity of materials based on the B/TM atomic ratio alone. The electrical conductivity of materials plays a critical role in catalytic reaction kinetics. Good conductivity promotes the transfer of charge between the electrode and electrolyte interface, thus increasing the rate of catalytic reaction. For example, the conductivity of amorphous transition metal borides can be improved by annealing at high temperature, borides with crystalline phase structure can be synthesized by selecting a specific synthesis method, or catalytic materials can be directly grown in situ on conductive substrates (e.g., iron foam, copper foam and carbon cloth, etc.). Phase engineering induced by annealing can adjust the electronic structure of TMB, improve its electrical conductivity and provide more active sites to regulate its electrocatalytic performance, which is worth further exploration. By adjusting the crystal phase structure, constituent atom ratio and constituent elements, the electronic structure can be changed, so as to optimize the adsorption energy of reaction intermediates on the surface of catalytic materials and thus improve the catalytic intrinsic reaction activity.

SYNTHESIS OF BORIDE-BASED ELECTROCATALYSTS

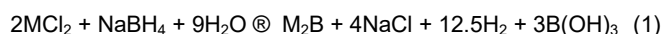
Unique structure and properties that endow metal borides with electrochemical activity and various strategies used to improve their activity are summarized. Transition metal boride/borate-based materials with different elemental composition, morphology, size and phase structure can be prepared by selecting specific synthesis methods. Therefore, in this section, this review sum-

marizes the progress of the synthesis of transition metal borides/borates for water electrolysis application. The characteristics of various synthesis methods are summarized in Table 1. In addition, the synthesis methods and the electrochemical properties of transition metal boride/borate-based materials involved in water electrolysis in recent years are listed in Table 3.

Synthesis of Borides

Transition metal borides (TMBs) can be synthesized by a variety of physical/chemical methods, including liquid phase synthesis (chemical reduction, chemical deposition, and electrodeposition), solid state heating, and chemical vapor deposition/boronization. This small section mainly focuses on the synthesis strategies of TMBs and the effects of these synthesis methods on the structure/property of borides.

Chemical Reduction. Chemical reduction is a common method for the synthesis of pure phase amorphous borides. The simple method can adjust the chemical composition of the product flexibly. General formula of chemical reduction reaction is as follows:



Among them, various transition metal boride electrocatalysts can be synthesized by selecting suitable precursors (metal salts, boron sources and solvents) and adjusting reaction parameters (e.g., reaction time and temperature, concentration of reactants, solvents and PH of the solution). It is noted that the borides are completely amorphous due to their spontaneous and exothermic properties of the reduction process.^[31] In addition, the borohydride is used as both reducing agent and boron source in these liquid phase reaction types. Among alkali borohydrides, sodium borohydride is the most commonly used reducing agent/boron source.^[74,75] Furthermore, borohydride can be hydrolyzed to

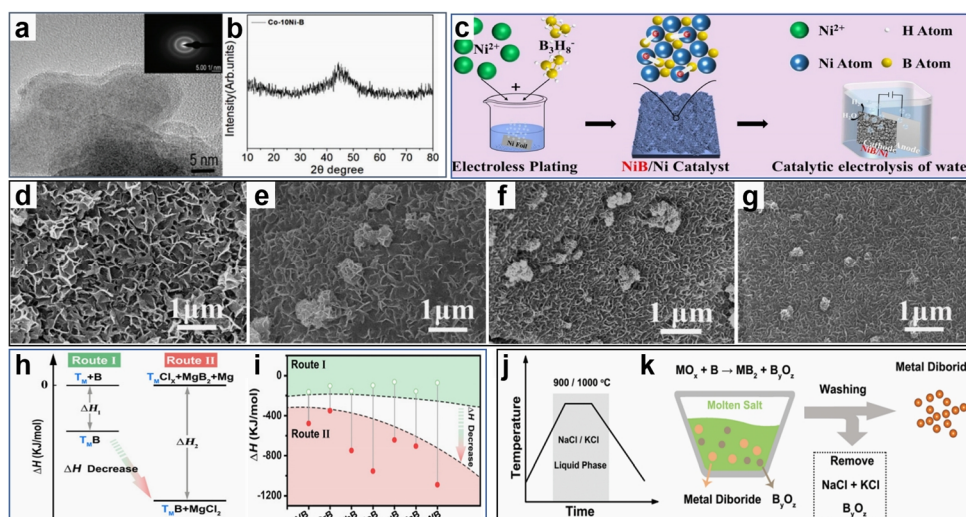


Figure 7. (a) The HR-TEM image and SAED pattern (inset). (b) The XRD pattern of the Co-10Ni-B catalyst. 75, Copyright 2020 Royal Society of Chemistry. (c) Schematic illustration of the fabrication process and application of NiB/Ni electrode. 67, Copyright 2020 Wiley-VCH. (d) SEM images for CoFeB-5-5/NF, (e) CoFeB-5-10/NF, (f) CoFeB-5-20/NF and (g) CoFeB-5-30/NF. 82, Copyright 2020 Elsevier. (h) The reaction routes for the synthesis of TMB intermetallics and (i) calculated reaction enthalpies of traditional element reaction (Route I) and magnesiothermic reduction in this work (Route II). 69, Copyright 2020 Wiley-VCH. (j) The reaction temperature between MO_x and B precursors occurs in the liquid phase domain of molten salts. (k) Schematic diagram of the synthesis of metal diborides. 42, Copyright 2019 Royal Society of Chemistry.

borates/boric acid in a protic solvent solution, and the hydrolysis of BH_4^- is strongly dependent on PH of the solution. In addition, borides are easily oxidized when exposed to air. Therefore, in this type of reaction, the molar ratio of $\text{BH}_4^-/\text{M}^{n+}$ is much larger than the stoichiometric ratio in order to ensure the complete removal of metal ions,^[76] the preparation, storage and drying of borides need to be carried out under anaerobic conditions, and NaOH/KOH solutions are often added to borohydride solutions to control the reaction rate.

For electrolytic water applications, a large number of literatures have been reported on the development of transition metal borides using chemical reduction methods.^[31,49,60,64,74-78] Zhang et al. synthesized amorphous boride (Co-10Ni-B) with an average particle diameter of 20 nm by chemically reducing metal precursors (CoCl_2 , NiCl_2) with sodium hydroxide solution containing sodium borohydride and drying it under nitrogen.^[75] HRTEM image without obvious lattice fringe and SAED image without points and rings confirm the amorphous state of the nanoparticles (Figure 7a). In addition, the amorphous phase of the catalyst powder is further confirmed by XRD with a single broad peak only at $2\theta = 45^\circ$ (Figure 7b). Additionally, the crystallinity of amorphous borides can be changed by high temperature annealing/calcination under inert conditions.^[60,64,77] For example, Masa et al. obtained Co_2B in crystal phase by annealing the amorphous Co_2B obtained via chemical reduction.^[60] Authors found by XRD that the amorphous structure of the product remained when annealing below 400°C , and then the diffraction peak pointing to Co_2B appeared when the annealing temperature is above 500°C (Figure 5a-b). In addition, using tetrahydrofuran (THF) as organic solvent can synthesize boron-rich compounds under the same conditions.^[66,79] For example, Li group reported that Fe_2B was prepared by solution synthesis and FeB_2 was obtained by chemical reduction of FeCl_2 by LiBH_4 in THF organic solvent.^[66]

Electroless Deposition. The borides obtained by the chemical reduction method discussed above are usually powder and need to be fixed to the substrate using an organic polymer binder before electrolysis, which increases the electrical resistance of the catalytic process and reduces the number of active sites available. Chemical deposition, in which a self-supporting boride catalytic material can be obtained through the same reduction reaction, seems to be more practical. The high dispersion of borides is facilitated by the porous three-dimensional structure of substrates (e.g., carbon cloth, nickel foam, iron foam and titanium foam). As a result, self-supported electrodes generally exhibit better catalytic performance than their powder counterparts due to the decrease of interfacial resistance, the increase of specific surface area and the improvement of mass transfer kinetics.^[80] Recently, some applications of water electrolysis using transition metal borides obtained by chemical deposition have been reported.^[61-63,67,81-86] Reductants/boron sources for chemical deposition are mainly divided into two types, namely dimethylaminoborane (DMAB) and sodium borohydride (NaBH_4).^[81-83] Boron content has a very obvious effect on the electrocatalytic intrinsic activity of transition metal borides, especially HER. Recently, Zhang et al. synthesized NiB/Ni with high

boron content using a novel reducing agent octahydridotriborate compound (B_3H_8^-) (Figure 7c), while $\text{NiB}_{0.25}/\text{Ni}$ was synthesized using conventional DMAB.^[67] Therefore, the use of B_3H_8^- compound instead of traditional reducing agent can significantly increase the boron content of boride species. Since chemical deposition reaction parameters such as deposition period and deposition time can affect the morphology of the boride and thus affect the electrocatalytic performance, the best deposition conditions should be determined by the actual situation and relevant literature reports during the preparation of the boride.^[82-84] For example, Li et al. synthesized different CoFeB-X-Y NSs/NF with different deposition periods/deposition time (where X and Y represent deposition periods and deposition time, respectively).^[82] It can be seen from the SEM images of CoFeB-5-Y/NF that all samples show nanosheet structure and the nanosheets become more compact with the increase of deposition time (Figure 7d-g). According to the SEM images of CoFeB-5-Y/NF, CoFeB-5-30/NF nanosheet became more complete (Figure 7g). The complete morphology of the nanosheet can effectively increase the reactive area of the reaction, which is conducive to improving the catalytic activity. In some borides prepared by chemical deposition, complexing agents such as ethylenediamine, $\text{NH}_3\cdot\text{H}_2\text{O}$ and $\text{Na}_3\text{C}_6\text{H}_5\text{O}_7\cdot 2\text{H}_2\text{O}$ can be added to the deposition solution to change the morphology.^[84-86] For example, Chen et al. synthesized CoB/NF using the latter two complexing agents.^[84] The authors found that the borides obtained with the stronger complexing agent $\text{Na}_3\text{C}_6\text{H}_5\text{O}_7\cdot 2\text{H}_2\text{O}$ exhibited a relatively smooth surface, while the borides obtained with the weaker complexing agent $\text{NH}_3\cdot\text{H}_2\text{O}$ became a rough surface. The change of morphology may be related to the deposition path and deposition speed. In a word, the advantages of chemical deposition method are far superior to the traditional chemical reduction method.

Electrodeposition. Electrodeposition is a widely used method for the synthesis of metal-based nanomaterials. Different from the chemical reduction and chemical deposition mentioned above, this method requires the external energy (electric energy) to grow nanomaterials in situ on conductive substrates. The advantage of electrodeposition is that various borides can be synthesized simply and quickly at room temperature and pressure.^[87] The key to the electrodeposition method is the selection of appropriate compositional precursors and electrodeposition parameters (e.g., electrolyte composition, electrodeposition potential and time). For example, Wu et al. prepared amorphous Ni-S-B coating by electrodeposition using nickel mesh as conductive substrate and $\text{NiSO}_4\cdot 6\text{H}_2\text{O}$, thiourea and borax as Ni, S and B sources.^[88] The amorphous phase of Ni-S-B coating was proved by electron diffraction and XRD. By adding boron element, the electrochemical active area and conductivity of binary Ni-S were improved, leading to excellent HER activity. In addition, Ahn group recently synthesized amorphous Co-P-B catalyst by electrodeposition on CP substrate by potentiostatic method.^[87] The composition of the catalyst (B/P ratio) was changed by adjusting the concentration of the precursor in the electrolyte. At the same time, it was found that HER intrinsic activity changed with the B/P ratio and showed a volcanic diagram. It was found that HER intrinsic activity was the highest when the B/P ratio is about 1.

High Temperature Treatment. In addition to the reactions discussed above in the liquid phase, various borides can also be synthesized in the solid and gas phases by means of high temperature conditions. Next, some important high temperature reaction processes are introduced.

Arc-Melting. In this method, a mixture of elemental metal and boron powder is extruded into pellets and then arc melted under inert gas or vacuum to obtain crystalline phase transition metal borides with a small number of impurities. The selection of appropriate arc melting conditions (e.g., current) is critical in the synthesis of the target product by this method. Some borides, including $\alpha\text{-Mo}_{0.7}\text{W}_{0.3}\text{B}_2$,^[46] AlFe_2B_2 ,^[89] and VB_2 ,^[90] were also synthesized by this method. For example, Park et al. used this technique to prepare four binary bulk molybdenum borides (Mo_2B , $\alpha\text{-MoB}$, $\beta\text{-MoB}$ and MoB_2) with small amounts of metal Mo and other binary borides as well as their size distributions ranging from 1 up to 15 nm.^[65]

Metal Flux. By using Sn as a solvent, not only do not form any borides, but also promote the dispersion of the molten mixture. Park et al. improved the arc melting method and synthesized pure phase Mo_2B_4 samples with particle distribution ranging from 1 to 10 nm by one-step method at 1100 °C.^[45] In addition, metal Sn can be removed by dissolution of the hydrochloric acid.

Ball-Milling. Ball milling is a mechanochemical synthesis method for the synthesis of crystalline borides.^[91] Experimental parameters (rotational speed and molar ratio of metal elements to boron powder, etc.) have a certain effect on the crystal phase structure of the product. For example, Chen et al. obtained three kinds of cobalt borides (i.e., CoB , Co_2B and Co_3B) by selecting appropriate molar ratio and rotational speed of elements.^[68]

Solid-State Metathesis (SSM). The solid-state metathesis reaction refers to redox reactions using a metal halide as a metal source (e.g., MCl_x) and an alkaline earth metal boride as a boron source (e.g., MgB_2) sealed in a vacuum/inert atmosphere and heated in a furnace.^[92] Because the reaction is highly exothermic, a relatively low heating temperature is required to carry out. For example, Li's group synthesized 12 nanoscale transition metal diborides MB_2 ($\text{M} = \text{Ti, Zr, Hf, V, Nb, Ta, Cr, Mo, W, Re, Ru, and Os}$), containing small number of impurities, through solid metathesis between MgB_2 and anhydrous chloride.^[92] In addition, FeB , NiB and MnB_4 were synthesized by this method, demonstrating its versatility and selectivity. In addition, Park et al. successfully synthesized nanocrystalline MoB_2 with particle size below 60 nm by SSM method.^[93] Among them, the synthesized product contained a small amount of Mo and MoB impurity phase. Therefore, this method can achieve rapid and selective synthesis of the target boride nanocrystals at the nanometer scale, but it tends to produce a small amount of impurity phase.

Metallurgical Reduction Reaction. The metallurgical reduction reaction between metal sources (such as metal oxides and metal halides), boron sources (such as boron and alkali earth metal borides) and reducing agents (such as Sn and Mg) is a simple and effective method to synthesize borides with different morphologies, stoichiometry and crystal phases at relatively low temperatures. The metallic elements (e.g., Sn and Mg) are both a reducing agent and a metallic solvent in such reactions. For

example, Zou's group proposed a general route for synthesizing pure phase transition metal borides.^[69] This method is based on the magnesiothermic reduction reaction, $\text{TMCl}_x + \text{Mg} + \text{MgB}_2 \rightarrow \text{MgCl}_2 + \text{TMB}$ (Route II in Figure 7h) followed by the removal of the by-product MgCl_2 . By comparing the enthalpy change (ΔH) of the elemental reaction route (Route I in Figure 7h) with that of the magnesiothermic reduction reaction, it is confirmed that the latter is more thermally advantageous (Figure 7i). Seven pure phase borides, including VB , NbB , TaB , CrB , MoB , WB and RuB , were synthesized by this method. In addition, Jothi et al. proposed a general metal thermal reduction reaction route to synthesize 3d, 4d and 5d transition metal borides with different morphologies by taking advantage of the redox properties of Sn/SnCl_2 .^[94] In short, in all cases, anhydrous metal chloride (MCl_n) was mixed with elemental boron and Sn powder. The mixed powders were then pressed into particles and sealed in a quartz ampoule. The quartz ampoule was heated in a furnace at 700 to 900 °C for approximately 4–8 h. The synthesized byproducts SnCl_2 and BCl_3 are gaseous at reaction temperatures.

Molten Salt Method. The method of molten salt is to provide a high temperature liquid phase environment for the reaction system by reaching a set temperature between the melting and the boiling points of the metal salt medium. The environmental condition enables rapid and uniform dispersion of reactants to generate thermodynamically stable nanomaterials. Molten salt synthesis methods often use sodium chloride, potassium chloride, and lithium chloride to provide only a liquid phase environment.^[95–97] In molten state of inorganic salt (KCl-NaCl), phase-pure borides were prepared by boron powder and metal salt/metal oxide through boron thermal reaction at a relatively low temperature of 900–1000 °C (Figure 7j–k). Recently, the Zou group has successfully prepared a series of MB_2 ($\text{M} = \text{Ti, V, Cr, Mn, Zr, Nb, Mo, Hf, Ta, W, Re}$ and Ru) by using this method.^[42] Sometimes, the metal salts in the system sometimes play a dual role in the metal source and ionic liquid phase environment.^[96,97] The key of the reaction is to choose the right metal salt, the melting temperature and time.

Chemical Vapor Deposition (CVD). Chemical vapor deposition takes place in a CVD tube furnace at a certain heating temperature using borane or a mixture of boron and oxide as boron source, foil as metal source and hydrogen as carrier gas and reducing gas. For example, by using boron and boron oxide as boron source placed at one end of a CVD furnace, Mo foil as metal source at the other end, and H_2 used to carry B_2O_3 to the Mo foil and then reduced to boride, Wang et al. obtained large-area ultra-thin hexagonal Mo_3B films by chemical vapor deposition.^[98]

Boronization. Direct boriding is a simple method of synthesizing metal borides by burying the metal substrate in a boron-derived reagent (boron powder, potassium tetrafluoroborate) and heating/calcination in an oven under an inert gas. For example, Zou et al. obtained single-phase M_2B layers on metal substrates ($\text{M} = \text{Fe, Co, Ni, and NiFe}$ alloys) by burying them in a mixture of amorphous boron powder and potassium tetrafluoroborate and heating them at a certain temperature.^[54] Among them, the borated NiFe alloy obtained exhibits excellent catalytic activity, stability and

Table 1. Comparison of Transition Metal Borides/Borates Synthesis Methods

Methods	Key parameters	Advantages	Disadvantages	Structure
chemical reduction	reaction time/temperature; B/TM ratio; solvent type	simplicity; variability; low cost	limited to a few TMBs; in powder form	amorphous borides
electroless deposition	substrate; B/TM ratio; solvents; pH; reaction time	low cost; large surface area	limited to a few TMBs	amorphous borides
electrodeposition	electrolyte; reaction time; pH	large surface area; simplicity; ambient temperature/pressure	extra electric power	amorphous borides
high temperature treatment	reaction temperature/time	obtain crystalline borides	high cost	crystalline borides

corrosion resistance in 30% KOH solution. Next, Zou improved the strategy by thermochemically treating the Ni plate directly with amorphous boron powder, and obtained an orthogonal Ni₃B directly on the metallic Ni substrate.^[53]

Synthesis of Borates

The transition metal borates discussed here are mainly formed by oxidation reactions on the surface of transition metal borides. In addition to oxidation caused by exposure of boride surfaces to air/water during preparation, storage and drying,^[39,99-106] electroactivation post-treatment is used to generate TM-B-O layers.^[52,53-55] More importantly, the oxygen-bearing species and core-shell structure formed on the surface are very important for electrocatalytic reactions, especially for the oxygen evolution.^[39,53-55,102]

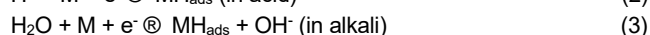
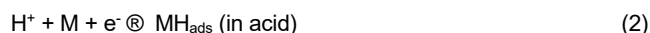
In conclusion, for traditional liquid phase synthesis methods, including chemical reduction, chemical deposition and electrodeposition, borides are often amorphous and have limited element composition. For example, molybdenum borides can hardly be synthesized by liquid phase synthesis method, which results in limited research on borides. However, high temperature treatment processes tend to result in boride formation with low specific surface area, accompanied by the formation of different boride impurity phases. After analyzing all the synthetic routes, the chemical reduction method is the easiest and most economical method to prepare metal borides. Because of its simplicity, it can also be used for large-scale production. High temperature boriding technology developed in recent years is a method to obtain stable catalyst surface, but due to the high energy consumption, further innovation is required to reduce the energy required. In the following sections, we discuss the application of transition metal boride/borate family in electrocatalysis.

n ELECTROCATALYTIC HYDROGEN EVOLUTION REACTION (HER)

After summarizing the structural characteristics and synthesis methods of the transition metal borides/borates, in the following part we will discuss the electrocatalytic mechanism of the water splitting and the electrocatalytic application of transition metal boride-based materials mainly including single-metal borides, multi-metal borides, borate derived, other nanocomposites containing boron (boron-doped nanocomposites/substrates with boron).

The electrolysis of water consists of two almost simultaneous semi-reactions, the oxygen evolution reaction at the anode and the hydrogen evolution reaction at the cathode. Of the two half reactions, hydrogen evolution involving two electron transfers is relatively simple. In acidic electrolytes, the first step of the hydrogen evolution reaction (Volmer reaction) is proton discharge and adsorption to the active site (M) to form adsorbed hydrogen atom (H_{ads}). Next, it depends on the coverage of the adsorbed hydrogen on the surface of the catalyst. When the coverage is low, H_{ads} combines with the proton discharge process to synthesize H₂ molecules (Heyrovsky reaction). When the coverage of adsorbed hydrogen is high, the two adjacent H_{ads} combine to form H₂ (Tafel reaction). Therefore, in terms of mechanism, hydrogen evolution reaction can be divided into Volmer-Heyrovsky and Volmer-Tafel paths. Under alkaline conditions, hydrolysis is required to produce protons to react. The HER process can be expressed by the following basic process (Figure 8a).^[107]

Volmer reaction:



Heyrovsky reaction:

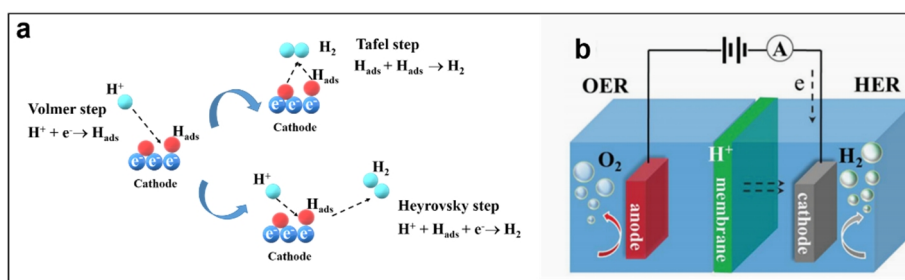
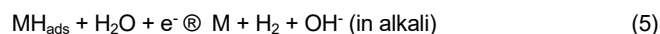
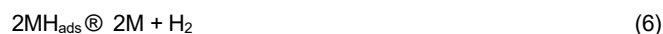


Figure 8. (a) Schematic representing possible reaction routes for HER on a cathode. (b) Schematic illustration of a typical ion-conducting membrane electrolyzer for the generation of H₂ and O₂ from water. 41, Copyright 2020 Royal Society of Chemistry.



Tafel reaction:



Both Volmer-Heyrovsky and Volmer-Tafel pathways are involved in the formation of H_{ads} intermediates. Therefore, the free energy change of adsorbed hydrogen atom (DG_{H^*}) is a key descriptor used to measure the HER activity of catalysts. That is to say, an ideal active site of HER should have a DG_{H^*} close to zero.^[108] The DG_{H^*} is related to the electronic structure and inherent chemical properties of catalyst materials. Platinum (Pt)-based materials are considered to be excellent catalytic materials in HER due to their suitable hydrogen adsorption energy ($\text{DG}_{\text{H}^*} \approx 0$). However, due to the small reserves and high price, the large-scale application of platinum-based materials in the field of electrocatalytic water splitting is limited. For transition metal borides/borates, the reaction path follows the basic rules described above. Among them, the transition metal boride/borate materials used in the field of electrocatalysis mainly include single-metal borides, multi-metal borides, borate derived and other nanocomposites containing boron (boron-doped nanocomposites/substrates with boron). The electrocatalytic performance of transition metal boride-based materials is comparable to that of other transition metal sulfides, carbides, phosphates and nitrides. In addition, in order to further realize the industrial application of borides in this field, researchers proposed a series of improvement strategies including morphology-controlled synthesis, composition regulation, phase engineering and hybridization to adjust the structure and properties of borides. As discussed in part 2, a widely recognized mechanism of high HER activity has not been established, while many reports on crystalline monometal borides have well confirmed the conclusion that increased boron content leads to high HER activity. In particular, for diborides, according to DFT theory calculation, the existence of planar B layer plays a key role in the excellent HER performance for crystalline phase diborides, on account of H-bonding strength on flat B layer being close to that of Pt (111) surface. In addition, many reports on amorphous Co and Ni-based borides have confirmed the phenomenon of reverse electron transfer for HER, which is the reason for the increase of HER activity.^[31,78,85] In this reverse electron transfer phenomenon, the d-band orbital of Co is filled with more electrons due to this reverse electron transfer, which is expected to be a favorable active site to promote HER. By giving electrons, B acts as a sacrificial agent, preventing oxidation of metal sites and improving their stability. For other borides, the theory of high HER activity of TMB catalyst and the important role of boron species were also proposed based on the calculation and experimental results. Further, we will discuss the mechanism of the corresponding catalytic activity enhancement in this section.

Single-Metal Borides

Single metal borides such as nickel borides, cobalt borides, molybdenum borides, vanadium borides and tungsten borides are remarkable HER electrocatalysts over a broad pH range, as shown in Table 3.

Nickel Borides. Zeng et al. synthesized a nanostructured amorphous nickel boride (Ni-B) alloy by chemical deposition.^[80] Amorphous Ni-B exhibited excellent catalytic efficiency and long-term stability of HER over a wide pH range, and its activity is close to that of Pt in lower concentrations of acidic and alkaline electrolytes. The authors demonstrate that the superior activity results from a large exposure of active sites and appropriate amorphous electronic structures. In addition, it was confirmed by XPS that B^0 transferred electron cloud density to Ni^0 and kept the valence state of nickel stable, thus contributing to good stability and oxidation resistance. Zeng et al. further explored the influence of catalyst particles on catalytic performance. It is found that the increase of thickness of the larger Ni-B film led to slow charge transfer, which reduced the catalytic performance.

Adjustment of the electronic structure of nickel boride can be achieved by changing the Ni to B ratio, which is a powerful strategy to achieve superior HER performance. According to the previous studies reported that intrinsic activity of TMB could be promoted by increasing the boron content.^[65] For example, Zhang et al. reported that nickel boride (NiB/Ni) with high boron content showed superior HER catalytic activity compared to $\text{Ni}_{0.25}\text{B}/\text{Ni}$, even comparable to Pt-C/Ni. Experimental results showed that TMB electrodes with high boron content can well achieve the combination of high ECSA, small reaction resistance and high intrinsic HER activity, and thus exhibited excellent HER performance. XPS confirmed that in NiB/Ni, the electron transfer from boron element to nickel occurred, and the electron enriched Ni may be more active to HER.^[80] Therefore, the increase in activity with boron content may be due to the higher boron content leading to more electron transfer to Ni atoms. In addition, due to the high covalence of Ni-B, the unsaturated active Ni sites were uniformly dispersed and the amorphous NiB was stable. In addition, the active structure of NiB/Ni electrode surface of post-HER was confirmed to be $\text{Ni}(\text{OH})_2@\text{NiB}$ rather than NiB by XPS and Raman spectroscopy. This evolved structure is beneficial to the performance of the electrode. On one hand, $\text{Ni}(\text{OH})_2$ can promote water dissociation and strengthen H^*/OH^* adsorption in HER process.^[109] On the other hand, there may be electron transfer between metal and metal oxide, and these effects jointly promoted the improvement of HER catalytic performance.^[110]

The catalytic activity of HER can be improved by coupling nickel boride with the hydroxides/metal oxides to form composite materials that can promote the dissociation of water in low alkaline or neutral reaction systems. Although nickel oxide/nickel hydroxides are not a superior HER catalyst, it can effectively promote water dissociation under alkaline conditions. When these materials are supported on the surface of the catalyst, the compounds can exhibit HER properties in alkaline electrolytes that approximate their activity under acidic conditions.^[109,111] For example, Li et al. designed a coupled borate intercalation of $\text{Ni}(\text{OH})_2$ of nickel boride ($\text{Ni-B}@\text{Ni}(\text{OH})_2\text{-BI}$) (Figure 9a).^[112] The electrocatalytic performance of Ni-B was compared with that of a-Ni(OH)₂ loaded on Ni-B ($\text{Ni-B}@\text{Ni}(\text{OH})_2$). The HER overpotential of $\text{Ni-B}@\text{Ni}(\text{OH})_2$ was significantly reduced (500 η_{10} mV vs 360 η_{10} mV), suggesting that $\text{Ni}(\text{OH})_2$ can promote water dissociation.

tion and provide more protons for HER. However, compared with the previous two, the catalytic activity of HER of Ni-B@Ni(OH)₂ inserted with borate (Ni-B@Ni(OH)₂-BI) was the best. Through infrared spectrum characterization, it was found that when borate ions were inserted into the α-Ni(OH)₂ layer, the peak intensity of H₂O molecular vibration was stronger at about 1636 and 3410 cm⁻¹, suggesting that more water molecules are in the interlayers (Figure 9b). In addition, the CV test showed that the reduction potential of α-Ni(OH)₂ in Ni(OH)₂-BI (-0.93 V vs. RHE) is lower than that in Ni(OH)₂ (-0.8 V vs. RHE), which indicated that the intercalation of borate ions can stabilize Ni(OH)₂.

Cobalt Borides. Cobalt borides proved to be also excellent non-noble metal electrocatalytic materials. However, limited by intrinsic activity and active sites, several effective strategies have been used to improve the catalytic performance of materials in recent years. Among them, modification of chemical composition by incorporation of foreign elements (e.g., anions, cations) proved to be a powerful strategy to optimize the electronic structure of the catalytic sites, resulting in a significant increase in catalytic activity.^[58,113] The Co-B-P/NF catalyst synthesized by Sun et al. showed the lowest overpotential and Tafel slope (42 mV, 42.1 mV dec⁻¹) compared with Co-B/NF (103 mV, 98.3 mV dec⁻¹) and Co-P/NF (65 mV, 59.7 mV dec⁻¹).^[58] The XPS characterization results indicated that there is electron transfer between the three elements in Co-B-P/NF materials. First, the electrons around B atom transferred to the d orbital of Co, and then from Co to P. Due to the synergistic effect of elements B and P, the electron cloud density of cobalt was optimized with appropriate positive charge (Co^{δ+}). At the same time, the Co⁰/Co²⁺ strength ratio of Co-B/NF and Co-B-P/NF is higher than that of Co-P/NF, which may be mainly attributed to the element boron preventing the oxidation of cobalt. Meanwhile, a two-step synergistic mechanism of Co-B-P for HER was proposed (Figure 9c). Firstly, the

interaction between Co^{δ+} and O²⁻ in water molecules, and the interaction between P^{δ-} and H⁺ in water molecules, together affect the adsorption of water and weaken the HO-H bonds, promoting water dissociation under alkaline conditions. Secondly, the H atoms formed were transferred to Co^{δ+} around P, and the OH⁻ generated was adsorbed to the nearby Co^{δ+}. The Co-H interaction was optimized by adjusting the binding energy of Co in Co-P due to the presence of boron. The synergistic effect of element P (accelerating the dissociation of water) and B (optimizing the free energy of hydrogen adsorption and inhibiting the oxidation of Co) significantly improved the intrinsic catalytic activity of the materials.

Phase engineering is an effective method to improve the catalytic performance of materials by changing the electronic structure of active sites, the number of active sites and electrical conductivity. The short-range order and long-range disorder in the structure of amorphous catalysts lead to a large number of coordination unsaturated sites, which enrich the available active sites. In addition, the loose arrangement structure leads to the porosity of materials and promotes the charge transfer.^[2,114] Bao et al., for example, reported that a series of Co-B_{RT} were obtained by adjusting the crystallinity of amorphous cobalt borides via annealing in an inert gas at different temperatures (300, 400 and 500 °C).^[113] The XRD results showed that the borides annealed at less than or equal to 400 °C remain amorphous state. However, amorphous Co-B₄₀₀ showed the best HER catalytic activity. Annealing at 400 °C improved the conductivity and increased the active area, leading to the improvement of Co-B performance. When the temperature got higher than 400 °C, the catalysts were clustered together and the active area were decreased. In addition, since amorphous materials often present poor conductivity and stability, combining the advantages of amorphous and crystalline materials to design a crystal-amorphous/partially amorphous structure can achieve the improvement of catalytic performance. Bao further designed the

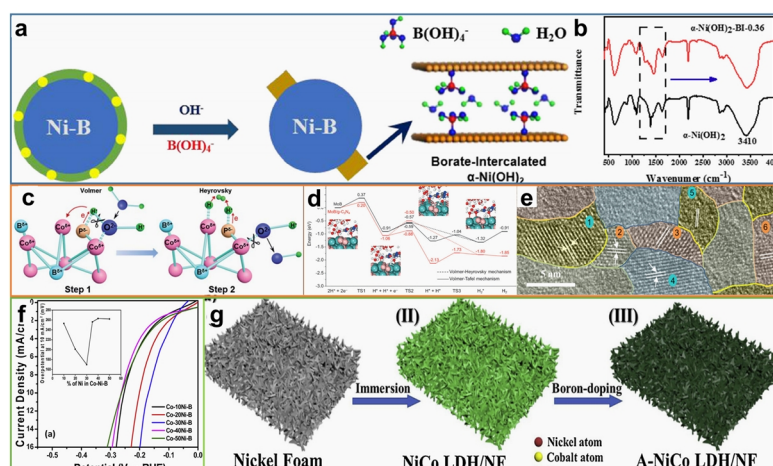


Figure 9. (a) Schematic transformation of Ni-B@oxide into Ni-B@Ni(OH)₂-BI. (b) Infrared spectra of α-Ni(OH)₂ and α-Ni(OH)₂-BI-0.36. 109, Copyright 2020 Elsevier B.V. (c) Schematic HER electrocatalysis on Co-B-P with a synergistic effect of Co, B and P. 58, Copyright 2018 The Royal Society of Chemistry. (d) Energy profiles of HER on pure MoB and MoB/g-C₃N₄ Schottky catalyst. 116, Copyright 2018 Wiley-VCH. (e) HR-TEM image of Ni₃B/MoB. (①, ④ and ⑤ correspond to (111), (200), (031) planes of Ni₃B, respectively; ②, ③ and ⑥ correspond to (110), (110), (021) planes of MoB, respectively.) 120, Copyright 2020 Elsevier B.V. (f) Linear polarization curves in pH 7 (0.5 M KPI solution) of Co-Ni-B with different Ni concentrations varying from 10% Ni to 50% Ni. Inset shows the plot of overpotential at 10 mA cm⁻² versus Ni concentration in Co-Ni-B catalyst. 31, Copyright 2016 Elsevier B.V. (g) The scheme of the preparation process for the A-NiCo LDH nanosheet arrays supported on the nickel foam. 127, Copyright 2019 Elsevier B.V.

Co-B-P composite consisting amorphous Co-B with crystalline cobalt phosphate ($\text{Co}_2\text{P}_2\text{O}_7$). Because the amorphous Co-B-O structure accelerated the electron transfer and the P-O bonds in the crystal phase structure promoted the dissociation of water molecules, the material exhibited excellent HER properties.

Molybdenum Borides. The earliest application of commercial molybdenum borides in electrocatalytic hydrogen evolution was reported by Hu Group in 2012 with MoB microparticles with appropriate catalytic activity.^[115] Until 2017, the application of molybdenum boride as HER catalyst was explored again. Through theoretical and experimental studies on boron-molybdenum with four different crystal phase structures, Zou et al. found that a-MoB₂ with borophene subunits is a highly efficient HER catalyst, with the activity in the following order: a-MoB₂ >> β -MoB₂ > MoB > Mo₂B.^[43] The main structural difference between these materials is the covalent bonding pattern between boron atoms. In contrast to b-MoB₂, a-MoB₂ has flat, graphene-like boron layers, which are efficient for superior catalytic activity. In addition, a-MoB₂ materials exhibit conductivity due to its unique Mo-based 3D frames and borophene subunits, and its resistivity is $6.6 \pm 1.7 \times 10^{-7} \Omega \cdot \text{m}$, much higher than that of Pt ($1.1 \pm 1.7 \times 10^{-7} \Omega \cdot \text{m}$). Through theoretical calculation, it is found that the Mo-terminated (001) and (100) surfaces and the B-terminated (100) of a-MoB₂ almost possess all possible active sites, and the Mo-terminated (001) and (100) surfaces should possess excellent HER catalytic activity,^[42] which is different from MoS₂ only with catalytic activity at its edges. In addition, Park et al. investigated HER performance of Mo₂B₄ containing flat and puckered boron layers.^[45] The experimental results showed that the catalytic performance of Mo₂B₄ ($\eta_{3.5}$: 270 mV, Tafel slope: 80 mV·dec⁻¹) and a-MoB₂ ($\eta_{3.5}$: 260 mV, Tafel slope: 75 mV·dec⁻¹) is almost similar, although the electrochemical active area of Mo₂B₄ was higher than that of a-MoB₂ (CdI: 156 vs. 101 mF·cm⁻²). These results indicated that the active site density of a-MoB₂ is very high. In addition, Park simultaneously found the dependence of HER activity on boron content of four binary bulk molybdenum borides (Mo₂B, a-MoB, b-MoB and MoB₂) under acidic conditions.^[65]

On one hand, nanocrystallization of materials can effectively increase surface area and expose more active sites. In addition, it can promote the interaction between electrolyte and electrode surface, and ultimately improve the catalytic performance. For example, Wang et al. designed the ultrathin hexagonal Mo₃B films by improving the synthesis strategy.^[98] The ultrathin crystalline phase Mo₃B can not only achieve more active site exposure but also improve the electrical conductivity of the crystalline and metallic structure characters.

For HER at the cathode, a metallic catalyst with abundant electron cloud density on its surface can stabilize hydrogen adsorption and improve catalytic activity.^[65] Molybdenum boride (a-MoB) is metallic, and it is an effective strategy to improve HER activity of metallic catalysts by establishing a Schottky junction to adjust the electronic structure of catalytic sites to achieve optimization of proton adsorption energy. A Schottky junction is formed between metal and semiconductor by introducing a built-in electric field to improve charge transfer. Therefore, Zhuang et al. reported that the surface charge density of metal catalyst

a-MoB was adjusted by selecting suitable semiconductor g-C₃N₄ to construct Schottky catalyst.^[116] A series of spectroscopic studies showed that the interface between MoB and g-C₃N₄ possessed obvious characteristics of charge redistribution, resulting in electron enrichment on the surface of MoB. The enhanced activity was mainly attributed to the increase of electron density on the MoB surface and the smooth electron transport in the matrix. Theoretical calculations further confirmed that kinetic barriers for proton adsorption and reduction were reduced on the established Schottky catalyst (Figure 9d).

Other Single-Metal Borides. In recent years, VB₂ was found to be an active catalyst for HER. Fokwa et al. performed DFT calculations on AlB₂-type VB₂ and their corresponding results showed that the B-terminated {001} (graphene-like boron layer), V-terminated {100} and V/B mixture {101} of VB₂ have free energy comparable to that of precious metal Pt, and therefore possess high HER activity. And its performance was comparable to similar surfaces in MoB₂.^[44] In addition, the authors also studied VB₂ at the nanoscale and bulk, and found that VB₂ significantly increased HER activity at the nanoscale due to a much higher density of active sites than VB₂ at bulk. Fokwa et al. further found that bulk crystalline vanadium boride materials (VB and V₃B₄) were highly active HER electrocatalysts.^[90] Importantly, the authors show that the high activity of vanadium borides can be rationalized by studying the effect of aggregating boron chains in vanadium boride as a function of HER activity. In addition, as mentioned before, the catalytic performance of HER of materials is related to the d-band properties of corresponding constituent metals. Zou et al. investigated the electronic structures and electrocatalytic properties of tungsten borides (W₂B, WB, WB₂, and WB₃).^[117] The activity trend (W₂B > WB > WB₂ > WB₃) was due to the different degree of hybridization between the d orbital of W and the sp orbital of element B, resulting in a difference in the properties of d-band (d-band center), which affected the surface H atom adsorption on each tungsten boride.

Multi-metal Borides

The successful development of single-metal borides in HER inspired researchers to further explore the application of multi-metal borides in this field. The catalytic application of HER for some multi-metal borides in a wide pH range is discussed, as shown in Table 3.

Mo-W/Ni/Co Borides. The catalytic performance of transition metal borides can be improved by inducing synergistic effect via adding other metal elements. Elemental doping can adjust the electron structure and lattice structure and prevent aggregation of the formation process. As discussed in the above section, a-MoB₂ containing only graphene-boron layers is a promising HER catalyst. By partially replacing molybdenum with element W in a-MoB₂ according to the doping strategy, Park et al. synthesized a-Mo_{1-x}W_xB₂ which showed better activity and stability than binary MoB₂ and WB₂ under acidic conditions, in an order of a-Mo_{0.7}W_{0.3}B₂ > a-MoB₂ > β -WB₂ > β -MoB₂.^[46] a-Mo_{0.7}W_{0.3}B₂ and a-MoB₂ contain only graphene-like B layers, while β -WB₂ and β -MoB₂ contain similar crystal phase structure, in which the flat and phosphorene-like boron layers exist simultaneously (Figure

3a). By adjusting the content of W ($a\text{-Mo}_{1-x}\text{W}_x\text{B}_2$), the catalytic activity improved with the increase of x until $x = 0.3$. This decrease of activity at $x > 0.3$ was due to the formation of the second phase of $b\text{-WB}_2$ with lower activity. The activity of $\beta\text{-WB}_2$ is slightly better than that of $\beta\text{-MoB}_2$, confirming that W is more active. These results led to a higher activity $a\text{-Mo}_{0.7}\text{W}_{0.3}\text{B}_2$ than $a\text{-MoB}_2$. Theoretical calculations confirmed that tungsten, in contrast to molybdenum, promoted hydrogen production by promoting the bonding of hydrogen atoms (Figure 3).

Grain boundaries in catalysts have been shown to possess high intrinsic catalytic activity due to charge transfer between different grain boundaries leading to changes in interface properties.^[118] Previous studies have reported that heterostructures containing grain boundaries formed by different phases can achieve adjustment of surface electronic structure.^[119] Huang et al. proposed an effective strategy to construct bimetallic boride $\text{Ni}_3\text{B}/\text{MoB}$ heterostructures with rich grain boundaries, which was confirmed by HRTEM and EDX scanning results (Figure 9e).^[120] Compared with mono-metal boride Ni_3B and MoB , the surface electronic states of $\text{Ni}_3\text{B}/\text{MoB}$ heterostructures were adjusted according to XPS results. The results of DFT calculation further showed that the electronic structure of $\text{Ni}_3\text{B}/\text{MoB}$ grain boundary was optimized, and DG_{H^+} was closer to the ideal value (zero) than that of Ni_3B and MoB single-metal borides. In addition to heterogeneous borides of different phases/compositions to achieve higher electrocatalytic activity than the corresponding individual, the combination of transition metal borides with other electroactive materials is another promising method for preparing high-performance catalysts. Therefore, selecting an excellent electroactive material can be hybridized with TMBs to construct a new type of EWS electrocatalyst. Lao et al. reported that the non-precious metal $\text{CoB}@\text{MoS}_2$ hybrid electrocatalysts was used for alkaline HER.^[121] MoS_2 is a promising transition metal dichalcogenides, which shows outstanding HER activity in acidic medium. In addition, CoB with excellent OER activity in alkaline medium can promote the adsorption and dissociation of water. At the same time, the electrical conductivity of the composite can be improved by hybridizing with CoB . The synergistic effect between CoB and MoS_2 resulted in $\text{CoB}@\text{MoS}_2\text{-0.5-300}$ exhibiting excellent HER activity under alkaline conditions. Some studies have shown that hybrid transition metal borides with transition metal oxides/hydroxides can improve the electrocatalytic performance. Recently, Ren et al. obtained an amorphous Co-Mo-B and $\text{O-vacancy-rich CoMoO}_{4-x}$ 3D layered nanostructured electrocatalyst by reducing CoMoO_4 with NaBH_4 .^[122] In addition to the fact that borides themselves are conductive and exhibit excellent HER in alkaline electrolytes, cobalt molybdenum oxides can effectively promote water dissociation and oxygen vacancies can promote water adsorption by causing electron delocalization at vacancies. In addition, the 3D layered nanopore structure can also provide sufficient active sites. These synergies contributed to $\text{Co-Mo-B}/\text{CoMoO}_{4-x}/\text{CF}$ showing excellent stability and activity in alkaline HER.

Ni-Co/W Borides. In this review, Co-B was found to be excellent catalysts for HER in a wide range of pH values (4-9).^[32] Meanwhile, electroless plated NiB_x films were reported to be very

active in all pH media, which provided a strong support for HER.^[85] By using the synergistic effect between metal elements, Gupta et al. synthesized amorphous Co-xNi-B electrocatalyst in the range of 10%-50% by adjusting the $\text{Ni}/(\text{Ni} + \text{Co})$ mole ratio (x) in Co-Ni-B , and determined the most appropriate composition of Co-30Ni-B .^[31] Among them, Co-30Ni-B (30% $\text{Ni}/(\text{Ni} + \text{Co})$) exhibited the highest activity of HER in the full PH range (Figure 9f). Considering the HER rates of Ni-B and Co-B , the former is more active. Therefore, with the increase of Ni concentration, the electronic structure of the cobalt active sites was optimized. However, when $x = 30\%$, the cobalt sites were replaced by less active Ni, resulting in the decrease of HER activity. In Co-Ni-B , as calculated by XPS, EXAFS, XANES and DFT theory, the addition of Ni resulted in boron enrichment on the surface and promoted more electron transfer to the Co sites. Compared with Co-B with similar morphology and surface area, the Co sites with higher electron density in Co-Ni-B improved the ability of Co itself to donate electrons, thus promoting HER. At the same time, boron can also protect the Co sites from oxidation and inactivation by transferring electrons, thus demonstrating excellent stability over the full PH range.

Metallic diboride materials have been widely studied in electrocatalysis due to their excellent electrical conductivity and high density of active sites. In this class of materials, $a\text{-MoB}_2$ reported by Zou and Fokwa groups is one of the materials with higher HER activity than other different structures of molybdenum borides.^[43,45,65] Subsequently, Zou et al. found that tungsten diboride was the best HER non-noble metal catalyst among 12 mono-metal borides (TiB_2 , VB_2 , CrB_2 , MnB_2 , ZrB_2 , NbB_2 , MoB_2 , HfB_2 , TaB_2 , WB_2 , ReB_2 and RuB_2).^[42] In order to further improve the catalytic activity of WB_2 , heteroatomic doping is considered to be an effective strategy to adjust the electronic structure. Due to the addition of nickel, the electronic structure of WB_2 was adjusted and the d-band center of Ni-WB_2 relative to WB_2 shifted from -1.55 to -1.69 eV, resulting in weaker H adsorption. In addition, according to Bader charge analysis, Ni doping reduced the negative charge of boron atoms on the surface (0.30 |e| for WB_2 and 0.22 |e| for Ni-WB_2), thus reducing the B-H bond strength. These results eventually led to the decrease of DG_{H^+} absolute value of Ni-WB_2 and the increase of its activity.

Other Nanocomposites Containing Boron

Due to unique structure and properties, boron can not only form transition metal compounds for electrocatalysis, but also form nanocomposites with other active catalytic materials for water electrolysis research.

Boron-Doped Nanocomposites. Boron as dopant is often the same as other heteroatoms, which can improve the performance of catalytic materials by adjusting the electronic structure and crystal phase structure of the active sites.

Among them, there are many related researches on the influence of dopants on the adjustment of electronic structure of catalytic materials, including boron as dopant.^[123-126] For example, boron doped molybdenum carbide (B-MoC) was reported by Lin et al.^[123] The electronegativity values of carbon and boron are 2.55 and 2.04, respectively. The addition of electron-deficient

Table 2. Classification and Comparison of Transition Metal Borides Adapted to Electrocatalytic Reactions of Her/Oer in Different Environments

Reaction	Alkaline	Neutral/acidic
HER	NiB _x , CoB _x , FeB _x , MoB _x	MoB _x , NiB _x , VB _x , WB _x
OER	NiB _x , CoB _x , FeB _x , MoB _x	None

boron atoms led to the polarization of carbon atoms, resulting in the transfer of a large number of electrons to molybdenum atoms. The increase of electron cloud density around Mo atoms endowed with the increase of proton adsorption sites, thus promoting electrocatalytic HER activity. In addition to improving the intrinsic catalytic activity, the addition of boron also increased the electrochemical active area and improved the conductivity. Similarly, Cao et al. designed boron doped CoP nanoparticles for HER in the full PH range.^[124] Experimental and theoretical studies showed that by modulating the electronic structure of catalytic materials, the B dopant changed the local electronic configuration and atomic arrangement of Co and neighboring P atoms, and improved the electron delocalization ability of Co atoms, thus achieving high conductivity. Meanwhile, the free energy of H adsorption and H₂ desorption at the active sites was optimized to obtain better HER kinetics.

In addition, boron as a dopant can also induce crystalline materials to amorphous, that is, B-doping-induced amorphization treatment. Compared with their crystalline counterparts, boron induced amorphous materials produce a large number of defects including dangling bonds, uncoordinated atoms, and oxygen defects, thus providing more active sites for catalytic processes. For example, Yang et al. reported that boron-doping induced the amorphous of NiCo LDH nanosheets loaded on Ni foam (Figure 9g).^[127] Partially amorphous (PA-NiCo LDH/NF) and completely amorphous NiCo LDH (A-NiCo LDH/NF) were obtained by controlling the boronation time. The obtained A-NiCo LDH/NF exhibited excellent catalytic activity and stability under alkaline conditions, especially under high current density. In the process of LDH amorphous induced by B doping, part of OH⁻ in crystalline NiCo LDH can be replaced by B doping, which existed in the form of BO₃³⁻ in different borate units. In alkaline electrolytes, the electronegative tri-coordinated BO₃ can readily react with the hydroxyl group to form tetra-coordinated BO₄. The formed BO₄ groups with strong proton acceptability would promote the dissociation of absorbed water molecules by absorbing H atoms, and then transfer them to the metal atoms nearby. In addition, borates and defects (such as unsaturated atoms, oxygen vacancies and dangling bonds) caused by amorphous crystals play a critical role in HER process.

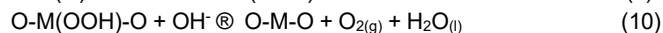
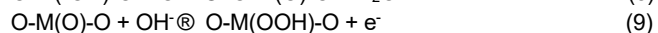
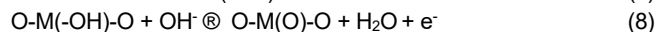
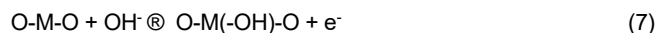
Substrates with Boron. Similarly, boron can also be used as dopant in the synthesis of conducting supports.^[128-130] Ye et al. proposed a simple pyrolysis method to synthesize Ru nanoclusters (NCs) anchored on B/N-doped graphene (BNG) (denoted as Ru NCs/BNG).^[128] In the pyrolysis process, boron was doped into graphene and promoted the formation of ultra-small Ru NCs with

a diameter of 0.5-1 nm. Density Functional theory (DFT) calculations showed that the electron configuration of boron (1s²s²p¹) can enable the delocalization of empty 2p orbitals to Ru NCs and graphene, which promoted the coordination between the oxygen atoms in H₂O molecules and Ru NCs, including the breaking of H-OH, thus accelerating the dissociation of water and promoting the dynamics of HER in alkaline solutions. At the end of this part, we classified transition metal borides/borates suitable for HER in different conditions as shown in Table 2. According to the borides used for electrocatalytic hydrogen evolution, most transition metal borides show excellent catalytic performance in alkaline electrolytes, while only a few metal borides (Ni and Mo group) are stable in acidic solutions.

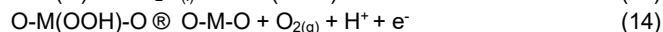
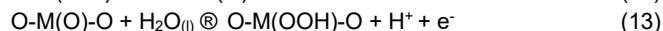
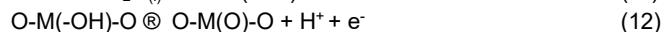
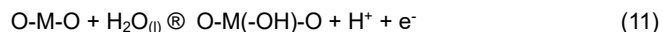
n ELECTROCATALYTIC OXYGEN EVOLUTION REACTION (OER)

Compared with HER, oxygen evolution reaction (OER) is a kinetically slow process involving four-electron coupled proton transfer. At present, OER catalytic mechanism can be divided into two widely accepted pathways,^[131] namely, adsorbate evolution mechanism (AEM) and lattice-oxygen-mediated mechanism (LOM), regardless of acid or alkaline conditions (Figure 10a). The elementary steps are as follows:

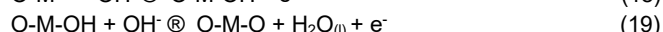
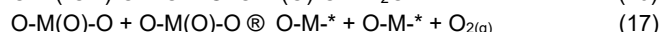
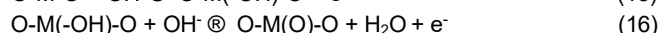
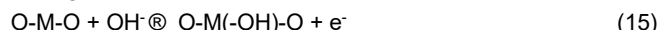
For AEM in alkaline conditions:



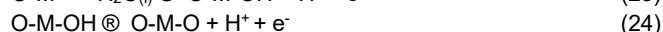
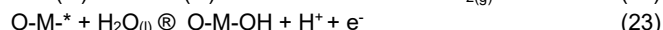
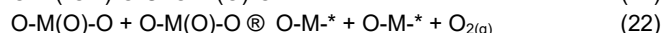
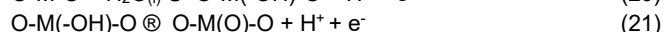
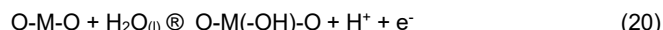
For AEM in acidic conditions:



For LOM in alkaline conditions:



For LOM in acidic conditions:



Where M represents the active sites of the catalysts. The formation of multiple intermediates (O*, OH*, and OOH*) is involved in the reaction process, and the formation of these intermediates is necessary for OER reaction and these intermediates form rate-limiting steps. Therefore, materials that can form surface species with a suitable bond energy are considered as ideal OER catalysts. Due to these characteristics, noble metal oxides (i.e., RuO₂ and IrO₂) have traditionally been highly active catalytic materials for both alkaline and acidic OER, but their poor stability in catalytic process and scarcity limit their large-scale application.^[9,10]

Therefore, a great deal of work has been done to develop low-cost and highly active materials that can replace RuO_2 and IrO_2 . In recent years, many non-noble metal catalytic materials including multi-metallic oxides,^[21,22] layered hydroxides,^[23,24] and non-oxide derived compounds^[11-20] have been developed as highly efficient OER electrocatalysts. For non-oxide catalytic materials, such as metal sulfides,^[11,12] phosphates^[15,16] and nitrides,^[19,20] OER process is catalyzed by surface oxides/hydroxides generated in situ. Borides catalyze reaction in a similar way.^[49,74]

For several mono-metal borides, excellent OER catalytic performance has been reported mainly from the active phase of oxide/hydroxide formed by surface oxidation of borides, while the role of boron has not been explained.^[63,79] However, other literature has mentioned that boron species play a certain role in OER properties of materials. Some studies on borides by Zou et al. pointed out that in OER electrocatalysis involving boronized Ni sheet, the ultrathin layer of amorphous oxyhydroxide composed of metaborate formed in situ on the boronized Ni sheet surface was identified as the OER catalytic sites (Figure 10b-d). The authors also found that metaborate can induce charge redistribution to regulate the electronic structure of the active sites, facilitating the optimization of the binding energy of NiOOH catalytic phase.^[53,54] Masa et al. conducted XAS studies on annealed Co_2B and showed that B induced lattice strain of Co due to electron interaction and hybridization between B 2p states and metal d orbitals. This lattice strain lowered the oxidation energy barrier for Co, making it easier to form OOH^* intermediates, thereby increasing the OER rate.^[60] In addition, in amorphous/nano-crystalline Co-B films, species B promoted the formation of CoOOH by contributing electrons to Co atoms to prevent the complete oxidation to form stable oxides that are not active to

OER, thus increasing the OER rate.^[132]

For multi-metal boride catalysts, although the oxides/hydroxides on the surface are the main active phase, there are other factors including synergies, crystallinity, etc., that contribute to the OER rate increase. For example, Chen et al. reported amorphous $\text{Co}_2\text{-Fe-B}$ catalysts for OER and demonstrated strong synergistic effects between Co and Fe by cyclic voltammetry, X-ray photoelectron spectroscopy, and long-term stability curve tests. The presence of Fe species stabilized the Co species at higher oxidation states, which in turn promoted the formation of OOH -like species (a key intermediate of OER), while the presence of cobalt species improved the electrical conductivity. Combined with previous reports, the authors also showed that B can lower the energy barrier for OOH species.^[49] However, Wang et al. recently have explored the OER mechanism of FeNi boride and found the activated boride was in situ converted to FeBO_3 and $\text{Ni}_2\text{B}_4\text{O}_7$ (Figure 4b-c). Theoretical calculations and experimental studies confirmed that $\text{Ni}_2\text{B}_4\text{O}_7$ exhibited the lowest thermodynamic overpotential compared to NiOOH , NiFeOOH and FeBO_3 (Figure 4e), demonstrating that $\text{Ni}_2\text{B}_4\text{O}_7$ achieved excellent OER performance and should be the active site of the activated FeNi boride.^[52] It is clear from the above discussion that OER activity can be increased in multi-metallic borides/borates for several reasons due to the contribution of synergistic effects between metals. However, in mono-metal borides/borates, the higher OER rate can only be explained in the context of surface metal oxide/hydroxide formation, and the role of boron is inconcludable, unlike the role of boron as a sacrificial electron donor in HER (see section 4). At present, most reports have pointed to the role of boron in regulating electronic structure. Due to the difference in electron density between the boron-oxygen species and the bonded metal active phase, the electronic structure of the

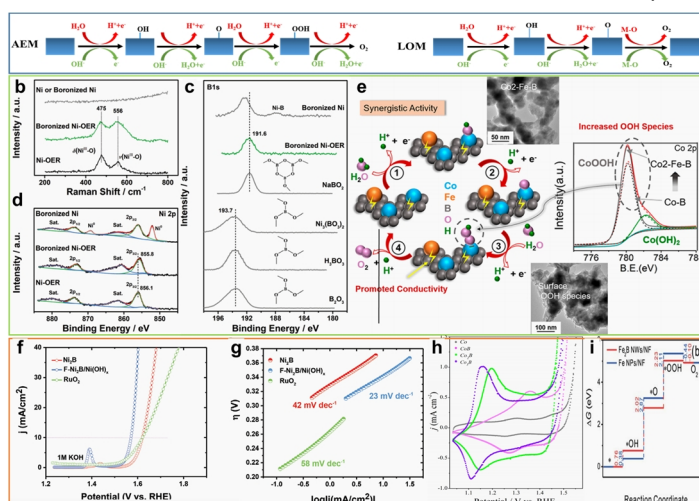


Figure 10. (a) Schematic illustration of OER reaction pathways on the catalyst surface under acidic (red) and alkaline (green) conditions. (b) Raman spectra of the boronized Ni sheet and the Ni sheets before and after the OER. (c) B1s XPS spectra of the boronized Ni sheet and the Ni sheet before and after the OER. The B1s XPS spectra of four reference materials are also shown for comparative purposes in the Figure. (d) Ni2p XPS spectra of the boronized Ni sheet before and after the OER. 53, Copyright 2019 The Royal Society of Chemistry. (e) Illustration of the Function Mechanism of the Synergistic Effect on OER Performance. 49, Copyright 2017 American Chemical Society. (f) LSV curves for $\text{F-Ni}_2\text{B/Ni(OH)}_x$ in 1M KOH and (g) their corresponding Tafel plots. 134, Copyright 2020 WILEY-VCH. (h) CV curves of Co_2B and cobalt electrodes measured in N_2 -saturated 1.0 M KOH solution at a scan rate of 2 mV s^{-1} . 68, Copyright 2017 American Chemical Society. (i) Free energy diagrams of Fe_2B and Fe-derived catalysts for OER at zero potential ($U = 0 \text{ V vs. RHE}$). * denotes adsorption sites. 139, Copyright 2020 The Royal Society of Chemistry.

active phase is adjusted, which ultimately optimizes the adsorption energy of the reaction intermediates on the catalytic surface and promotes the OER activity. Throughout these theories, it can be concluded that boron is not the active site of OER, but plays a crucial role in the formation of intermediates. Although much progress has been made in boride work, understanding how boride catalysts really work in the OER process is still limited. Therefore, further efforts are needed to study the structure-activity relationship of the OER process of borides.

Single-Metal Borides

Single-metal borides for electrocatalytic OER including nickel, iron and cobalt borides are discussed and their properties are shown in Table 3.

Nickel Borides. Nickel-based electrodes are still the best choice for commercial alkaline hydrolysis due to their moderate catalytic activity, good corrosion resistance under corrosive alkali conditions, low cost and easy processing. Zou et al. proposed a simple boronization strategy that can convert commercially available metal sheets (nickel, cobalt and iron) into efficient, stable, corrosion-resistant, inexpensive oxygen evolution electrodes.^[53] The boronized metal sheets (M_2B , $M = Co, Ni$ and Fe) have been shown more active and significantly enhanced corrosion resistance in operating environments than metal sheets. The boronized metal sheets exhibited similar trend of OER catalytic activity as the corresponding metal sheets ($Ni > Co > Fe$), suggesting that the catalytic activity can be negatively correlated with the oxophilicity of metallic active sites. In addition, ultrathin (25 nm) metaborate-containing $NiOOH$ films were formed on the surface of the boronized Ni during OER process, and were identified as the catalytic active phase of OER (Figure 10b-d). Then, the group further improved the boronization strategy to design a nickel boride plate composed uniformly by Ni_3B particles.^[54] The authors confirmed that the initial electrochemical OER testing process resulted in the in-situ generation of nanosheets consisting of metaborate-containing oxyhydroxides on nickel boride as a potent catalytic active phase. Specifically, the improvement of catalytic performance of the materials in the electrochemical activation process was due to the synergistic catalytic effect of structural characteristics of the nanosheets of hydroxides (geometric optimization) and the modification of electronic structure of hydroxides by metaborate (electronic optimization).

As mentioned above, adjusting appropriately the crystallinity of the target catalyst and studying its effect on electrocatalytic activity provides an opportunity to improve catalytic performance. For example, Jiang et al. investigated the crystallinity of the $Ni(II)$ borate thin layer on Ni_3B ($Ni-B_i@NB$) to modulate OER electrocatalytic activity.^[51] The authors show that the crystallinity of nickel borate could be regulated by annealing and the OER activity of $Ni-B_i@NB$ is strongly dependent on the crystallinity of $Ni-B_i$ shells (Figure 5f-h). Among them, the partially crystalline $Ni-B_i$ catalysts (annealed at 350 °C, pc- $Ni-B_i@NB$) showed higher catalytic activity than its amorphous (as-prepared sample, a- $Ni-B_i@NB$) or crystalline (annealed at 350 °C) counterparts. The higher activity of pc- $Ni-B_i@NB$ catalysts was attributed to the increased intrinsic activity of catalytic sites.

By hybridizing different active species together to form a hierarchical hybrid, the material can not only increase the number of active sites but also promote the intrinsic activity through synergistic action. For example, Liang et al. directly designed nickel hydroxide grown in situ on the Ni foam as a conductive substrate to hybridize with nickel boride nanoparticles to form layered porous nanocomposite material (i.e., $Ni-B@Ni(OH)_2@Ni$ foam), exhibiting significantly enhanced electrocatalytic activity and durability to OER.^[133] The hierarchical hybridization of $Ni-B$ with $Ni(OH)_2$ supported on the nickel foam effectively promoted oxygen evolution in the alkaline medium. In addition, Hong et al. proposed a “two-phase engineering” strategy to synthesize a highly metallic transition metal boride phase in conjunction with transition metal hydroxide with a large number of adsorption sites (i.e., $F-Ni_2B/Ni(OH)_x$). The $F-Ni_2B/Ni(OH)_x$ exhibited good alkaline OER properties due to its good adsorption energy and reaction kinetics (Figure 9f-g). The coexistence of transition metal boride phase and transition metal hydroxide phase on the catalyst surface promoted the two-phase effect, including providing rich adsorption sites for the reaction intermediates and efficient charge transfer pathway.^[134]

Cobalt Borides. Among OER catalysts, cobalt-based materials have attracted much attention due to their abundance and moderate activity. However, electrochemical studies on cobalt borides are very few so far. Recently, Ma et al. prepared a series of cobalt boride (Co_xB , $x = 1-3$) by ball milling and investigated their OER activity.^[68] Among them, the OER performance of Co_2B ($\eta_{10} = 287$ mV) in 1.0 M KOH solution showed better activity than CoB ($\eta_{10} = 340$ mV) and Co_3B ($\eta_{10} = 312$ mV) thanks to its high intrinsic activity, abundant active sites and good electrical conductivity. The experimental results demonstrated that the formation of Co_3O_4 and $CoOOH$ and the good electrical conductivity of Co_xB alloy core were conducive to the OER properties of the product. XPS and cyclic voltammetry showed that the B in Co_xB made the oxidation of cobalt easier, resulting in higher OER activity than metal Co (Figure 10 h).

In addition, the catalytic activity can be significantly improved by hybridizing various active components into composite materials.^[135,136] Similarly, by combining cobalt boride with other conductive materials, the conductivity and the stability of the active material can be improved.^[103] For example, Chen et al. designed an ultrathin h-BN shell encapsulated CoB_x NPs by heat treatment of amorphous CoB NPs in NH_3 .^[137] The h-BN shell prevented the accumulation and leaching of Co NPs and the interaction between B atoms in the metal core and Co, resulting in the formed $CoB_x@h-BN$ core-shell nanostructures exhibiting excellent OER activity.

Iron Borides. Because iron is the most abundant metal in the earth's crust, iron-based catalysts are cheap to make. However, compared with cobalt and nickel, iron based OER electrocatalysts, especially iron (oxy) hydroxides, have not been widely developed. Boettcher et al. reported that the intrinsic activity of iron oxyhydroxide ($FeOOH$) is limited by its low conductivity and does not perform well.^[138] Therefore, the addition of metallic boron to iron-based materials can improve the conductivity of the

catalyst and modify the catalyst surface to accelerate OER. For example, Zhou et al. demonstrated that Fe_2B nanowires (NWs) can be deposited onto NF via a simple one-step chemical reduction in an applied magnetic field.^[139] During OER in an alkaline solution, these interconnected Fe_2B NWs are converted into thicker, larger networks covered with metaborate and FeOOH . Metal oxyhydroxides acted as the active phase, while boron promoted OER by regulating the electronic structure of the iron-active sites to optimize the adsorption energy of the reaction intermediates (Figure 10i). Experimental and theoretical calculations showed that the higher intrinsic catalytic activity of Fe_2B NWs was mainly due to: (I) the unique electronic structure of iron modulated by metal boron, (II) accelerated charge transfer, and (III) the hydrophilic surface of the catalyst. At the same time, excellent stability resulted from the presence of metaborate species in the active layer which significantly improved the corrosion resistance.

Multi-metal Borides

The synergies between the metals should be realized in the improvement of OER catalytic activity of borides. There are a few reports on bimetallic boride OER catalysts, and the synergistic effect and related internal mechanism caused by the introduction of second metal into mono-metallic boride are rarely reported.

Ni-Co/Fe Borides. Zhang et al. prepared a series of nickel-cobalt based bimetallic boride catalysts (Co-xNi-B , x is the molar content of Ni, $x = \text{Ni}/(\text{Ni} + \text{Co})\%$) and evaluated their activity.^[75] Among them, the Co-10Ni-B catalyst showed good catalytic activity for oxygen evolution reaction in 1 M KOH electrolyte. By

CV test and XPS analysis, the introduction of nickel into cobalt boride resulted in an increase in the electrochemical active area and a change in the electronic structure of Co. These synergistic effects promoted the catalytic performance of borides. In addition, XPS and XRD results further confirmed that Co-10Ni-B can easily form CoOOH and NiOOH under OER condition, which can be committed to the OER catalytic process. Wang et al. reported that self-supporting FeNi@FeNiB-700 , developed by a simple and environmentally friendly solid phase boriding process.^[140] FeNi@FeNiB-700 exhibited excellent catalytic activity for OER in a series of boronized FeNi samples (FeNi@FeNiB-X , X is boronization temperature, $X = 600, 700, 800$, and 900), due to the porous and loose structure and the best crystallinity, which guaranteed enhanced active surface area and rapid charge/mass transfer.

The activity of the catalyst can be improved by supporting it on an appropriate high surface area conductive substrate. The use of conductive substrate can not only improve the electrical conductivity of materials but also promote the uniform distribution of active sites. Zhang et al. prepared Ni-Co-B nanosheets coupled with reduced graphene oxide (rGO) as advanced OER electrocatalysts.^[48] The use of rGO not only served as an effective substrate to ensure the uniform and orderly vertical alignment of Ni-Co-B nanosheets, ensuring exposure of more specific surface area, but also improved the electrical conductivity of the material and thus accelerated OER dynamics. In addition, Zou et al. designed a multilayer oxygen evolution electrode to meet the multiple needs of anodic materials for seawater electrolysis.^[55] The

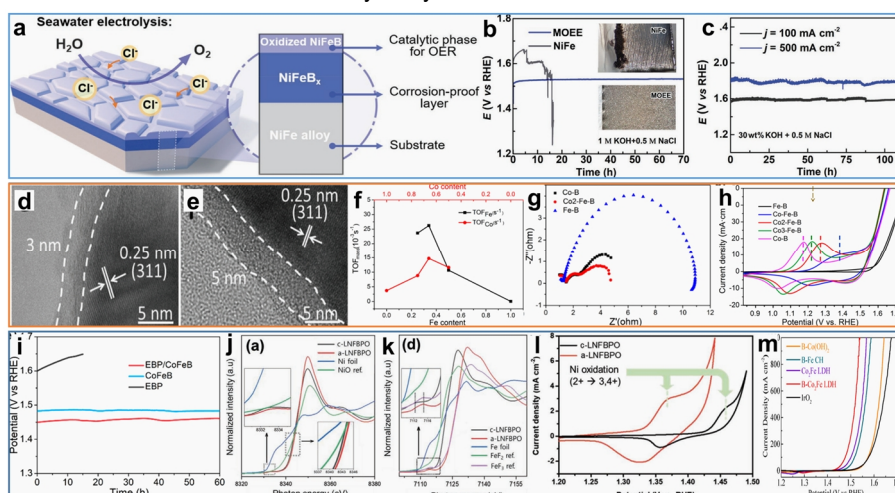


Figure 11. (a) Structural illustration of a multilayered alloy electrode for seawater electrolysis. (b) Chronopotentiometric curves with NiFe and MOEE as the electrode in 1 M KOH solution containing 0.5 M NaCl. The photographs of the electrodes after OER electrocatalysis are provided in the insets. (c) Chronopotentiometric curves of MOEE as an electrode in 30 wt% KOH electrolyte with 0.5 M NaCl at current densities of 100 and 500 mA cm^{-2} for 100 h. 55, Copyright 2021 Wiley-VCH. (d) HRTEM images of NiCo_2O_4 after OER electrolysis. (e) HRTEM images of $\text{NiCo}_2\text{O}_4@\text{Ni-Co-B}$ after OER electrolysis. 142, Copyright 2017 The Partner Organisations. (f) TOF plots depicted based on assuming that only Co sites are available for catalysis (TOF_{Co}) and only Fe sites are available for catalysis (TOF_{Fe}). (g) EIS of the samples (on Cu substrates) at 1.58 V (vs. RHE) in 1 M KOH aqueous electrolyte. (h) The second CV cycle of samples (catalyst loading 0.2 mg cm^{-2}) on stainless steel substrate at a scan rate of 100 mV s^{-1} in 1 M KOH aqueous electrolyte; dashed lines indicate the positions of oxidation peaks. 49, Copyright 2017 American Chemical Society. (i) Chronopotentiometry tests for OER at a current density of 10 mA cm^{-2} . 145, Copyright 2021 American Chemical Society. (j) Ni K-edge XANES spectra of c-LNFBPO, a-LNFBPO, Ni foil, and NiO reference. (k) Fe K-edge XANES spectra of c-LNFBPO and a-LNFBPO. (l) The cyclic voltammetry of c-LNFBPO and a-LNFBPO. 149, Copyright 2021 Wiley-VCH. (m) OER polarization curves of B-Co(OH)_2 , B-Fe CH, $\text{Co}_2\text{Fe LDH}$, B- $\text{Co}_2\text{Fe LDH}$, and IrO_2 catalysts in 1 M KOH electrolyte. 151, Copyright 2021 Elsevier B.V.

multilayer electrode (MOEE) was synthesized by direct thermal boriding of NiFe alloy plate with boron powder and then electrochemical oxidation. The MOEE was composed of the surface oxidized NiFeBx alloy layer, NiFeBx alloy interlayer, and NiFe alloy substrate (Figure 11a). Boron species existed in the outermost oxide layer in the form of metaborate, and their presence can facilitate the formation and stabilization of the catalytically active γ -(Ni,Fe)OOH. The introduction of NiFeBx interlayer can effectively prevent excessive oxidation, corrosion in seawater electrolyte and improve the electrical conductivity of anode materials (Figure 11b-c). Yan et al. prepared amorphous Fe-Ni-P-B-O nanocages by simple chemical reduction method.^[141] When appropriate P and Fe were added to Ni-B-O catalyst, the overpotential of j_{10} can be as low as 236 mV, and the Tafel slope can be greatly reduced to 39 mV dec⁻¹. The excellent OER catalytic activity was mainly attributed to the following factors: the introduction of P and O may weaken the metal-metal bonding, resulting in the rearrangement of the electron density at the catalytic active center and the reduction of the energy barrier formed by the reaction intermediates. Second, the introduced phosphorus species can act as adsorption sites for oxygen-containing intermediates, accelerating the OER process. Third, doped iron can stabilize the Ni active center. Sun et al. reported that the formation of amorphous Ni-Co-B layers on NiCo₂O₄ nanowire arrays was an effective method to improve their OER activity in alkaline media.^[142] As a 3D catalyst electrode, the core-shell NiCo₂O₄@Ni-Co-B nanoarray was durable and provided a geometric catalytic current density of 10 mA cm⁻² only at 270 mV overpotential, 100 mV lower than that of the NiCo₂O₄ nanoarray. The significant increase in OER activity was attributed to the fact that the Ni-Co-B layer promoted the formation of surface-active species during OER (Figure 11d-e).

Co-Fe Borides. Some studies have shown that with the incorporation of Fe into 3d transition-metal oxides, oxyhydroxides can promote the formation of OOH species with high chemical valence, which are favorable to OER.^[143] Ye et al. synthesized binary metal Cox-Fe-B catalyst by simple chemical reduction method.^[49] Obviously, the addition of Fe improved the catalytic activity of the catalyst. The overpotential of CO₂-Fe-B decreased by 42 and 61 mV at 10 and 100 mA cm⁻² current density, compared with Co-B, respectively. For CO₂-Fe-B, the overpotential was 0.298 V and a smaller Tafel slope was 62.6 mV dec⁻¹ (the Tafel slope of Co-B is 97.3 mV dec⁻¹). The calculation of turnover frequency (TOF) showed that Co and Fe ions were OER available (Figure 11f). The reasons for the improvement of electrocatalytic performance were investigated by cyclic voltammetry, X-ray photoelectron spectroscopy, long-term stability test and electrochemical impedance spectroscopy. The results confirmed the synergistic effect of Co and Fe on COx-Fe-B catalyst. The addition of Co increased the conductivity (Figure 11g), while iron induced the formation and stabilization of M-OOH species with high oxidation state (Figure 11h), simultaneously promoting OER activity. In addition, Wang et al. reported a simple and systematic method for the preparation of metal borides by chemical reduction, in which the morphology change from nano-particles to nanosheets was achieved by careful selection of metal salt solu-

tions.^[144] The authors chose to use cobalt nitrate to prepare Co-B with two-dimensional nanosheet morphology as the precursor. The optimized Fe₃Co₇-B/CNT showed excellent catalytic activity and stability for water oxidation in 1 M KOH electrolyte through iron doping and hybridization with carbon nanotubes (CNT). The activity of Fe₃Co₇-B/CNT catalyst surpassed that of Fe₃Co₇-B, Co- or Fe-B and IrO₂, suggesting a synergy between transition metals in ternary borides. In addition to iron doping, coupling with CNT also improved the conductivity to optimize the electrocatalytic activity. In addition, using the two-dimensional (2D) layered structure of exfoliated black phosphorus (EBP) nanosheets with high carrier mobility, but limited by the absorption of excessive oxygen-containing intermediates and rapid deterioration in air, Qin et al prepared a 2D/2D nanosheet hybrid electrocatalyst for OER by hybridizing EBP nanosheets with amorphous CoFeB nanosheets.^[145] The EBP/CoFeB hetero-structure showed good catalytic performance for OER, with an overpotential of 227 mV at 10 mA cm⁻², fast reaction kinetics with a smaller Tafel slope of 36.7 mV dec⁻¹, and long-term durability. The authors confirmed that the heterostructure can exhibit excellent OER catalytic performance for the following reasons: Firstly, the heterostructure optimized the absorption energy of oxygen-containing intermediates because of the strong absorption capacity of EBP and the weak absorption capacity of CoFeB. Secondly, EBP (crystalline) and CoFeB (amorphous) improved the conductivity and the number of active sites of the hybrid, respectively. Thirdly, CoFeB nanosheets can protect EBP from degradation in the environment to improve electrochemical stability (Figure 11i). By combining the nanostructure optimization strategy with the composite strategy of materials and conductive substrates, Lin et al. reasonably designed a series of CoFeB-X-Y nanosheet arrays grown in situ on conductive nickel foam by means of chemical deposition.^[82] By adjusting the parameters of chemical deposition (X is the deposition period and Y is the time) to optimize the morphology of nanomaterials (Figure 7d-g), the obtained partially amorphous CoFeB-5-30 NS/NF exhibited excellent OER catalytic activity and stability. The excellent electrocatalytic activity can be attributed to the partial amorphous structure that increased defect sites, the synergistic effect between metal Co and Fe that promoted electron transfer, and the nanosheet structure that increased the available active sites. In addition, the contact resistance and stability of the active material were improved by growing directly on a conductive nickel substrate.

Other Multi-metal Borides. Multi-metallic electrocatalysts based on Fe, Co and Ni usually show strong electrocatalytic activity for oxygen evolution reactions (OER). Zhang et al successfully synthesized FeCoNiBOx/PPy/rGO nanocomposites by one-step reduction method.^[146] Compared with monometallic and bimetallic electrocatalysts prepared under the same conditions, the trimetal FeCoNiBOx/PPy/rGO exhibited excellent OER activity, with the lowest over potential ($\eta_{\text{onset}} = 230$ mV, $\eta_{10} = 290$ mV) and the best Tafel slope of 47 mV dec⁻¹, attributed to the synergistic effects of Fe, Co, Ni and lamellar conductive PPy/rGO. Much work has been done to optimize the electrocatalytic performance of TMBs by doping transition metal atoms to modify the electronic structure. In addition, according to energy valance bond

theory, electronic d orbitals and empty 4f orbitals of rare earth metals have the ability to diffuse each other, thus promoting the proper arrangement of catalytic orbital required in the OER process.^[147] Haik et al. improved the alkaline OER performance of electrodeposited cobalt boride (CoB) nanosheets by the combined effect of using gadolinium as a dopant and gold film as a support.^[148] As the controllable doping of Gd not only promoted the smooth growth of nanosheets but also modulated the surface electronic structure of catalyst material, the obtained Gd-CoB@Au catalyst exhibited high activity, faster kinetics, smaller charge transfer resistance and durability even at high current density. The characterization after long-term stability showed that it possessed chemical and mechanical stability, and confirmed that active and stable species were formed on the borate surface. Song et al. reported amorphous LiNiFe borophosphate (a-LNFBPO) for efficient and durable oxygen evolution reaction (OER).^[149] The crystalline phase LNFBPO obtained by hydrothermal method was amorphous by high-energy ball milling. The amorphous structure engineering of LNFBPO induced the high oxidation states of Ni and Fe and contracted the M-O bond length, which led to the enhanced increase of M-O covalency (Figure 11j-k). The strong M-O covalency of a-LNFBPO facilitated charge transfer between catalyst and electrolyte. In addition, due to the large number of defects and long-range disordered arrangements induced by the amorphous, the structural flexibility was improved, resulting in a simpler transformation of the initially inert species into the active phase during the OER process (Figure 11l). At the same time, the electronic structure adjustment caused by Ni and Fe interaction can also improve OER.

Other Nanocomposites Containing Boron

Boron-Doped Nanocomposites. As mentioned in this paper, boron species and their derivatives borate have also been reported in a large number of literature as dopants for improving the catalytic performance of materials. In addition, H^- derived from NaBH_4 has a strong reducing ability and can be used as an oxygen scavenger to produce oxygen defects and change the crystallinity of the precursor.^[150] Ren et al. synthesized a partially amorphous boron modified cobalt-iron layered hydroxide (B- Co_2Fe LDH).^[151] The resulting B- Co_2Fe LDH catalyst showed excellent OER catalytic activity in 1 M KOH, requiring overpotential of 205 and 246 mV to drive current densities of 10 and 100 mA cm^{-2} , respectively (Figure 11m). NaBH_4 , in the process of introducing boron, as a boron source and reducing agent, can not only react with metal cations to form borides, but also produce a large number of oxygen defects by extracting oxygen and adjust the Co_2Fe LDH precursor to partially amorphous structure. The modification of boron also enhanced the intrinsic catalytic kinetics of partially amorphous B- Co_2Fe LDH, expanded its ECSA, and made it show excellent OER catalytic activity and stability in both fresh and seawater. Liu et al. developed a feasible strategy to introduce a large number of oxygen vacancies (O_v) into CoO nanowires through B doping.^[152] The results of XAS, XPS and EPR analysis clearly showed that B doping caused the local structure disorder and formed O_v . The B-doped CoO-O_v

showed excellent OER activity, requiring only 280 mV overpotential to drive the current density of 10 mA cm^{-2} in 1 M KOH, with the Tafel slope to be 71 mV dec^{-1} . Theoretical calculation demonstrated that the O_v caused by B doping reduced the reaction barrier of Co-O bond breaking, leading to the excellent electrocatalytic activity. Huang et al. successfully prepared boron-doped amorphous iridium oxide (IrO_x -B) by a simple boric acid-assisted method, achieving an ultrahigh OER mass activity of 2779 $\text{A g}^{-1}_\text{Ir}$ at 300 mV overpotential.^[153] Because boric acid not only promoted Ir exposure, but also can be embedded into amorphous IrO_x in the form of metaborate and further modify the electronic structure and local ligand structure of Ir, thus improving the intrinsic activity. Chai et al. prepared a pyrite selenide by dual-cation substitution (Fe, Ni) and boron doping to obtain better activity and stability.^[154] The overpotential of the Ni-pyrite selenide catalyst ($\text{Fe}_5\text{Co}_4\text{Ni}_{20}\text{Se}_{36}\text{B}_\text{x}$) decreased from 543 to 279.8 mV at the current density of 10 mA cm^{-2} , and the Tafel slope decreased from 161 to 59.5 mV dec^{-1} . Theoretical calculation showed that the doped cations and boron can effectively optimize the adsorption energy of OER intermediates, promote the charge transfer between heteroatoms, and improve the OER performance.

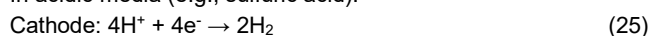
Substrates with Boron. The electrochemical properties of catalytic materials can be improved by combining them with conductive materials such as graphene and carbon nanotubes. Boron can be doped into graphene and used as a conductive material. For example, Manthiram et al. investigated a simple and scalable method for the preparation of Co_3O_4 coated N- and B-doped graphene hollow spheres ($\text{Co}_3\text{O}_4/\text{NBGHSS}$).^[155] The results showed that $\text{Co}_3\text{O}_4/\text{NBGHSS}$ exhibited higher electrocatalytic activity due to the coupling between Co_3O_4 and NBGHSS, strong interaction with O_2 adsorption, high conductivity and specific hollow structure. In addition, boron nitride (BN) has many unique advantages of carbon-based materials, such as low density, large surface area and low cost. More importantly, it has higher chemical and thermal stability, making it resistant to electrochemical corrosion.^[156] However, the application of boron nitride in electrocatalysis is hindered by its low electrical conductivity due to its interlayer insulation. Du et al reported carbon, oxygen doped boron nitride modified by pulsed laser ablation (L-BN) is an excellent OER catalyst support that can replace carbon black (CB).^[157] The results showed that B-B dipole interaction was formed in the L-BN, which led to a significant increase in electrical conductivity. L-BN was then used as a support to load IrO_x catalyst for OER applications. Obviously, IrO_x on L-BN ($\text{IrO}_\text{x}/\text{L-BN}$) performed better than IrO_x on CB ($\text{IrO}_\text{x}/\text{CB}$): the overpotential (η_{10}) decreased from 276 mV for $\text{IrO}_\text{x}/\text{CB}$ to 259 mV for $\text{IrO}_\text{x}/\text{L-BN}$ (Figure 12a), and the Tafel slope dropped from 56.92 to 36.68 mV dec^{-1} (Figure 12b). The performance improvement was due to the strong interaction between IrO_x and L-BN, which can not only effectively prevent the aggregation of IrO_x , but also oxidize Ir ions to higher valence states. In addition, at the end of this part, we classified transition metal borides suitable for OER in different environments, as shown in Table 2. Literature has reported the activity of transition metal borides as active HER catalysts in

different environments, such as acidic, alkaline and other wide pH range. According to the OER report, borides show good OER activity only in alkaline media, indicating they cannot achieve a balance of activity and stability over a wide PH range.

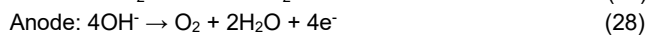
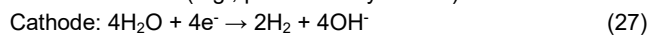
n BIFUNCTIONAL ELECTROCATALYSTS FOR OVERALL WATER SPLITTING

The complete water splitting mechanism consists of two almost simultaneous semi-reactions, i.e., HER at the cathode and OER at the anode (Figure 8b). Water splitting to produce hydrogen (H_2) and oxygen (O_2) seems simple but the process is different in various PH solutions.^[7] The equation of electrolytic water reaction in different media is listed below:

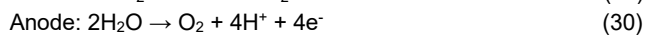
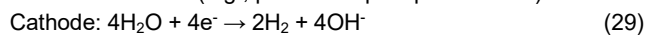
In acidic media (e.g., sulfuric acid):



In alkaline media (e.g., potassium hydroxide):



In neutral medium (e.g., potassium phosphate buffer):



Regardless of the electrolyte medium, bifunctional catalysts must have properties suitable for catalyzing both HER and OER.

In this section, the application of transition metal borides in dual-function electrocatalysis is discussed from the point of view of single-metal borides, the multi-metal borides and other boron-containing composites. The bifunctional catalytic properties of some borides are listed in Table 3.

Single-Metal Borides

Nickel Borides. According to previous studies, most metal boride catalysts such as Ni_3B have abundant active sites and can achieve efficient HER,^[65,99] while the real active form of OER is mainly the surface oxide/hydroxide formed under reaction conditions.^[53] In addition, nickel borides (Ni_3B) have good ductility and corrosion resistance compared with other borides. A series of nickel borides with oxide layer (Ni_3B , Ni_2B and NiB_2) were prepared by Guo et al through a simple chemical reduction of Ni^{2+} with borohydride and exposure of the precipitates to air.^[47] The authors confirmed that the oxide layer on the surface of the catalyst consisted of nickel oxide/hydroxide and boron-oxo species. This oxide layer promoted the formation of OOH^* active intermediates, which was detrimental to HER, leading to a decrease in HER activity. In addition, boron in Ni_3B can promote the oxidation of nickel and produce more Ni^{2+} on Ni_3B surface, so boron-rich nickel boride expressed good OER activity. Compared with $Ni-B-O@Ni_2B$ (1.67 V) and $Ni-B-O@NiB_2$ (1.68 V), $Ni-B-O@NiB_3$ alkaline electrolyzer required only 1.58 V cell voltage to afford the

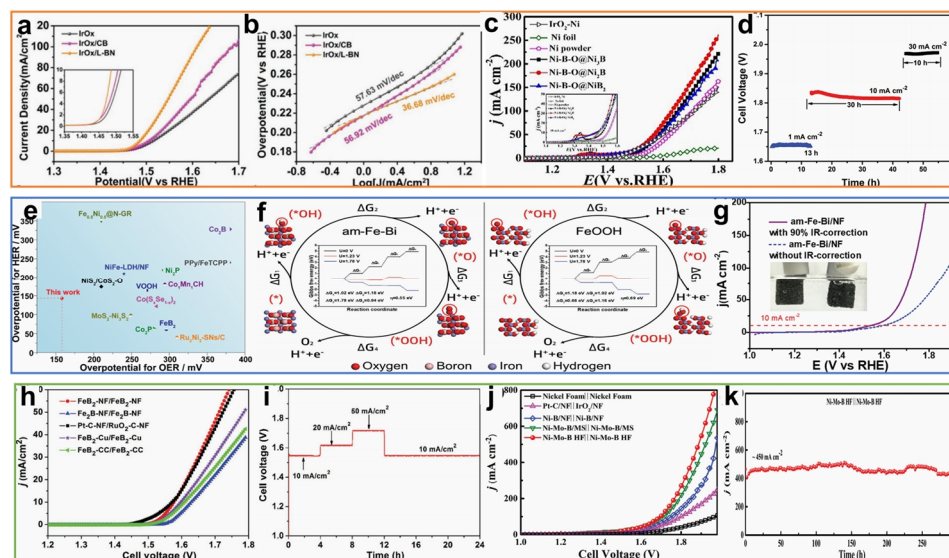


Figure 12. (a) The OER polarization curves of different materials supporting IrO_x , with loading of 0.28 mg cm^{-2} catalyst on glassy carbon electrode (GCE). (b) Tafel plots of catalysts loaded on GCE at 5 mV s^{-1} scan rate. 157, Copyright 2020 WILEY-VCH. (c) LSV curves of overall water electrolysis for $Ni-B-O@Ni_3B$, $Ni-B-O@Ni_2B$, and $Ni-B-O@NiB_2$ in a two-electrode configuration at a scan rate of 2 mV s^{-1} without iR correction. 47, Copyright 2019 Wiley-VCH. (d) Chronopotentiometric stability curves at different current densities during electrolysis of water in a two-electrode cell using Co_2B-500 supported on carbon cloth both as the anode and Co_2B-500/NG supported on carbon cloth as the cathode, and 3 M KOH as the electrolyte. 60, Copyright 2016 WILEY-VCH. (e) Overpotential for OER and HER at 10 mA cm^{-2} of state-of-the-art bifunctional electrocatalysts on 1 M KOH . (f) Gibbs free energies of Fe-Bi (left) and FeOOH (right) were calculated as follows. As shown in the Figure, when $U > 1.78 \text{ V}$, all steps are thermodynamically accessible for Fe-Bi; while when $U > 1.92 \text{ V}$, all steps are thermodynamically accessible for FeOOH. The red, cyan, brown, and white atoms represent O, Fe, B, and H, respectively. (g) Two-electrode polarization curve of am-Fe-Bi/NF/am-Fe-Bi/NF in 1 M KOH at room temperature with 90% IR-correction (purple line) and without IR-correction (blue line). 159, Copyright 2018 WILEY-VCH. (h) Polarization curves obtained in a two-electrode configuration (5 mV s^{-1}). (i) Chronopotentiometric curve of FeB_2-NF under different current density. 66, Copyright 2017 WILEY-VCH. (j) Polarization curves of overall water splitting using different electrodes. (k) The long-term stability test of water splitting with $Ni-Mo-B \text{ HF}||Ni-Mo-B \text{ HF}$ under 450 mA cm^{-2} at a cell voltage of 1.8 V . 163, Copyright 2021 Wiley-VCH.

current density of 10 mA cm⁻² (Figure 12c).

Cobalt Borides. In the research of cobalt-based materials as electrocatalysts, cobalt borides with high catalytic performance and good stability have attracted more and more attention as potential OER and HER electrocatalysts.^[58,68] Yang et al. successfully synthesized surface oxidized multifunctional Co_xB (Co₂B, CoB and CoB₂) through chemical reduction and simple air oxidation treatment.^[79] The prepared Co-B-O@Co_xB catalysts showed excellent catalytic activity in both OER and HER in alkaline. By investigating the influence of oxide layer and B content on catalytic performance, it is found that oxide layer and low boron content were both favorable to OER of cobalt borides, while high B content was favorable to HER and surface oxidation basically would have no effect on HER.^[115] Due to boron rich content, the proportion of active Co species on the surface decreased, which was not conducive to OER activity. By using optimized Co-B-O@CoB₂/Ni as the cathode and Co-B-O@Co₂B/Ni as the anode, the cell can afford the current density of 10 mA cm⁻² with only 1.54 V cell voltage and no significant attenuation within 60 h. Schuhmann et al. reported amorphous cobalt boride (Co₂B) as a highly efficient non-noble metal electrocatalyst.^[60] Cobalt boride after annealing (Co₂B-500) showed excellent OER properties. Annealing not only improved the electrical conductivity of the material, but also adjusted the surface electronic structure of cobalt boride, promoting OER. In addition, when Co₂B-500 was impregnated on nitrogen-doped graphene (NG), overpotential for HER was significantly reduced from 328 to 127 mV relative to Pt/C, mainly due to the highly conductive NG promoting charge transfer. With Co₂B-500 as anode material and Co₂B-500/NG as cathode material, the cell required a 1.81 V cell voltage at a current density of 10 mA cm⁻² in 3 M KOH and showed almost no performance loss after 53 h of continuous testing at different current densities (Figure 12d). Therefore, is an effective method to support nanoscale cobalt boride with carbon-based materials, which can not only prevent the accumulation of nanoscale cobalt boride, but also accelerate the charge transfer during the reaction process, thus improving the catalytic activity. Zang et al prepared the in situ carbon support Co-based catalysts of Co₂B/Co/N-B-C/B₄C derived from nano-B₄C by solvothermal carbonization.^[158] The catalyst Co₂B/Co/N-B-C/B₄C hybrid exhibited excellent OER, HER and ORR multifunctional electrocatalytic activity in alkaline media. The excellent catalytic performance of the catalyst is due to the multiple synergies of Co₂B, metal Co, Co/N doped carbon, B self-doped carbon, B₄C stiff support in the hybrid material. The alkaline electrolytic cell composed of Co₂B/Co/N-B-C/B₄C carbon paper electrodes as both anode and cathode can achieve a current density of 10 mA cm⁻² at a 1.622 V cell voltage. In addition, the electrolytic cell also showed good stability in overall water-splitting work for 10 h, suggesting that Co₂B/Co/N-B-C/B₄C can be a promising overall water-splitting electrocatalyst.

Iron Borides. Iron boride-based catalysts have also attracted the attention of electrochemical research in recent years due to their economic benefits, earth-abundant and excellent electrocatalytic performance. Wu et al. managed to grow amorphous iron borate

(am-Fe-Bi) cross-linked nanocrystals on nickel foam by a mild wet-chemical process.^[159] It is noteworthy that am-Fe-Bi on NF showed good OER activity (158 mV at 10 mA cm⁻²), high HER (143 mV at 10 mA cm⁻²) and ORR activity (Figure 12e). The reasons for the high activity of amorphous iron-borate electrode are as follows: First, the introduction of borohydride in the synthesis process led to a cross-linked ordered and amorphous structure, which accelerated mass transfer and exposed more active sites. Secondly, am-Fe-Bi with a lower d-band center can balance the adsorption of reactants and desorption of products. In addition, according to theoretical calculations, am-Fe-Bi possessed higher intrinsic activity due to its smaller Gibbs free energy and lower theoretical overpotential, which accelerated the OER process (Figure 12f). At the same time, the synergy between borate and iron was also aimed at multifunctional catalysis. The results showed that am-Fe-Bi/NF based overall water-splitting cell can drive 10 mA cm⁻² current density at 1.56 V cell voltage and 100 mA cm⁻² at 1.73 V (Figure 12g), and the activity cannot be significantly decreased at the chronoamperometric test. This proved to be one of the best electrocatalysts in alkaline solutions. Geyer et al. synthesized boron-rich iron diboride nanoparticles (FeB₂) by chemical reduction of iron ion (Fe²⁺) with LiBH₄ in THF organic medium, and then annealing in inert argon.^[66] The prepared FeB₂ electrode possessed significant catalytic activity and long-term stability for both HER and OER in alkaline electrolyte. FeB₂ itself is favorable for HER and OER reactions due to its high electrical conductivity. In addition, for HER, the abundance of active sites led to highly efficient catalysis, while for OER, the active FeOOH/FeB₂ heterojunction formed during the reaction led to highly efficient OER. The alkaline water electrolytic cell constructed with two identical FeB₂/NF electrodes as cathode and anode required only 1.57 V cell voltage to provide a current density of 10 mA cm⁻² and showed a nearly 100% Faraday efficiency at 20 mA cm⁻². In addition, when the applied potential exceeded 1.58 V, the catalytic capacity of FeB₂-based electrolyzer was better than Pt-C-NF/RuO₂-C-NF (Figure 12h). In addition, when the current density changed continuously in the range of 10-50 mA cm⁻², the cell voltage of the FeB₂-based electrolyzer immediately responded and remained stable in the 24 h long-term OER measurement, demonstrating the excellent stability (Figure 12i).

Multi-metal Borides

Most of the multi-metal borides reported in the literature for multifunction electrocatalysis mainly include Ni-Fe/Mo borides and Fe-Co borides. The electrochemical performance parameters of corresponding electrocatalysts are also listed in Table 3.

Ni-Fe/Mo Borides. Recent studies have shown that bimetallic borides formed by doping the second metal into mono-metallic borides can significantly improve their HER or OER performance. Guo et al. synthesized Fe/Co doped Ni₂B catalysts by high pressure and high temperature method.^[160] The obtained highly crystallized Fe-doped nickel boride (FeNiB) electrode exhibited excellent alkaline OER performance, requiring only 257 mV overpotential to get 10 mA cm⁻² current density. The electrolytic water

system consisting of FeNiB/NF anode and Pt foil cathode required only 1.54 V cell voltage to drive the current density of 10 mA cm⁻². Experimental results showed that the incorporation of iron weakened the binding strength of TM-B, which is beneficial to the adsorption of oxygen. In addition, in the OER process, the addition of iron led to an increase in the dissolution of boron oxide, which promoted the effective exposure of the metal active center and improved the catalytic performance. Theoretical calculations showed that the DOS of FeNiB near Fermi level is 2.78 times higher than that of the original Ni₂B, leading to improvement of electronic conductivity and catalytic performance. Cai et al. successfully synthesized pure phase ternary boride Mo₂NiB₂ by simple solid phase reaction.^[161] The performance of the synthesized Mo₂NiB₂ was significantly better than that of the mono-metal borides Ni₂B and MoB. For excellent OER activity, the introduction of Mo atoms into nickel boride slightly increased the density of the active sites and optimized the adsorption energy of intermediate species, resulting in easy charge transfer at the interface. At the same time, Mo dopant can greatly improve the intrinsic activity of catalytic sites. For HER, the electron transfer from Ni to Mo atoms in Mo₂NiB₂ lattice made Mo atoms have higher Bader charge and enhance the adsorption capacity of H. Therefore, the energy barrier for HER at the Mo sites was significantly reduced from 0.84 eV for MoB to 0.27 eV for Mo₂NiB₂. Considering its good OER and HER activities, Mo₂NiB₂ was used as the anode and cathode to perform overall water splitting in 1 M KOH. The electrolyzer required 1.57 V cell voltage to drive a current density of 10 mA cm⁻², and demonstrated better durability compared to the Pt/C//IrO₂/C (1.56 V). Although excellent performance has been achieved through reasonable design of structure of traditional supported catalyst, the problem of catalyst/substrate interface still inevitably exists in this kind of electrode, resulting in low catalytic surface efficiency, high charge resistance and poor stability.^[162] Shen et al. developed a novel three-dimensional hollow foam monolithic Ni-Mo-B electrode through a simple electroless plating and calcination strategy.^[163] Due to its high catalytic activity, large ECSA, high electrical conductivity, good mechanical strength and fast mass transfer capability, this novel Ni-Mo-B hollow foam electrode (Ni-Mo-B HF) not only exhibited significant catalytic activity, but also showed long-term stability at high current densities comparable to conventional supported electrodes. In view of its outstanding performance in HER and OER, the Ni-Mo-B HF as both cathode and anode constructed a two electrode electrolyzer with a 1 M KOH electrolyte, and the assembled electrolyzer can drive 10, 50 and 500 mA cm⁻² current density at cell voltage of only 1.39, 1.42 and 1.88 V (Figure 12j). In addition, Ni-Mo-B HF electrolyzer system also showed a very high stability at about 450 mA cm⁻² large current under 1.8 V for 300 h in 1 M KOH (Figure 12k).

Fe-Co Borides. Transition metal borides are considered as potential electrocatalytic materials due to their low cost, good stability and excellent electrical conductivity. After that, the electronic structure and morphology structure of borides have been optimized by various improvement strategies, and the improved borides showed excellent properties. For the borides developed, most materials are excellent OER catalysts, and the corre-

sponding HER activity is often not very ideal. According to reports, most metal phosphide or P-doped hybrids exhibit excellent HER activity.^[15,16] Therefore, the synergistic effect of the incorporation of P element into metal borides to adjust the chemical composition can be used to design bifunctional electrocatalysts. Additionally, to synthesize unique, high-specific surface nano-structured borides via morphological control can expose more active sites and facilitate mass/electron transfer than boride particles synthesized by conventional methods. Liu et al. reported phosphorus-doped Co-Fe-B material (Co₁-Fe₁-B-P) with chain structure and confirmed that it is a novel and highly efficient OER, HER and overall water-splitting electrocatalyst.^[164] In addition, the experimental results showed that the molar ratio of Co/Fe affected the morphology and catalytic performance of the prepared catalysts. Due to its excellent bi-functional properties, the Co₁-Fe₁-B-P nanochain can drive 10 mA cm⁻² current density at a low voltage of 1.68 V in 1.0 M KOH to achieve efficient water splitting. The prepared Co₁-Fe₁-B-P nanochain showed excellent electrocatalytic performance due to the following points: 1D chain-like structure can expose more catalytic active sites. Secondly, the coupling effect between phosphorus and boron promoted the electrocatalytic process by reducing the reaction energy, and at the same time enabled the catalyst to have excellent bi-functional properties. In addition, the interface between different components can regulate the reaction kinetics and promote the charge transfer in the catalytic process. Finally, the synergistic effect of Co and Fe can significantly promote the electrocatalytic reaction. Fang et al. successfully synthesized Co-Fe-B ternary boride catalyst by chemical reduction and then calcination.^[165] Co-Fe-B showed good bifunctional electrocatalytic performance with 129 mV overpotential at 10 mA cm⁻² current density and 67.3 mV dec⁻¹ Tafel slope for HER, 280 mV overpotential and 38.9 mV dec⁻¹ Tafel slope for OER. Combined with experimental and theoretical results, the excellent performance of Co-Fe-B was due to the synergistic effect between Co and Fe, optimized electronic structure, improved charge transfer, larger specific surface area of electrochemical activity and lower kinetic barrier.

Other Multi-metal Borides. The introduction of other heteroatoms into the transition metal borides can help to regulate the local disorder, improve the thermal stability and catalytic activity of the amorphous phase, and optimize the properties of the materials combined with the structural design. Guo et al. synthesized a series of Co-based metal boride nanochains doped with other metal elements (Ni,Fe) by using simple one-pot chemical reduction. The NiCoFeB obtained showed remarkable HER and OER activities and outstanding working stability.^[166] The presence of cobalt played a key role in the formation of the nanochain structure in borides. Density functional theory calculations confirmed that the excellent catalytic performance came from the incorporation of Ni and Fe, which adjusted potentially existing Co⁰ surface state and led to the optimization of electronic structure. In addition, the incorporation of Ni and Fe led to Co-B sublattice distortion, not only causing the loss of long-range order, but also widening the p-d band overlap, which was the key to the strong surface charge transfer effect. The alkaline electrolyzer

composed of NiCoFeB as HER and OER electrodes can drive a 10-mA cm^{-2} current density at a cell voltage of 1.81 V without significant performance loss at over 20 h stability test in 1.0 M KOH. Taking advantage of the ultrathin 2D porous nanostructures of ultrathin nanomeshes, ultrathin metal borate nanomeshes with well-ordered nanopores (e.g., Co-B_i, Ni-B_i and Fe-B_i) have been successfully synthesized in one step by He et al.^[167] The as-synthesized Co-B_i nanomeshes supported on 3D bark-like N-doped carbon (denoted BNC) showed excellent OER properties which is due to the porous nanostructure promoting the exposure of the active site, the highly electronegative N optimizing the electronic structure of Co-Bi to improve the intrinsic activity, and the strong coupling of BNC and Co-Bi heterojunction accelerating the charge transfer. However, Co-B_i/BNC can only observe negligible HER current density, possibly due to the weak interaction between hydrogen and Co-B_i. Meanwhile, Ru-doped Co-B_i/BNC (Ru-Co-B_i/BNC) showed excellent HER activity. The water splitting device based on Co-B_i and Ru-Co-B_i nanomeshes can achieve a current density of 10 mA cm^{-2} at a small cell voltage of 1.53 V. Co-B_i/BNC-based nanocomposites exhibited no obvious loss of water-splitting current density for 20 h, which indicated excellent water splitting stability.

Other Nanocomposites Containing Boron

Boron-Doped Nanocomposites. When boron is introduced into the electrocatalytic active material in the form of dopant, first of all, the activity is optimized by modulating the electron cloud density and electronic properties of the active sites to change the interface electron transfer capacity and the energy barrier formed by the reaction intermediates. Secondly, defects (i.e., oxygen vacancies and amorphous state) are often formed during the

introduction of borides through borohydride reduction, which can bring abundant active sites and conductivity. For example, Song et al. proposed a simple two-step preparation strategy to synthesize B, N co-doped carbon nanosheets (B5/GCS). B atoms can be introduced by borate crosslinking, while N element was introduced into the carbon networks with anion intercalation stripping agent.^[168] B5/GCS, as an advanced carbon-based bifunctional catalyst, showed excellent HER performance (with a low overpotential of $\sim 51.96\text{ mV}$ at 10 mA cm^{-2}) and OER performance (170 mV at 10 mA cm^{-2}) in acidic media. HER and OER performance improvement was mainly due to the synergy of B and N co-doping and the formation of nanosheets through intercalating cationic stripping, in which the B atoms at the center of the BO_3 plane acted as the main active sites and N atoms as cocatalyst to optimize the adsorption of reaction intermediates and facilitate the transfer of electrons. It is noteworthy that an efficient water-splitting electrolyzer consisting of B5/GCS as anode and cathode can reach 10 mA cm^{-2} at only 1.45 V cell voltage in 0.5 M H_2SO_4 . Moreover, the synthesized B, N co-doped molybdenum carbide nanoparticles embedded in B,N-doped carbon (BCN) networks (B,N:Mo₂C@BCN) exhibited excellent electrocatalytic HER and OER activities in alkaline media.^[169] It was confirmed that the improved performance of the hybrid material was mainly attributed to the adjustment of electronic structure induced by B and N co-doping, which promoted the charge transfer and improved the surface wettability (Figure 13a), as well as the formation of tiny nanoparticles on the BCN network. When the current density got to 100 mA cm^{-2} , the cell voltage ($E_{100} = 1.84\text{ V}$) was 110 mV lower than that of Pt/RuO₂ ($E_{100} = 1.95\text{ V}$) in the electrolyzer composed of B,N:Mo₂C@BCN (Figure 13b). Besides, B,N:Mo₂C@BCN showed high reversibility

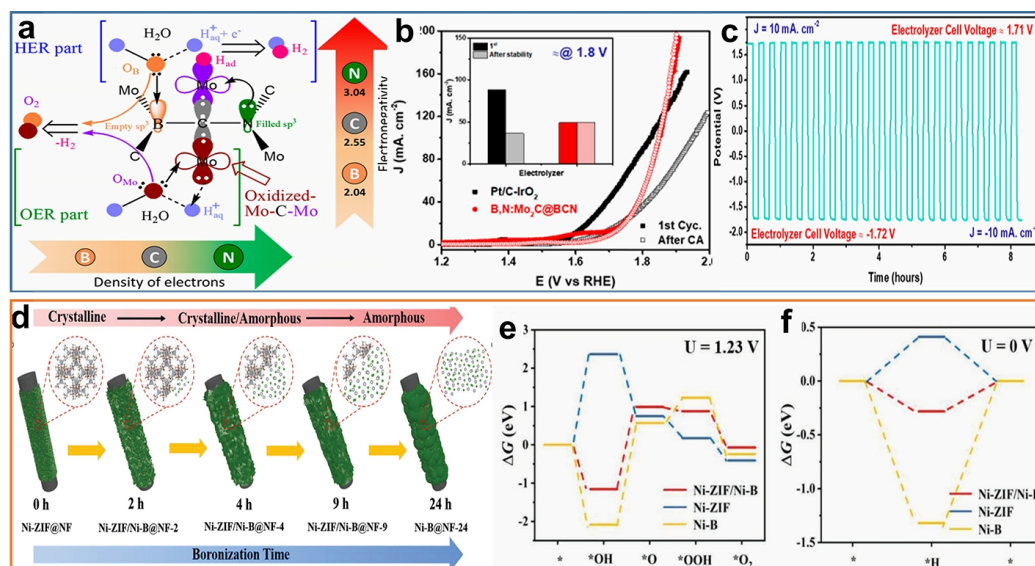


Figure 13. (a) Proposed mechanism of overall water splitting on a B,N:Mo₂C@BCN nanoparticle showing the synergistic effect of B and N attached to the C atom of Mo₂C for the HER and OER. (b) Polarization curves of the two-electrode electrolyzer using cathode-anode combinations of B,N:Mo₂C@BCN-B,N:Mo₂C@BCN and Pt/C-RuO₂@NF at a sweep rate of 2 mV s^{-1} and comparison of current densities at a cell voltage of 1.8 V before and after CA (inset). (c) Pulse chronopotentiometric curve for H₂/O₂ evolution in a B,N:Mo₂C@BCN electrolyzer with a current density of $-10/10\text{ mA cm}^{-2}$. 169, Copyright 2018 American Chemical Society. (d) Schematic illustration of the synthetic process of Ni-ZIF/Ni-B@NF. (e) The calculated free-energy diagram of OER at the thermodynamic equilibrium potential 1.23 V. (f) The calculated free-energy diagram of the HER. 170, Copyright 2019 WILEY-VCH.

Table 3. Summary of the Electrochemical Parameters for Transition Metal Boride/Borate-Based Catalysts Reported in Literature

Electrocatalyst	Synthesis method	Reaction	Performance			Ref.
			η_{10} (mV)	Tafel slope (mV·dec ⁻¹)	Electrolyte	
Co-30Ni-B	chemical reduction	HER	170	51	0.5 M KPi	[31]
10%Ni-WB ₂	molten salt-assisted method	HER	144	63	0.5 M H ₂ SO ₄	[42]
nano-VB ₂	arc-melting	HER	192	68	0.5 M H ₂ SO ₄	[44]
a-Mo _{0.7} W _{0.3} B ₂	arc-melting	HER	201	63.8	0.5 M H ₂ SO ₄	[46]
Ni-B-O@Ni ₃ B	chemical reduction, oxidation	HER	64	80.9	1 M KOH	[47]
Co-B-P/NF	electroless deposition	HER	42	42.1	1 M KOH	[58]
CNBO-NSs	chemical reduction	HER	140	116	1 M KOH	[59]
Co ₂ B-500	chemical reduction, annealing	HER	328	136.2	1 M KOH	[60]
Co-Ni-B@NF	electroless plating, calcination	HER	205	—	1 M KOH	[61]
annealed Co-W-B/NF	electroless plating, annealing	HER	98	83	1 M KOH	[62]
FeB ₂ NPs	chemical reduction, annealing	HER	61	87.5	1M KOH	[66]
NiB/NF	electroless plating	HER	41.2	91.3	1 M KOH	[67]
NiB/Ni	electroless plating	HER	78.2	106.5	1 M KOH	[67]
Co-3Mo-B	chemical reduction	HER	66	67	1 M NaOH	[76]
Co-B-O@CoB ₂	chemical reduction, oxidation	HER	106	234.9	1 M KOH	[79]
Ni-B/GC	electroless plating	HER	132(η_{20})	53(η_{10-40}) 112(η_{40-120})	1 M HClO ₄	[80]
Co-B/Ni	electroless plating	HER	70	68	1 M KOH	[83]
calcined CoB/NF	electroless plating, calcination	HER	110	96	1 M KOH	[84]
Ni-B _{0.54} film	electroless plating	HER	45	43	0.5 M H ₂ SO ₄	[85]
		HER	54	77	1 M PBS	[85]
		HER	135	88	1 M KOH	[85]
Ni-S-B	electrodeposition	HER	240	121.2	30 wt% KOH	[88]
VB ₂	arc-melting	HER	204	108.3	0.5 M H ₂ SO ₄	[90]
MoB ₂	solid state metathesis (ssm)	HER	154	49	0.5 M H ₂ SO ₄	[93]
ultrathin Mo ₃ B films	chemical vapor deposition	HER	249(η_{20})	52	0.5 M H ₂ SO ₄	[98]
Ni-B@Ni(OH) ₂ -BI	chemical reduction	HER	256	114	0.1 M Na ₂ SO ₄ containing 0.36 M NaB(OH) ₄ (pH = 12.5)	[109]
Co-B-P	hydrothermal, boronization-phosphidation	HER	51	44	1 M KOH	[113]
MoB/g-C ₃ N ₄	machinery mixing	HER	152	46	1 M KOH	[116]
WB ₂	metallothermic reduction	HER	198	53.1	0.5 M H ₂ SO ₄	[117]
Ni ₃ B/MoB	hydrothermal, boronization	HER	75	61	0.5 M H ₂ SO ₄	[120]
		HER	119	79	1 M KOH	[120]
CoB@MoS ₂ -0.5-300	hydrothermal, chemical reduction	HER	146	80.9	1 M KOH	[121]
Co-Mo-B/CoMoO _{4-x} /CF	hydrothermal, calcination, chemical reduction	HER	55	66	1 M KOH	[122]
B-MoC	calcination	HER	285	128	0.5 M H ₂ SO ₄	[123]
B-CoP/CNT	chemical reduction	HER	39	50	0.5 M H ₂ SO ₄	[124]
		HER	79	80	1 M PBS	[124]
		HER	56	69	1 M KOH	[124]
B-Fe ₇ S ₈ /FeS ₂	chemical reduction	HER	113	57.4	1 M KOH	[125]
NiCo ₂ -B-P	chemical reduction	HER	78	73	1 M KOH	[126]
A-NiCo LDH/NF	chemical reduction	HER	36	57	1 M KOH	[127]
Ru NCs/BNG	pyrolyzation	HER	10	28.9	1 M KOH	[128]
Ru@B-Ti ₃ C ₂ Tx	pyrolyzation	HER	62.9	100	0.5 M H ₂ SO ₄	[129]
BC ₃ N@Pt	pyrolyzation	HER	26.1	41.59	1 M KOH	[130]
		HER	38.5	59.05	1 M PBS	[130]
		HER	23.1	61.07	0.05 M H ₂ SO ₄	[130]
Co ₂ B/Co/N-B-C/B ₄ C	solvothermal carbonization	HER	220	105	0.1 M KOH	[158]
am-Fe-Bi/NF	solvent thermal method	HER	143	75	1 M KOH	[159]

Mo ₂ NiB ₂	solid state sintering	HER	160	71	1 M KOH	[161]
		HER	125	81	0.5 M H ₂ SO ₄	[161]
Ni-Mo-B HF	electroless plating, calcination	HER	68(η_{50})	58	1 M KOH	[163]
Co ₁ -Fe ₁ -B-P	water-bath, phosphorization	HER	173	96	1 M KOH	[164]
Co-Fe-B	chemical reduction, calcination	HER	129	67.3	1 M KOH	[165]
NiCoFeB	chemical reduction	HER	345	98	1 M KOH	[166]
Ru-Co-B _i /BNC	chemical reduction	HER	145	65.6	1 M KOH	[167]
Ni-B-O@NiB ₂	chemical reduction, oxidation	OER	219	126.2	1 M KOH	[47]
Ni-Co-B/rGO	chemical reduction, calcination	OER	280	56	1 M KOH	[48]
Co ₂ -Fe-B	chemical reduction	OER	298	62.6	1 M KOH	[49]
pc-Ni-B _i @NB	chemical reduction, annealing	OER	302	52	1 M KOH	[51]
NiFe-Boride	chemical reduction,	OER	167	25	1 M KOH	[52]
activation, boronized Ni	boronization	OER	300	43	1 M KOH	[53]
MOEE	boronization,	OER	263	47.1	1 M KOH	[55]
	electrochemical oxidation					
Fe-B-O@FeB ₂	chemical reduction, oxidation	OER	260	57.9	1 M KOH	[56]
CNBO-NSs	chemical reduction	OER	300	60	1 M KOH	[59]
Co ₂ B-500	chemical reduction, annealing	OER	380	45	0.1 M KOH	[60]
Co-Ni-B@NF	electroless plating, calcination	OER	313	120	1 M KOH	[61]
annealed Co-W-B/NF	electroless plating, annealing	OER	360	--	1 M KOH	[62]
NiB _{0.45} -250/Cu	electroless plating,	OER	296	58	1 M KOH	[63]
	annealing					
Ni _x B-300	chemical reduction	OER	380	89	1 M KOH	[64]
FeB ₂ NPs	chemical reduction, annealing	OER	296	52.4	1M KOH	[66]
Co ₂ B	ball milling	OER	287	50.7	1 M KOH	[68]
Co-10Ni-B	chemical reduction	OER	330	73.3	1 M KOH	[75]
Co-3Mo-B	chemical reduction	OER	320	155	1 M NaOH	[76]
(Co _{0.9} Ni _{0.1}) ₂ B	chemical reduction, annealing	OER	371	77	1 M KOH	[77]
Co-B-O@Co ₂ B/Ni	chemical reduction, oxidation	OER	221	139.9	1 M KOH	[79]
Ni-B/GC	electroless plating	OER	194(η_{20})	--	1 M KOH	[80]
Ir/CoNiB	electroless plating, oil bath heating	OER	178	35.1	1 M KOH	[81]
CoFeB-5-30 NS/NF	electroless plating	OER	260(η_{20})	38	1 M KOH	[82]
Co-B/Ni	electroless plating	OER	140	89	1 M KOH	[83]
calcined CoB/NF	electroless plating, calcination	OER	315	80	1 M KOH	[84]
AlFe ₂ B ₂	arc-melting, ball-milling	OER	240	42	1 M KOH	[89]
Ni@B _i /RGO	chemical reduction	OER	329	79	1 M KOH	[100]
Co-B _i NS/G	chemical reduction	OER	290	53	1 M KOH	[101]
m-B-FeNiNH/IF	boronization	OER	246(η_{100})	26.5	1 M KOH	[102]
rGO/CB/Co-B _i	chemical reduction	OER	350	95.5	0.1 M KOH	[103]
Co-B _i /Ti	electrodeposition	OER	469	138	0.1 M K-B _i	[104]
Ni-B _i /CC	electrodeposition	OER	470	107	0.1 M K-B _i	[105]
Ni-Co-B _i /CC	electrodeposition	OER	388	142	0.1 M K-B _i	[106]
Co-B film	pulsed laser deposition	OER	280	60	1 M KOH	[132]
Ni-B@Ni(OH) ₂ @Ni	hydrothermal technique,	OER	300(η_{100})	49	1 M KOH	[133]
	dip-coating					
F-Ni ₂ B/Ni(OH) _x	chemical reduction, chemical	OER	340	23	1 M KOH	[134]
	surface etching					
Co@Co-Bi/Ti	chemical reduction	OER	329	46	1 M KOH	[136]
CoB _x @h-BN	chemical reduction, ammonization	OER	290	81.9	1 M KOH	[137]
Fe ₂ B NWs/NF	chemical reduction	OER	240	30	1 M KOH	[139]
FeNi@FeNiB-700	boronization	OER	272	89.2	1 M KOH	[140]
Fe _{6.4} Ni _{16.1} P _{12.9} B _{4.3} O _{60.2}	chemical reduction	OER	236	39	1 M KOH	[141]
NiCo ₂ O ₄ @Ni-Co-B/CC	oxidative polarization	OER	270	62	1 M KOH	[142]
Fe ₃ Co ₇ -B/CNT	chemical reduction	OER	265	30	1 M KOH	[144]
EBP/CoFeB	chemical reduction	OER	227	36.7	1 M KOH	[145]
FeCoNiBO _x /PPy/rGO	chemical reduction	OER	290	47	1 M KOH	[146]

Gd-CoB@Au	electrodeposition, chemical reduction	OER	230	42	1 M KOH	[148]
a-LNFBPO	hydrothermal, ball milling	OER	242	37	1 M KOH	[149]
B-Co ₂ Fe LDH	hydrothermal, chemical reduction	OER	205	39.2	1 M KOH	[151]
B-doped CoO-Ov	hydrothermal, calcination	OER	280	71	1 M KOH	[152]
Fe ₅ Co ₄ Ni ₂₀ Se ₃₆ B _x	chemical reduction, selenization	OER	279.8	59.5	1 M KOH	[154]
IrO _x /L-BN	chemical vapor deposition, laser irradiation	OER	259	36.68	1 M KOH	[157]
Co ₂ B/Co/N-B-C/B ₄ C	solvothermal carbonization	OER	300	111	0.1 M KOH	[158]
am-Fe-Bi/NF	solvent thermal method	OER	158	53	1 M KOH	[159]
FeNiB	ball-milling	OER	257	110	1 M KOH	[160]
Mo ₂ NiB ₂	solid state sintering	OER	280	57	1 M KOH	[161]
Ni-Mo-B HF	electroless plating, calcination	OER	293(η_{50})	79	1 M KOH	[163]
Co ₁ -Fe ₁ -B-P	water-bath, phosphorization	OER	225	40	1 M KOH	[164]
Co-Fe-B	chemical reduction, calcination	OER	280	38.9	1 M KOH	[165]
NiCoFeB	chemical reduction	OER	284	46	1 M KOH	[166]
Co-B ₂ /BNC	chemical reduction	OER	286	70.9	1 M KOH	[167]
Co ₂ B-500-OER// Co ₂ B-500/NG-HER	chemical reduction, calcination	water splitting	1.81 V	--	3 M KOH	[60]
FeB ₂ -NF	chemical reduction, annealing	water splitting	1.57 V	--	1 M KOH	[66]
Ni ₃ B/f-MWCNT	chemical reduction	water splitting	1.6 V	--	1 M KOH	[99]
Co ₂ B/Co/N-B-C/B ₄ C	solvothermal carbonization	water splitting	1.622 V	--	1 M KOH	[158]
am-Fe-Bi/NF	solvent thermal method	water splitting	1.56 V	--	1 M KOH	[159]
FeNiB-OER//Pt-HER	ball-milling	water splitting	1.54 V	--	1 M KOH	[160]
Mo ₂ NiB ₂	solid state sintering	water splitting	1.57 V	--	1 M KOH	[161]
Ni-Mo-B HF	electroless plating, calcination	water splitting	1.39 V	--	1 M KOH	[163]
Co ₁ -Fe ₁ -B-P	water-bath, phosphorization	water splitting	1.68 V	--	1 M KOH	[164]
NiCoFeB	chemical reduction	water splitting	1.81 V	--	1 M KOH	[166]
Co-B ₂ /BNC-OER// Ru-Co-B ₂ /BNC-HER	chemical reduction	water splitting	1.53 V	--	1 M KOH	[167]
B5/GCS	borate crosslinking, cationic intercalation stripping	water splitting	1.45 V	--	0.5 M H ₂ SO ₄	[168]
B,N:Mo ₂ C@BCN	annealing	water splitting	1.71 V	--	1 M KOH	[169]
Ni-ZIF/Ni-B@NF	hydrothermal, chemical reduction	water splitting	1.54 V	--	1 M KOH	[170]
V ₀ B-Co ₃ O ₄ /NF	hydrothermal, annealing, chemical reduction	water splitting	1.67 V	--	1 M KOH	[171]
B-BCN/N-BCN	annealing	water splitting	1.52 V	--	1 M KOH	[172]
Co/NBC	carbonization	water splitting	1.68 V	--	1 M KOH	[175]

and can be cycled 50 times in 30,000 seconds (Figure 13c). The excellent reversibility between OER and HER was attributed to the synergistic effect between the BCN network and the flexible change of the valence state of Mo on the material surface within the potential window. Considering the advantages of ultrathin MOF materials and the characteristics of sodium borohydride boronization at room temperature, Wu et al. converted Ni-ZIF nanorods into ultrathin Ni-ZIF/Ni-B nanosheets with abundant crystalline-amorphous grain boundaries as a highly efficient bi-functional electrocatalyst.^[170] By changing the boriding time (0, 2, 4, 9 and 24 h), the degree of MOFs transformation (i.e., morphology, chemical composition and microstructure) can be regulated to obtain the best catalytic materials (Figure 13d). The experimental results showed that the Ni-ZIF/Ni-B nanosheets supported on nickel foam after boronization for 4 h (Ni-ZIF/Ni-B@NF-4) possessed an outstanding electrocatalytic performance toward overall water splitting, requiring only an ultralow cell

voltage of 1.54 V at 10 mA cm⁻², representing an outstanding MOF-based electrocatalyst. The excellent catalytic performance can be attributed to the 2D ultrathin nanosheets with abundant crystalline-amorphous grain boundaries that can promote the increase and exposure of active sites and accelerate mass diffusion and charge transfer capabilities, as well as the optimized electronic structure that can regulate the adsorption energy of intermediates (Figure 13e-f). Wang et al. prepared self-supported B-doped Co₃O₄ (V₀B-Co₃O₄) nanowires with controllable O vacancy on the nickel foam by alternating the treatment of Co salt and NaBH₄.^[171] Experimental and theoretical calculations confirmed that the O-vacancy engineering realized the modulation of Co₃O₄ energy band to promote the electron transfer. Meanwhile, the boron doping led to the rearrangement of the electronic structure of metal and promoted the release of hydrogen through the dissociation of water. The two-electrode alkaline electrolyzer was prepared using V₀B-Co₃O₄/NF as cathode and anode, which

needed the cell voltage of 1.67 V to drive 10 mA cm⁻² current density with remarkable stability over 20 h. Conventional carbon materials exhibit electrochemical inertness due to their high graphitization. Hao et al. reported, based on theoretical calculation and Lewis's theory of acids and bases, that boron carbonitride (BCN) systems with different enrichment degrees of B/N heteroatoms can introduce stronger adsorption for OH^{*}/H₂O.^[172] The authors designed and synthesized a series of self-supported BCN materials with different levels of B/N enrichment. By adjusting the contents of B and N, the best catalytic performance of overall water-splitting was obtained. Finally, the optimized material B-BCN/N-BCN has an onset voltage of 1.52 V under alkaline conditions. Furthermore, Chakraborty et al. designed 2D a-CN with P, Si, and B dopants as catalysts for HER and OER.^[173] Theoretical calculations showed that the doping of P and B can modulate the electronic properties of CN and reduce its energy band to the position required for HER and OER. The authors found that P replacing C sites and B replacing N sites in CN were beneficial to HER and OER, respectively.

Substrates with Boron. Boron imidazolate frameworks (BIFs) are a new type of zeolite-like metal-organic framework consisting of the crosslinking of preassembled boron-imidazolate complex and metal ions. BIFs have a high density of boron and nitrogen components and have B-H groups to directly reduce encapsulated metal ions to nanoparticles without any external stimulation.^[174] Multiple heteroatom co-doped carbon nanocomposites can be prepared by using the ordered arrangement of MOF precursors. Based on these advantages, Zhang et al. reported a novel cobalt-imidazolate framework (BIF-82-Co), which was converted into a nitrogen-boron co-doped carbon shell (Co/NBC) decorated with cobalt nanoparticles by direct carbonization without the introduction of additional heteroatomic ligands.^[175] By controlling the calcination temperature to adjust the composition and surface structure of the material to optimize the catalytic performance, the optimized Co/NBC-900 displayed high catalytic performance of HER and OER in alkaline solution. In addition, thanks to the synergistic effect between partially oxidized cobalt metal, conducting N and B co-doped graphite carbon and carbon nanotubes, as well as the coupling between these components, the Co/NBC-900 acted as both anode and cathode for water splitting to achieve a current density of 10 mA cm⁻² at a cell voltage of 1.68 V. In addition, transition metal (TM) single atom catalysts (SACs) supported by two-dimensional (2D) materials are excellent electrocatalytic materials.^[176] Due to the difference in electronegativity between boron, nitrogen and carbon atoms, combining graphene with hexagonal boron nitride (h-BN) to prepare single atom anchored on hybrid BCN is an effective strategy for improving performance. Jiang et al. developed a single-Ni atom anchoring on a BCN nanosheet with defect (Ni@BCN) bi-functional HER and OER electrocatalyst.^[177] Due to the effective charge polarization and synergistic effect between graphene, BN domain and Ni atoms, Ni@BCN displayed significant electrocatalytic activity and a very low overpotential 0.47/0.02 V for OER/HER.

n CONCLUSIONS AND PERSPECTIVES

In this review, the structural characteristics, synthesis methods and recent research progress of transition metal borides as non-noble metals and low-cost electrocatalysts for HER, OER and overall water splitting are reviewed in detail. Transition metal boride-based catalysts can exhibit remarkable electrochemical performance due to their excellent properties and structures such as electrical conductivity and unique electronic structure. Obviously, transition metal borides are excellent catalytic materials for electrocatalytic hydrogen production. Previous studies have even shown that TMBs are superior to commonly used TM based materials, including TM phosphating, TM sulfides and TM oxides. The excellent performance of TMBs includes high electrocatalytic activity, excellent stability and good electrical conductivity mainly due to the unique electronic structure, crystal phase structure and other structural characteristics of borides. However, despite recent advances in transition metal boride-based electrocatalysts, possible challenges and room for improvement remain, as detailed below.

Material Synthesis and Design. I) Material synthesis: It is important to design transition metal boride-based catalysts via effective, environmentally friendly and economical synthesis methods as well as innovative strategies for the development of commercial-oriented catalysts. Borides synthesized by traditional liquid phase synthesis methods, including chemical reduction, chemical deposition, and electrodeposition, are often amorphous and of limited elemental composition, such as molybdenum borides, which is difficult to synthesize by this kind of liquid phase synthesis method. This has resulted in limited research on borides. However, high temperature treatment process often produces borides with low specific surface area and is often accompanied by the synthesis of boride impurity phases with different stoichiometry and crystal phase structures. This not only results in a decrease in the number of active sites but also makes it impossible to accurately determine the activity of the target boride. After examining all the synthetic routes, it can be concluded that chemical reduction is the simplest and most economical method to prepare metal borides. Owing to its simplicity, it is also suitable for factory scale production. However, in order to develop pure phase Mo-based borides, more research work is needed to find low energy consumption technologies. Boriding, which has been developed in recent years, is an impressive way to obtain stable catalyst surfaces, but requires more efforts to adjust the lower temperatures it can achieve. In addition, precursors, solvents and specific conditions in the synthesis process can affect the morphology and crystal structure of borides. These factors that can affect performance also vary from system to system. Therefore, it is of guiding significance for precise control of boride materials to explore the inner correlation between synthesis-structure-properties. II) Material design: For the construction of high-performance boride electrocatalysts, four principles should be followed. Abundant active sites, excellent electrocatalytic activity, good electrical conductivity and long-term stability are necessary conditions for electrocatalysts. Based on the previous discussion, general principles for the construction of high-performance transition metal boride based catalysts for electrocatalytic applications will be elaborated. Abundant active

sites can ensure sufficient contact between electrolyte/reactant and catalyst to facilitate the electrochemical reaction. More active sites can be exposed by nanomatization, nanostructure control, hybridization with porous substrates, and ion doping. The intrinsic electrocatalytic activity determines the electrocatalytic performance of TMBs to a certain extent. It has been reported that the catalytic activity can be improved by regulating the electronic structure and surface properties of hosts, including composition regulation, surface oxidation, phase engineering and heterogenization. In the electrochemical reaction, efficient electron transfer is very important to improve the reaction kinetics, for high electrical conductivity can promote interfacial charge transfer and avoid unnecessary resistance. Proper composition adjustment of TMBs and loading of TMB onto a conductive substrate can also significantly improve the conductivity of the entire electrocatalyst/electrode. The strong covalent bond properties of metal-like bonds in TMB are the main reason for their chemical and mechanical stability. Composition regulation (e.g., B/TM atomic ratio optimization and doping), hybridization, morphology and nanostructure control can further improve the durability of TMB based electrocatalysts. In addition, it is very important to accurately design boron-rich/metal-rich borides and diborides with highly active graphene-like 2D boron layers for electrocatalytic water splitting. In addition, heteroatom doping is a useful but limited method for borides. The hybridization of borides with other active catalysts or conductive materials is also an effective strategy for the preparation of highly active electrocatalysts, but only limited literature has been reported, so there is a lot of room for improvement. Therefore, further optimization of chemical composition and structure to develop high-performance electrocatalysts requires further exploration of innovative design strategies.

Structure-Activity. Revealing the structure-activity relationship is not only helpful to understand the catalytic mechanism and the active sites, but also crucial for improving the catalytic activity accurately. I) Surface oxidation: Borides cannot avoid oxidation during preparation, drying and storage. The surface oxide layer is composed of transition metal oxide/oxyhydroxide and boron oxide/borate. Importantly, the formation of oxygen-bearing species and core-shell structure TMB@TMB oxide/oxyhydroxide composites has not been determined as to the mechanism of electrocatalysis. Currently, emphasis is placed on the formation of transition metal oxide/oxyhydroxide species that are beneficial to the OER process. However, evolving boron oxide/borate species is rarely investigated, although they show great promise for OER applications. Another issue to be considered is the effect of oxidation on HER performance. Several studies have shown that the oxide layer on the surface of TMBs is detrimental to HER, while oxidation has also been reported to promote alkaline HER by forming TM hydroxides. II) Catalytic mechanism: Many aspects of the transition metal boride/borate family remain unclear from the perspective of electrocatalytic mechanisms. In HER, for amorphous metal borides, the most commonly accepted reaction mechanism is that transition metal atoms (Co and Ni) serve as the active center, and boron provides electrons to enrich its d-band, thus effectively preventing the oxidation of metal active sites and improving the stability of the

material. The mechanism for HER is verified by experiments and theoretical calculations. However, the reason for the phenomenon of “reverse electron transfer” in amorphous metal borides needs to be solved. For OER, most of the literature reports that boron is not the active center. Some references do not clearly explain the role of boron, but only mention that the catalyst evolves into core-shell structure TMB/TM oxides/oxyhydroxides during OER. In this structure model, the active phase is transition metal oxides or oxyhydroxides, and the boride nucleus enhance electrical conductivity. It has also been reported that boron species dissolve into the electrolyte, creating defects that provide active sites. In other reports, boron species mainly assist the formation of metal oxides/hydroxides/oxyhydroxides. Therefore, the exact role and mechanism of boron in OER process have not been determined. In addition, anionic or cationic doping strategy is an effective method to improve the intrinsic properties of boride materials. However, electron transfer and electron structure optimization are mainly discussed at present, and the overall and deep doping mechanism is not very clear. Hence, further experiments should be carried out on the basis of the in situ/operando methods to observe changes in the chemical behavior of borides before, during and after water splitting test. By combining the electrocatalytic process with advanced characterization technology such as in situ XPS, XAS, TEM, XRD and Raman, real-time reaction changes during the catalytic process can be monitored to determine the active sites and reaction mechanism. In addition, the combination of theoretical calculations and operando characterization technologies can facilitate the design of highly efficient catalytic materials.

Stability. HER, OER and overall water-splitting are usually carried out in strong acid or alkali media, so the electrochemical stability of transition metal boride-based electrocatalysts under such harsh conditions is also an important part of their electrocatalytic performance. For OER, the use of metal borides in acidic media is rarely reported, reflecting the instability of this family in acids. Even for HER, few metal borides (Ni and Mo based borides) are stable in acidic solutions. As a result, most borides can only be used in alkaline water electrolyzer. Due to the stability of borides, their application in proton exchange membrane (PEM) water electrolyzers is problematic. Fortunately, the only molybdenum-based borides show good stability in acidic media. However, the synthesis of pure molybdenum borides is a challenge and requires new synthesis strategies to develop molybdenum-based borides. The success of these synthesis techniques will provide a major breakthrough for the development of acid stable metal borides. Among the existing OER catalysts, some transition metal borates are effective for OER in neutral media but inert for HER. Therefore, transition metal boride electrocatalysts with OER and HER activities in neutral electrolytes need to be developed in the future. In addition, future work on metal borides/borates should focus on improving the overall testing techniques, especially under industrial conditions, and must focus on extreme conditions ($\gg 30$ bar, $80\text{ }^{\circ}\text{C}$, > 200 h, $> 100\text{ mA cm}^{-2}$ stability) for application testing, which will establish its reliability in industrial alkaline water electrolyzers. Finally, in order to realize the industrial application of borides, the key pa-

parameters for the catalyst are high stability, low cost and good performance under high current density. In the case of high current density, it is difficult to strike a balance between good performance and excellent stability. It can only be achieved if appropriate design strategies are adopted to regulate the different types of borides.

Commercial Prospects. First, boron is relatively cheap and abundant. Most reported transition metal borides use transition metals that are also inexpensive and abundant. In addition, the metal borides/borates synthesis method consumes less energy and is non-toxic compared to those required for the synthesis of other transition metal non-oxide electrocatalysts (sulfides and phosphides). And in alkaline medium, the performance of most metal borides is comparable to that of precious metals. These conditions make it possible for transition metal borides to replace precious metals. Therefore, it has a realistic application prospect in the substitution of precious metal catalyst, especially in alkaline electrolyzers. In addition to water electrolysis, potential applications for borides can be extended to other related fields, including batteries, supercapacitors, photocatalysis and other catalytic reactions, such as N_2 and CO_2 reduction and $NaBH_4$ hydrolysis. Therefore, the development of borides displays important guiding significance for promoting high performance and multifunctional energy storage conversion materials.

n ACKNOWLEDGEMENTS

This work was financially supported by National Natural Science Foundation of China (Nos. 22078362 and 21808243) and the Postgraduate Innovation Engineering Project of China University of Petroleum (East China) (YCX2021063).

n AUTHOR INFORMATION

Corresponding authors. Emails: liubin@upc.edu.cn (B. Liu) and dongbin@upc.edu.cn (B. Dong)

n COMPETING INTERESTS

The authors declare no competing interests.

n ADDITIONAL INFORMATION

Full paper can be accessed via
<http://manu30.magtech.com.cn/jghx/EN/10.14102/j.cnki.0254-5861.2022-0117>

For submission: <https://www.editorialmanager.com/cjschem>

n REFERENCES

- (1) Dong, B.; Xie, J. Y.; Wang, N.; Gao, W. K.; Ma, Y.; Chen, T. S.; Yan, X. T.; Li, Q. Z.; Zhou, Y. L.; Chai, Y. M. Zinc ion induced three-dimensional Co_9S_8 nano-neuron network for efficient hydrogen evolution. *Renew. Energ.* **2020**, 157, 415-423.
- (2) Radwan, A.; Jin, H.; He, D.; Mu, S. Design engineering, synthesis protocols, and energy applications of MOF-derived electrocatalysts. *Nanomicro. Lett.* **2021**, 13, 132.
- (3) Zhang, L. C.; Zhao, H. T.; Xu, S. R.; Liu, Q.; Li, T. S.; Luo, Y. L.; Gao, S. Y.; Shi, X. F.; Asiri, A.; Sun, X. P. Recent advances in 1D electrospun nanocatalysts for electrochemical water splitting. *Small Struct.* **2021**, 2, 2000048.
- (4) Wang, Y.; Huang, J.; Wang, L.; She, H.; Wang, Q. Research progress of ferrite materials for photoelectrochemical water splitting. *Chin. J. Struct. Chem.* **2022**, 41, 2201054-2201068.
- (5) Zhang, J. Y.; Wang, H.; Tian, Y.; Yan, Y.; Xue, Q.; He, T.; Liu, H.; Wang, C.; Chen, Y.; Xia, B. Y. Anodic hydrazine oxidation assists energy-efficient hydrogen evolution over a bifunctional cobalt perselenide nanosheet electrode. *Angew. Chem. Int. Ed.* **2018**, 57, 7649-7653.
- (6) Gong, L.; Yang, H.; Wang, H.; Qi, R.; Wang, J.; Chen, S.; You, B.; Dong, Z.; Liu, H.; Xia, B. Y. Corrosion formation and phase transformation of nickel-iron hydroxide nanosheets array for efficient water oxidation. *Nano Res.* **2021**, 14, 4528-4533.
- (7) Long, X.; Meng, J.; Gu, J.; Ling, L.; Li, Q.; Liu, N.; Wang, K.; Li, Z. Interfacial engineering of $NiFeP/NiFe-LDH$ heterojunction for efficient overall water splitting. *Chin. J. Struct. Chem.* **2022**, 41, 2201019-2201024.
- (8) Shao, L. Y.; Sun, H. M.; Miao, L. C.; Chen, X.; Han, M.; Sun, J. C.; Liu, S.; Li, L.; Cheng, F. Y.; Chen, J. Facile preparation of NH_2 -functionalized black phosphorene for the electrocatalytic hydrogen evolution reaction. *J. Mater. Chem. A* **2018**, 6, 2494-2499.
- (9) Yang, Y.; Yu, Y.; Li, J.; Chen, Q.; Du, Y.; Rao, P.; Li, R.; Jia, C.; Kang, Z.; Deng, P.; Shen, Y.; Tian, X. Engineering ruthenium-based electrocatalysts for effective hydrogen evolution reaction. *Nanomicro. Lett.* **2021**, 13, 160.
- (10) Yang, S.; Qin, L.; Zhang, W.; Cao, R. The mechanism of water oxidation from mn-based heterogeneous electrocatalysts. *Chin. J. Struct. Chem.* **2022**, 41, 2204022-2204033.
- (11) Qin, J. F.; Yang, M.; Chen, T. S.; Dong, B.; Hou, S.; Ma, X.; Zhou, Y. N.; Yang, X. L.; Nan, J.; Chai, Y. M. Ternary metal sulfides $MoCoNiS$ derived from metal organic frameworks for efficient oxygen evolution. *Int. J. Hydrogen Energy* **2020**, 45, 2745-2753.
- (12) Huang, C. Q.; Yu, L.; Zhang, W.; Xiao, Q.; Zhou, J. Q.; Zhang, Y. L.; An, P. F.; Zhang, J.; Yu, Y. N-doped Ni-Mo based sulfides for high-efficiency and stable hydrogen evolution reaction. *Appl. Catal. B* **2020**, 276, 119137.
- (13) Yuan, J.; Cheng, X.; Wang, H.; Lei, C.; Pardiwala, S.; Yang, B.; Li, Z.; Zhang, Q.; Lei, L.; Wang, S.; Hou, Y. A superaerophobic bimetallic selenides heterostructure for efficient industrial-level oxygen evolution at ultra-high current densities. *Nanomicro. Lett.* **2020**, 12, 104.
- (14) Li, M.; Feng, L. $NiSe_2-CoS_2$ with a hybrid nanorods and nanoparticles structure for efficient oxygen evolution reaction. *Chin. J. Struct. Chem.* **2022**, 41, 2201019-2201024.
- (15) Yan, T.; Zhang, X.; Liu, H.; Jin, Z. CeO_2 particles anchored to Ni_2P nanoplate for efficient photocatalytic hydrogen evolution. *Chin. J. Struct. Chem.* **2022**, 41, 2201047-2201053.
- (16) Shi, Y.; Li, M.; Yu, Y.; Zhang, B. Recent advances in nanostructured transition metal phosphides: synthesis and energy-related applications. *Energy Environ. Sci.* **2020**, 13, 4564-4582.
- (17) Li, P.; Hong, W.; Liu, W. Fabrication of large scale self-supported $WC/Ni(OH)_2$ electrode for high-current-density hydrogen evolution. *Chin. J. Struct. Chem.* **2021**, 40, 1365-1371.
- (18) Han, N.; Yang, K. R.; Lu, Z.; Li, Y.; Xu, W.; Gao, T.; Cai, Z.; Zhang, Y.; Batista, V. S.; Liu, W.; Sun, X. Nitrogen-doped tungsten carbide nanoarray as an efficient bifunctional electrocatalyst for water splitting in acid. *Nat. Commun.* **2018**, 9, 924.
- (19) Shu, X.; Chen, S.; Pan, W.; Zhang, J. Cobalt nitride embedded holey N-doped graphene as advanced bifunctional electrocatalysts for

Zn-air batteries and overall water splitting. *Carbon* **2020**, 157, 234-243.

(20) Saad, A.; Shen, H.; Cheng, Z.; Arbi, R.; Guo, B.; Hui, L. S.; Liang, K.; Liu, S.; Atfield, J. P.; Turak, A.; Wang, J.; Yang, M. Mesoporous ternary nitrides of earth-abundant metals as oxygen evolution electrocatalyst. *Nanomicro. Lett.* **2020**, 12, 79.

(21) Guo, B. Y.; Zhang, X. Y.; Ma, X.; Chen, T. S.; Chen, Y.; Wen, M. L.; Qin, J. F.; Nan, J.; Chai, Y. M.; Dong, B. RuO₂/Co₃O₄ nanocubes based on Ru ions impregnation into Prussian blue precursor for oxygen evolution. *Inter. J. Hydrogen Energy* **2020**, 45, 9575-9582.

(22) Xie, J. Y.; Fan, R. Y.; Fu, J. Y.; Zhen, Y. N.; Li, M. X.; Liu, H. J.; Ma, Y.; Wang, F. L.; Chai, Y. M.; Dong, B. Double doping of V and F on Co₃O₄ nanoneedles as efficient electrocatalyst for oxygen evolution. *Int. J. Hydrogen Energy* **2021**, 46, 19962-19970.

(23) Fu, C.; Wang, Y.; Huang, J. Hybrid of quaternary layered double hydroxides and carbon nanotubes for oxygen evolution reaction. *Chin. J. Struct. Chem.* **2020**, 39, 1807-1816.

(24) Li, R.; Xu, H.; Yang, P.; Wang, D.; Li, Y.; Xiao, L.; Lu, X.; Wang, B.; Zhang, J.; An, M. Synergistic interfacial and doping engineering of heterostructured NiCo(OH)_x-Co₂W as an efficient alkaline hydrogen evolution electrocatalyst. *Nanomicro. Lett.* **2021**, 13, 120.

(25) Shi, L.; Chen, H.; Liang, X.; Liu, Y.; Zou, X. Theoretical insights into nonprecious oxygen-evolution active sites in Ti-Ir-based perovskite solid solution electrocatalysts. *J. Mater. Chem. A* **2020**, 8, 218-223.

(26) Chen, D.; Qiao, M.; Liu, Y. R.; Hao, L.; Liu, D.; Dong, C. L.; Li, Y.; Wang, S. Preferential cation vacancies in perovskite hydroxide for the oxygen evolution reaction. *Angew. Chem. Int. Ed.* **2018**, 57, 8691-8696.

(27) Chen, Y.; Li, H.; Wang, J.; Du, Y.; Xi, S.; Sun, Y.; Sherburne, M.; Ager, J. W.; Fisher, A. C.; Xu, Z. J. Exceptionally active iridium evolved from a pseudo-cubic perovskite for oxygen evolution in acid. *Nat. Commun.* **2019**, 10, 572.

(28) Guo, H. P.; Ruan, B. Y.; Luo, W. B.; Deng, J. Q.; Wang, J. Z.; Liu, H. K.; Dou, S. X. Ultrathin and edge-enriched holey nitride nanosheets as bifunctional electrocatalysts for the oxygen and hydrogen evolution reactions. *ACS Catal.* **2018**, 8, 9686-9696.

(29) Li, R. C.; Zhou, D.; Luo, J. X.; Xu, W. M.; Li, J. W.; Li, S. S.; Cheng, P. P.; Yuan, D. S. The urchin-like sphere arrays Co₃O₄ as a bifunctional catalyst for hydrogen evolution reaction and oxygen evolution reaction. *J. Power Sources* **2017**, 341, 250-256.

(30) Chen, H.; Zou, X. X. Intermetallic borides: structures, synthesis and applications in electrocatalysis. *Inorg. Chem. Front.* **2020**, 7, 2248-2264.

(31) Gupta, S.; Patel, N.; Fernandes, R.; Kadrekar, R.; Dashora, A.; Yadav, A. K.; Bhattacharyya, D.; Jha, S. N.; Miotello, A.; Kothari, D. C. Co-Ni-B nanocatalyst for efficient hydrogen evolution reaction in wide pH range. *Appl. Catal. B* **2016**, 192, 126-133.

(32) Gupta, S.; Patel, N.; Miotello, A.; Kothari, D. C. Cobalt-boride: an efficient and robust electrocatalyst for hydrogen evolution reaction. *J. Power Sources* **2015**, 279, 620-625.

(33) Masa, J.; Andronesco, C.; Antoni, H.; Sinev, I.; Seisel, S.; Elumeeva, K.; Barwe, S.; Marti-Sanchez, S.; Arbiol, R. C.; Muhler, S. W. Role of boron and phosphorus in enhanced electrocatalytic oxygen evolution by nickel borides and nickel phosphides. *ChemElectroChem* **2019**, 6, 235-240.

(34) Hulm, J. K.; Matthias, B. T. New superconducting borides and nitrides. *Phys. Rev.* **1951**, 82, 273-274.

(35) Hardy, G. F.; Hulm, J. K. The superconductivity of some transition metal compounds. *Phys. Rev.* **1954**, 93, 1004-1016.

(36) Chung, H. Y.; Weinberger, M. B.; Levine, J. B.; Kavner, A.; Yang, J. M.; Tolbert, S. H.; Kaner, R. B. Synthesis of ultra-incompressible superhard rhenium diboride at ambient pressure. *Science* **2007**, 316, 436-438.

(37) Gabani, S.; Flachbart, K.; Siemensmeyer, K.; Mori, T. Magnetism and superconductivity of rare earth borides. *J. Alloy. Compd.* **2020**, 821, 153201.

(38) Sussardi, A.; Tanaka, T.; Khan, A. U.; Schlappbach, L.; Mori, T. Enhanced thermoelectric properties of samarium boride. *J. Materials* **2015**, 1, 196-204.

(39) Chen, Z. J.; Duan, X. G.; Wei, W.; Wang, S. B.; Zhang, Z. J.; Ni, B. J. Boride-based electrocatalysts: emerging candidates for water splitting. *Nano Res.* **2020**, 13, 293-314.

(40) Gupta, S.; Patel, M. K.; Miotello, A.; Patel, N. Metal boride-based catalysts for electrochemical water-splitting: a review. *Adv. Funct. Mater.* **2019**, 30, 1906481.

(41) Jiang, Y. Y.; Lu, Y. Z. Designing transition-metal-boride-based electrocatalysts for applications in electrochemical water splitting. *Nanoscale* **2020**, 12, 9327-9351.

(42) Guo, F. F.; Wu, Y. Y.; Ai, X.; Chen, H.; Li, G. D.; Chen, W.; Zou, X. X. A class of metal diboride electrocatalysts synthesized by a molten salt-assisted reaction for the hydrogen evolution reaction. *Chem. Commun.* **2019**, 55, 8627-8630.

(43) Chen, Y. L.; Yu, G. T.; Chen, W.; Liu, Y. P.; Li, G. D.; Zhu, P. W.; Tao, Q.; Li, Q. J.; Liu, J. W.; Shen, X. P.; Li, H.; Huang, X. R.; Wang, D. J.; Asefa, T.; Zou, X. X. Highly active, nonprecious electrocatalyst comprising borophene subunits for the hydrogen evolution reaction. *J. Am. Chem. Soc.* **2017**, 139, 12370-12373.

(44) Jothi, P. R.; Zhang, Y.; Yubuta, K.; Culver, D. B.; Conley, M.; Fokwa, B. P. T. Abundant vanadium diboride with graphene-like boron layers for hydrogen evolution. *ACS Appl. Energy Mater.* **2019**, 2, 176-181.

(45) Park, C. H.; Zhang, Y.; Scheifers, J. P.; Jothi, P. R.; Encinas, A.; Fokwa, B. P. T. Graphene- and phosphorene-like boron layers with contrasting activities in highly active Mo₂B₄ for hydrogen evolution. *J. Am. Chem. Soc.* **2017**, 139, 12915-12918.

(46) Park, H.; Zhang, Y. M.; Lee, E.; Shankari, P.; Fokwa, B. P. T. High-current-density HER electrocatalysts: graphene-like boron layer and tungsten as key ingredients in metal diborides. *ChemSusChem* **2019**, 12, 3726-3731.

(47) Yuan, W. Y.; Zhao, X. S.; Hao, W. J.; Li, J. X.; Wang, L. C.; Ma, X. H.; Guo, Y. H. Performance of surface-oxidized Ni₃B, Ni₂B, and NiB₂ electrocatalysts for overall water splitting. *ChemElectroChem* **2019**, 6, 764-770.

(48) Sun, J. K.; Zhang, W.; Wang, S. Y.; Ren, Y. B.; Liu, Q. Y.; Sun, Y. F.; Tang, L.; Guo, J. X.; Zhang, X. Ni-Co-B nanosheets coupled with reduced graphene oxide towards enhanced electrochemical oxygen evolution. *J. Alloy. Compd.* **2019**, 776, 511-518.

(49) Chen, H. Y.; Ouyang, S.; Zhao, M.; Li, Y. X.; Ye, J. H. Synergistic activity of Co and Fe in amorphous Co_x-Fe-B catalyst for efficient oxygen evolution reaction. *ACS Appl. Mater. Interfaces* **2017**, 9, 40333-40343.

(50) Masa, J.; Piontek, S.; Wilde, P.; Antoni, H.; Eckhard, T.; Chen, Y. T.; Muhler, M.; Apfel, U. P.; Schuhmann, W. Ni-metalloid (B, Si, P, As, and Te) alloys as water oxidation electrocatalysts. *Adv. Energy Mater.* **2019**, 9, 1900796.

(51) Jiang, W. J.; Niu, S.; Tang, T.; Zhang, Q. H.; Liu, X. Z.; Zhang, Y.; Chen, Y. Y.; Li, J. H.; Gu, L.; Wan, L. J.; Hu, J. S. Crystallinity-modulated electrocatalytic activity of a nickel(II) borate thin layer on Ni₃B for efficient

water oxidation. *Angew. Chem. Int. Ed.* **2017**, 56, 6572-6577.

- (52) Wang, N.; Xu, A.; Ou, P. F.; Hung, S. F.; Ozden, A.; Lu, Y. R.; Abed, J.; Wang, Z. Y.; Yan, Y.; Sun, M. J.; Xia, Y. J.; Han, M.; Han, J. R.; Yao, K. L.; Wu, F. Y.; Chen, P. H.; Vomiero, A.; Seifitokaldani, A.; Sun, X. H.; Sinton, D.; Liu, Y. C.; Sargent, E. H.; Liang, H. Y. Boride-derived oxygen-evolution catalysts. *Nat. Commun.* **2021**, 12, 6089.
- (53) Li, J. H.; Chen, H.; Liu, Y. P.; Gao, R. Q.; Zou, X. X. In situ structural evolution of a nickel boride catalyst: synergistic geometric and electronic optimization for the oxygen evolution reaction. *J. Mater. Chem. A* **2019**, 7, 5288-5294.
- (54) Guo, F. F.; Wu, Y. Y.; Chen, H.; Liu, Y. P.; Yang, L.; Ai, X.; Zou, X. X. High-performance oxygen evolution electrocatalysis by boronized metal sheets with self-functionalized surfaces. *Energy Environ. Sci.* **2019**, 12, 684-692.
- (55) Li, J.; Liu, Y.; Chen, H.; Zhang, Z.; Zou, X. Design of a multilayered oxygen-evolution electrode with high catalytic activity and corrosion resistance for saline water splitting. *Adv. Funct. Mater.* **2021**, 31, 2101820.
- (56) Wang, L. C.; Li, J. X.; Zhao, X. S.; Hao, W. J.; Ma, X. H.; Li, S. J.; Guo, Y. H. Surface-activated amorphous iron borides (Fe_xB) as efficient electrocatalysts for oxygen evolution reaction. *Adv. Mater. Interfaces* **2019**, 6, 1801690.
- (57) Gong, Z. C.; Liu, R.; Gong, H. S.; Ye, G. L.; Liu, J. J.; Dong, J. C.; Liao, J. W.; Yan, M. M.; Liu, J. B.; Huang, K.; Xing, L. L.; Liang, J. F.; He, Y. M.; Fei, H. L. Constructing a graphene-encapsulated amorphous/crystalline heterophase NiFe alloy by microwave thermal shock for boosting the oxygen evolution reaction. *ACS. Catal.* **2021**, 11, 12284-12292.
- (58) Sun, H. M.; Xu, X. B.; Yan, Z. H.; Chen, X.; Jiao, L. F.; Cheng, F. Y.; Chen, J. Superhydrophilic amorphous Co-B-P nanosheet electrocatalysts with Pt-like activity and durability for the hydrogen evolution reaction. *J. Mater. Chem. A* **2018**, 6, 22062-22069.
- (59) He, T.; Nsanzimana, J. M. V.; Qi, R. J.; Zhang, J. Y.; Miao, M.; Yan, Y.; Qi, K.; Liu, H. F.; Xia, B. Y. Synthesis of amorphous boride nanosheets by the chemical reduction of prussian blue analogs for efficient water electrolysis. *J. Mater. Chem. A* **2018**, 6, 23289-23294.
- (60) Masa, J.; Weide, P.; Peeters, D.; Sinev, I.; Xia, W.; Sun, Z. Y.; Somsen, C.; Muhler, M.; Schuhmann, W. Amorphous cobalt boride (Co₂B) as a highly efficient nonprecious catalyst for electrochemical water splitting: oxygen and hydrogen evolution. *Adv. Energy Mater.* **2016**, 6, 1502313.
- (61) Xu, N.; Cao, G. X.; Chen, Z. J.; Kang, Q.; Dai, H. B.; Wang, P. Cobalt nickel boride as an active electrocatalyst for water splitting. *J. Mater. Chem. A* **2017**, 5, 12379-12384.
- (62) Cao, G. X.; Xu, N.; Chen, Z. J.; Kang, Q.; Dai, H. B.; Wang, P. Cobalt-tungsten-boron as an active electrocatalyst for water electrolysis. *ChemistrySelect* **2017**, 2, 6187-6193.
- (63) Jiang, J.; Wang, M.; Yan, W. S.; Liu, X. F.; Liu, J. X.; Yang, J. L.; Sun, L. C. Highly active and durable electrocatalytic water oxidation by a NiB_{0.45}/NiO_x core-shell heterostructured nanoparticulate film. *Nano Energy* **2017**, 38, 175-184.
- (64) Masa, J.; Sinev, I.; Mistry, H.; Ventosa, E.; Mata, M.; Arbiol, J.; Muhler, M.; Roldan, C. B.; Schuhmann, W. Ultrathin high surface area nickel boride (Ni_xB) nanosheets as highly efficient electrocatalyst for oxygen evolution. *Adv. Energy Mater.* **2017**, 7, 1700381.
- (65) Park, H.; Encinas, A.; Scheifers, J. P.; Zhang, Y. M.; Fokwa, B. P. T. Boron-dependency of molybdenum boride electrocatalysts for the hydrogen

evolution reaction. *Angew. Chem. Int. Ed.* **2017**, 56, 5575-5578.

- (66) Li, H.; Wen, P.; Li, Q.; Dun, C.; Xing, J.; Lu, C.; Adhikari, S.; Jiang, L.; Carroll, D. L.; Geyer, S. M. Earth-abundant iron diboride (FeB₂) nanoparticles as highly active bifunctional electrocatalysts for overall water splitting. *Adv. Energy Mater.* **2017**, 7, 1700513.
- (67) Zhang, R. Q.; Liu, H. X.; Wang, C. F.; Wang, L. C.; Yang, Y. J.; Guo, Y. H. Electroless plating of transition metal boride with high boron content as superior HER electrocatalyst. *ChemCatChem* **2020**, 12, 3068-3075.
- (68) Ma, X. Z.; Wen, J.; Zhang, S.; Yuan, H. R.; Li, K. Y.; Yan, F.; Zhang, X. T.; Chen, Y. J. Crystal Co_xB (x = 1-3) synthesized by a ball-milling method as high-performance electrocatalysts for the oxygen evolution reaction. *ACS Sustain. Chem. Eng.* **2017**, 5, 10266-10274.
- (69) Ai, X.; Zou, X.; Chen, H.; Su, Y. T.; Feng, X. L.; Li, Q. J.; Liu, Y. P.; Zhang, Y.; Zou, X. X. Transition-metal-boron intermetallics with strong interatomic d-sp orbital hybridization for high-performance electrocatalysis. *Angew. Chem. Int. Ed.* **2020**, 59, 3961-3965.
- (70) Zou, X.; Wang, L.; Ai, X.; Chen, H.; Zou, X. X. Crystal phase-dependent electrocatalytic hydrogen evolution performance of ruthenium-boron intermetallics. *Chem. Commun.* **2020**, 56, 3061-3064.
- (71) Xu, Q. C.; Liu, Y.; Jiang, H.; Hu, Y. J.; Liu, H. L.; Li, C. Z. Unsaturated sulfur edge engineering of strongly coupled MoS₂ nanosheet-carbon macroporous hybrid catalyst for enhanced hydrogen generation. *Adv. Energy Mater.* **2019**, 9, 1802553.
- (72) Dinca, M.; Surendranath, Y.; Nocera, D. G. Nickel-borate oxygen-evolving catalyst that functions under benign conditions. *PNAS* **2010**, 107, 10337-10341.
- (73) Surendranath, Y.; Dinca, M.; Nocera, D. G. Electrolyte-dependent electrosynthesis and activity of cobalt-based water oxidation catalysts. *J. Am. Chem. Soc.* **2009**, 131, 2615-2620.
- (74) Nsanzimana, J. M. V.; Peng, Y. C.; Xu, Y. Y.; Thia, L.; Wang, C.; Xia, B. Y.; Wang, X. An efficient and earth-abundant oxygen-evolving electrocatalyst based on amorphous metal borides. *Adv. Energy Mater.* **2018**, 8, 1701475.
- (75) Zhang, J.; Li, X. X.; Liu, Y. T.; Zeng, Z. W.; Cheng, X.; Wang, Y. D.; Tu, W. M.; Pan, M. Bi-metallic boride electrocatalysts with enhanced activity for the oxygen evolution reaction. *Nanoscale* **2018**, 10, 11997-12002.
- (76) Gupta, S.; Patel, N.; Fernandes, R.; Hanchate, S.; Miotello, A.; Kothari, D. C. Co-Mo-B nanoparticles as a non-precious and efficient bifunctional electrocatalyst for hydrogen and oxygen evolution. *Electrochim. Acta* **2017**, 232, 64-71.
- (77) Schuch, J.; Klemenz, S.; Schuldt, P.; Zieschang, A. M.; Dolique, S.; Connor, P.; Kaiser, B.; Kramm, U. I.; Albert, B.; Jaegermann, W. Efficient oxygen evolution electrocatalyst by incorporation of nickel into nanoscale dicobalt boride. *ChemCatChem* **2021**, 13, 1772-1780.
- (78) Yang, Y. S.; Zhuang, L. Z.; Rufford, T. E.; Wang, S. B.; Zhu, Z. H. Efficient water oxidation with amorphous transition metal boride catalysts synthesized by chemical reduction of metal nitrate salts at room temperature. *RSC Adv.* **2017**, 7, 32923-32930.
- (79) Guo, Y. H.; Zhang, R. Q.; Hao, W. J.; Zhang, J. K.; Yang, Y. J. Multifunctional Co-B-O@Co₂B catalysts for efficient hydrogen generation. *Int. J. Hydrogen Energy* **2020**, 45, 380-390.
- (80) Zeng, M.; Wang, H.; Zhao, C.; Wei, J. K.; Qi, K.; Wang, W. L.; Bai, X. D. Nanostructured amorphous nickel boride for high-efficiency electrocatalytic hydrogen evolution over a broad pH range. *ChemCatChem* **2016**, 8, 708-712.

- (81) Wang, C.; Zhai, P. L.; Xia, M. Y.; Wu, Y. Z.; Zhang, B.; Li, Z. W.; Ran, L.; Gao, J. F.; Zhang, X. M.; Fan, Z. Z.; Sun, L. C.; Hou, J. G. Engineering lattice oxygen activation of iridium clusters stabilized on amorphous bimetal borides array for oxygen evolution reaction. *Angew. Chem. Int. Ed.* **2021**, 60, 27126-27134.
- (82) Li, Y.; Jiang, X. L.; Tang, M. Y.; Zheng, Q. J.; Huo, Y.; Xie, F. Y.; Lin, D. M. A high-performance oxygen evolution electrocatalyst based on partially amorphous bimetallic cobalt iron boride nanosheet. *Int. J. Hydrogen Energy* **2020**, 45, 28586-28597.
- (83) Hao, W. J.; Wu, R. B.; Zhang, R. Q.; Ha, Y.; Chen, Z. L.; Wang, L. C.; Yang, Y. J.; Ma, X. H.; Sun, D. L.; Fang, F.; Guo, Y. H. Electroless plating of highly efficient bifunctional boride-based electrodes toward practical overall water splitting. *Adv. Energy Mater.* **2018**, 8, 1801372.
- (84) Chen, Z. J.; Kang, Q.; Cao, G. X.; Xu, N.; Dai, H. B.; Wang, P. Study of cobalt boride-derived electrocatalysts for overall water splitting. *Int. J. Hydrogen Energy* **2018**, 43, 6076-6087.
- (85) Zhang, P. L.; Wang, M.; Yang, Y.; Yao, T. Y.; Han, H. X.; Sun, L. C. Electroless plated Ni-B films as highly active electrocatalysts for hydrogen production from water over a wide pH range. *Nano Energy* **2016**, 19, 98-107.
- (86) Yang, Y.; Wang, M.; Zhang, P. L.; Wang, W. H.; Han, H. X.; Sun, L. C. Evident enhancement of photoelectrochemical hydrogen production by electroless deposition of M-B (M = Ni, Co) catalysts on silicon nanowire arrays. *ACS Appl. Mater. Interfaces* **2016**, 8, 30143-30151.
- (87) Kim, J.; Kim, H.; Kim, S. K.; Ahn, S. H. Electrodeposited amorphous Co-P-B ternary catalyst for hydrogen evolution reaction. *J. Mater. Chem. A* **2018**, 6, 6282-6288.
- (88) Wu, Y. H.; Gao, Y.; He, H. W.; Zhang, P. Novel electrocatalyst of nickel sulfide boron coating for hydrogen evolution reaction in alkaline solution. *Appl. Surf. Sci.* **2019**, 480, 689-696.
- (89) Mann, D. K.; Xu, J.; Mordvinova, N. E.; Yannello, V.; Ziouani, Y.; Gonzalez-Ballesteros, N.; Sousa, J. P. S.; Lebedev, O. I.; Kolen'ko, Y. V.; Shatruk, M. Electrocatalytic water oxidation over AlFe_2B_2 . *Chem. Sci.* **2019**, 10, 2796-2804.
- (90) Lee, E.; Park, H.; Joo, H.; Fokwa, B. P. T. Unexpected correlation between boron chain condensation and hydrogen evolution reaction (HER) activity in highly active vanadium borides: enabling predictions. *Angew. Chem. Int. Ed.* **2020**, 59, 11774-11778.
- (91) Carenco, S.; Portehault, D.; Boissiere, C.; Mezailles, N.; Sanchez, C. Nanoscaled metal borides and phosphides: recent developments and perspectives. *Chem. Rev.* **2013**, 113, 7981-8065.
- (92) Li, Q. J.; Zou, X.; Ai, X.; Chen, H.; Sun, L.; Zou, X. X. Revealing activity trends of metal diborides toward pH-universal hydrogen evolution electrocatalysts with Pt-like activity. *Adv. Energy Mater.* **2019**, 9, 1803369.
- (93) Jothi, P. R.; Zhang, Y. M.; Scheifers, J. P.; Park, H.; Fokwa, B. P. T. Molybdenum diboride nanoparticles as a highly efficient electrocatalyst for the hydrogen evolution reaction. *Sustain. Energy Fuels* **2017**, 1, 1928-1934.
- (94) Jothi, P. R.; Yubuta, K.; Fokwa, B. P. T. A simple, general synthetic route toward nanoscale transition metal borides. *Adv. Mater.* **2018**, 30, 1704181.
- (95) Xiao, M.; Zhang, L.; Luo, B.; Lyu, M.; Wang, Z. L.; Huang, H. M.; Wang, S. C.; Du, A. J.; Wang, L. Z. Molten-salt-mediated synthesis of an atomic nickel Co-catalyst on TiO_2 for improved photocatalytic H_2 evolution. *Angew. Chem. Int. Ed.* **2020**, 59, 7230-7234.
- (96) Wang, F. G.; Liu, B.; Wang, H. Y.; Lin, Z. Y.; Dong, Y. W.; Yu, N.; Luan, R. N.; Chai, Y. M.; Dong, B. Motivating borate doped FeNi layered double hydroxides by molten salt method toward efficient oxygen evolution. *J. Colloid Interface Sci.* **2022**, 610, 173-181.
- (97) Zhou, Y. N.; Wang, F. L.; Dou, S. Y.; Shi, Z. N.; Dong, B.; Yu, W. L.; Zhao, H. Y.; Wang, F. G.; Yu, J. F.; Chai, Y. M. Motivating high-valence Nb doping by fast molten salt method for NiFe hydroxides toward efficient oxygen evolution reaction. *Chem. Eng. J.* **2022**, 427, 131643.
- (98) Wang, X. F.; Tai, G. A.; Wu, Z. H.; Hu, T. S.; Wang, R. Ultrathin molybdenum boride films for highly efficient catalysis of the hydrogen evolution reaction. *J. Mater. Chem. A* **2017**, 5, 23471-23475.
- (99) Chen, X. C.; Yu, Z. X.; Wei, L.; Zhou, Z.; Zhai, S. L.; Chen, J. S.; Wang, Y. Q.; Huang, Q. W.; Karahan, H. E.; Liao, X. Z.; Chen, Y. Ultrathin nickel boride nanosheets anchored on functionalized carbon nanotubes as bifunctional electrocatalysts for overall water splitting. *J. Mater. Chem. A* **2019**, 7, 764-774.
- (100) Cao, X. Y.; Cui, L.; Wang, X. X.; Yang, W. R.; Liu, J. Q. Nickel-borate/reduced graphene oxide nanohybrid: a robust and efficient electrocatalyst for oxygen evolution reaction in alkaline and near neutral media. *ChemCatChem* **2018**, 10, 2826-2832.
- (101) Chen, P. Z.; Xu, K.; Zhou, T. P.; Tong, Y.; Wu, J. C.; Cheng, H.; Lu, X. L.; Ding, H.; Wu, C. Z.; Xie, Y. Strong-coupled cobalt borate nanosheets/graphene hybrid as electrocatalyst for water oxidation under both alkaline and neutral conditions. *Angew. Chem.* **2016**, 128, 2534-2538.
- (102) Wang, F. G.; Liu, B.; Lin, Z. Y.; Liu, X.; Ma, Y.; Zhou, Y. L.; Yu, J. F.; Chai, Y. M.; Dong, B. Constructing partially amorphous borate doped iron-nickel nitrate hydroxide nanoarrays by rapid microwave activation for oxygen evolution. *Appl. Surf. Sci.* **2022**, 592, 153245.
- (103) Sun, J. Q.; Yang, D. J.; Lowe, S.; Zhang, L. J.; Wang, Y. Z.; Zhao, S. L.; Liu, P. R.; Wang, Y.; Tang, Z. Y.; Zhao, H. J.; Yao, X. D. Sandwich-like reduced graphene oxide/carbon black/amorphous cobalt borate nanocomposites as bifunctional cathode electrocatalyst in rechargeable zinc-air batteries. *Adv. Energy Mater.* **2018**, 8, 1801495.
- (104) Yang, L. B.; Liu, D. N.; Hao, S.; Kong, R. M.; Asiri, A. M.; Zhang, C. X.; Sun, X. P. A cobalt-borate nanosheet array: an efficient and durable non-noble-metal electrocatalyst for water oxidation at near neutral pH. *J. Mater. Chem. A* **2017**, 5, 7305-7308.
- (105) Ji, X. Q.; Cui, L.; Liu, D. N.; Hao, S.; Liu, J. Q.; Qu, F. L.; Ma, Y. J.; Du, G.; Asiri, A. M.; Sun, X. P. A nickel-borate nanoarray: a highly active 3D oxygen-evolving catalyst electrode operating in near-neutral water. *Chem. Commun.* **2017**, 53, 3070-3073.
- (106) Ma, M.; Qu, F. L.; Ji, X. Q.; Liu, D. N.; Hao, S.; Du, G.; Asiri, A. M.; Yao, Y. D.; Chen, L.; Sun, X. P. Bimetallic nickel-substituted cobalt-borate nanowire array: an earth-abundant water oxidation electrocatalyst with superior activity and durability at near neutral pH. *Small* **2017**, 13, 1700394.
- (107) Sun, H. M.; Yan, Z. H.; Liu, F. M.; Xu, W. C.; Cheng, F. Y.; Chen, J. Self-supported transition-metal-based electrocatalysts for hydrogen and oxygen evolution. *Adv. Mater.* **2020**, 32, 1806326.
- (108) She, Z. W.; Kibsgaard, J.; Dickens, C. F.; Chorkendorff, I.; Norskov, J. K.; Jaramillo, T. F. Combining theory and experiment in electrocatalysis: insights into materials design. *Science* **2017**, 355, 146.
- (109) Zheng, Y.; Jiao, Y.; Vasileff, A.; Qiao, S. Z. The hydrogen evolution reaction in alkaline solution: from theory, single crystal models, to practical electrocatalysts. *Angew. Chem. Int. Ed.* **2018**, 57, 7568-7579.

- (110) Peng, L. S.; Zheng, X. Q.; Li, L.; Zhang, L.; Yang, N.; Xiong, K.; Chen, H. M.; Li, J.; Wei, Z. D. Chimney effect of the interface in metal oxide/metal composite catalysts on the hydrogen evolution reaction. *Appl. Catal. B* **2019**, 245, 122-129.
- (111) Zhao, Z. P.; Liu, H. T.; Gao, W. P.; Xue, W.; Liu, Z. Y.; Huang, J.; Pan, X. Q.; Huang, Y. Surface-engineered PtNi-O nanostructure with record-high performance for electrocatalytic hydrogen evolution reaction. *J. Am. Chem. Soc.* **2018**, 140, 9046-9050.
- (112) Li, Y. X.; Zhang, W. Z.; Li, H.; Yang, T. Y.; Peng, S. Q.; Kao, C.; Zhang, W. Y. Ni-B coupled with borate-intercalated Ni(OH)₂ for efficient and stable electrocatalytic and photocatalytic hydrogen evolution under low alkalinity. *Chem. Eng. J.* **2020**, 394, 124928.
- (113) Bao, X. H.; Li, Y. T.; Wang, J.; Zhong, Q. Amorphous-crystalline Co-B-P catalyst for synergistically enhanced hydrogen evolution reaction. *ChemCatChem* **2020**, 12, 6259-6264.
- (114) Han, H.; Choi, H.; Mhin, S.; Hong, Y. R.; Kim, K. M.; Kwon, J.; Ali, G.; Chung, K. Y.; Je, M.; Umh, H. N.; Lim, D. H.; Davey, K.; Qiao, S. Z.; Paik, U.; Song, T. Advantageous crystalline-amorphous phase boundary for enhanced electrochemical water oxidation. *Energy Environ. Sci.* **2019**, 12, 2443-2454.
- (115) Vrubel, H.; Hu, X. Molybdenum boride and carbide catalyze hydrogen evolution in both acidic and basic solutions. *Angew. Chem. Int. Ed.* **2012**, 51, 12703-12706.
- (116) Zhuang, Z. C.; Li, Y.; Li, Z. L.; Lv, F.; Lang, Z. Q.; Zhao, K. N.; Zhou, L.; Moskaleva, L.; Guo, S. J.; Mai, L. Q. MoB/g-C₃N₄ interface materials as a schottky catalyst to boost hydrogen evolution. *Angew. Chem. Int. Ed.* **2018**, 57, 496-500.
- (117) Li, Q.; Wang, L. N.; Ai, X.; Chen, H.; Zou, J. Y.; Li, G. D.; Zou, X. X. Multiple crystal phases of intermetallic tungsten borides and phase-dependent electrocatalytic property for hydrogen evolution. *Chem. Commun.* **2020**, 56, 13983-13986.
- (118) Zhang, J.; Wang, T.; Pohl, D.; Rellinghaus, B.; Dong, R. H.; Liu, S. H.; Zhuang, X. D.; Feng, X. L. Interface engineering of MoS₂/Ni₃S₂ heterostructures for highly enhanced electrochemical overall-water-splitting activity. *Angew. Chem. Int. Ed.* **2016**, 55, 6702-6707.
- (119) Diao, J. X.; Qiu, Y.; Liu, S. Q.; Wang, W. T.; Chen, K.; Li, H. L.; Yuan, W. Y.; Qu, Y. T.; Guo, X. H. Interfacial engineering of W₂NWC heterostructures derived from solid-state synthesis: a highly efficient trifunctional electrocatalyst for ORR, OER, and HER. *Adv. Mater.* **2020**, 32, 1905679.
- (120) Huang, H. W.; Jung, H.; Jun, H.; Woo, D. Y.; Han, J. W.; Lee, J. Design of grain boundary enriched bimetallic borides for enhanced hydrogen evolution reaction. *Chem. Eng. J.* **2021**, 405, 126977.
- (121) Lao, J.; Li, D.; Jiang, C. L.; Luo, C. H.; Qi, R. J.; Lin, H. C.; Huang, R.; Waterhouse, G. I. N.; Peng, H. Synergistic effect of cobalt boride nanoparticles on MoS₂ nanoflowers for a highly efficient hydrogen evolution reaction in alkaline media. *Nanoscale* **2020**, 12, 10158-10165.
- (122) Ren, Y. M.; Wang, J. J.; Hu, W. J.; Wen, H.; Qiu, Y. P.; Tang, P. P.; Chen, M. H.; Wang, P. Hierarchical nanostructured Co-Mo-B/CoMoO_{4-x} amorphous composite for the alkaline hydrogen evolution reaction. *ACS Appl. Mater. Interfaces* **2021**, 13, 42605-42612.
- (123) Lin, Q.; Shang, C. Q.; Chen, Z. H.; Wang, X.; Zhou, G. F. Boron-doped molybdenum carbide as a pH-independent electrocatalyst for the hydrogen evolution reaction. *Int. J. Hydrogen Energy* **2020**, 45, 30659-30665.
- (124) Cao, E. P.; Chen, Z. M.; Wu, H.; Yu, P.; Wang, Y.; Xiao, F.; Chen, S.; Du, S. C.; Xie, Y.; Wu, Y.; Ren, Z. Y. Boron-induced electronic-structure reformation of CoP nanoparticles drives enhanced pH-universal hydrogen evolution. *Angew. Chem. Int. Ed.* **2020**, 59, 4154-4160.
- (125) Wu, J.; Zhang, Q.; Shen, K.; Zhao, R.; Zhong, W. D.; Yang, C. F.; Xiang, H.; Li, X. K.; Yang, N. J. Modulating interband energy separation of boron-doped Fe₇S₈/FeS₂ electrocatalysts to boost alkaline hydrogen evolution reaction. *Adv. Funct. Mater.* **2021**, 32, 2107802.
- (126) Liu, M. Y.; He, Q.; Huang, S. W.; Zou, W. H.; Cong, J.; Xiao, X. Q.; Li, P.; Cai, J. G.; Hou, L. X. NiCo-layered double hydroxide-derived B-doped CoP/Ni₂P hollow nanoprisms as high-efficiency electrocatalysts for hydrogen evolution reaction. *ACS Appl. Mater. Interfaces* **2021**, 13, 9932-9941.
- (127) Yang, H. Y.; Chen, Z. L.; Guo, P. F.; Fei, B.; Wu, R. B. B-doping-induced amorphization of LDH for large-current-density hydrogen evolution reaction. *Appl. Catal. B* **2020**, 261, 118240.
- (128) Ye, S. H.; Luo, F. Y.; Xu, T. T.; Zhang, P. Y.; Shi, H. D.; Qin, S. Q.; Wu, J. P.; He, C. X.; Ouyang, X. P.; Zhang, Q. L.; Liu, J. H.; Sun, X. L. Boosting the alkaline hydrogen evolution of Ru nanoclusters anchored on B/N-doped graphene by accelerating water dissociation. *Nano Energy* **2020**, 68, 104301.
- (129) Bat-Erdene, M.; Batmunkh, M.; Sainbileg, B.; Hayashi, M.; Bati, A. S. R.; Qin, J. D.; Zhao, H. J.; Zhong, Y. L.; Shapter, J. G. Highly dispersed Ru nanoparticles on boron-doped Ti₃C₂T_x (MXene) nanosheets for synergistic enhancement of electrocatalytic hydrogen evolution. *Small* **2021**, 17, 2102218.
- (130) Zhao, X.; Zheng, M.; Zhang, Z. Y.; Wang, Y. F.; Zhou, Y. T.; Zhou, X. H.; Zhang, H. B. Supramolecular nanosheet evolution into BC₃N matrix improves the hydrogen evolution reaction activity in the pH universality of highly dispersed Pt nanoparticles. *J. Mater. Chem. A* **2021**, 9, 16427-16435.
- (131) Song, J. J.; Wei, C.; Huang, Z. F.; Liu, C. T.; Zeng, L.; Wang, X.; Xu, Z. C. A review on fundamentals for designing oxygen evolution electrocatalysts. *Chem. Soc. Rev.* **2020**, 49, 2196-2214.
- (132) Gupta, S.; Jadhav, H.; Sinha, S.; Miotello, A.; Patel, M. K.; Sarkar, A.; Patel, N. Cobalt-boride nanostructured thin films with high performance and stability for alkaline water oxidation. *ACS Sustain. Chem. Eng.* **2019**, 7, 16651-16658.
- (133) Liang, X. G.; Dong, R. T.; Li, D. P.; Bu, X. M.; Li, F. Z.; Shu, L.; Wei, R. J.; Ho, J. Coupling of nickel boride and Ni(OH)₂ nanosheets with hierarchical interconnected conductive porous structure synergizes the oxygen evolution reaction. *ChemCatChem* **2018**, 10, 4555-4561.
- (134) Hong, Y. R.; Kim, K. M.; Ryu, J. H.; Mhin, S.; Kim, J.; Ali, G.; Chung, K. Y.; Kang, S.; Han, H. Dual-phase engineering of nickel boride-hydroxide nanoparticles toward high-performance water oxidation electrocatalysts. *Adv. Funct. Mater.* **2020**, 30, 2004330.
- (135) Leng, X.; Wu, K. H.; Su, B. J.; Jang, L. Y.; Gentle, I.; Wang, D. W. Hydrotalcite-wrapped Co-B alloy with enhanced oxygen evolution activity. *Chin. J. Catal.* **2017**, 38, 1021-1027.
- (136) Xie, C.; Wang, Y. Y.; Yan, D. F.; Tao, L.; Wang, S. Y. In situ growth of cobalt@cobalt-borate core-shell nanosheets as highly-efficient electrocatalysts for oxygen evolution reaction in alkaline/neutral medium. *Nanoscale* **2017**, 9, 16059-16065.
- (137) Chen, S.; Li, Y. Q.; Zhang, Z. H.; Fu, Q.; Bao, X. H. The synergetic effect of h-BN shells and subsurface B in CoB_x@h-BN nanocatalysts for enhanced oxygen evolution reactions. *J. Mater. Chem. A* **2018**, 6, 10644-10648.
- (138) Zou, S. H.; Burke, M.; Kast, M.; Fan, J.; Danilovic, N.; Boettcher, S.

Fe (Oxy)hydroxide oxygen evolution reaction electrocatalysis: intrinsic activity and the roles of electrical conductivity, substrate, and dissolution. *Chem. Mater.* **2015**, 27, 8011-8020.

(139) Liu, Q. H.; Zhao, H.; Jiang, M.; Kang, Q.; Zhou, W.; Wang, P. C.; Zhou, F. M. Boron enhances oxygen evolution reaction activity over Ni foam-supported iron boride nanowires. *J. Mater. Chem. A* **2020**, 8, 13638-13645.

(140) Yuan, H. F.; Wang, S. M.; Gu, X. D.; Tang, B.; Li, J. P.; Wang, X. G. One-step solid-phase boronation to fabricate self-supported porous FeNiB/FeNi foam for efficient electrocatalytic oxygen evolution and overall water splitting. *J. Mater. Chem. A* **2019**, 7, 19554-19564.

(141) Ren, H.; Sun, X. L.; Du, C. F.; Zhao, J.; Liu, D. B.; Fang, W.; Kumar, S.; Chua, R.; Meng, S.; Kidkhunthod, P.; Song, L.; Li, S. Q.; Madhavi, S.; Yan, Q. Y. Amorphous Fe-Ni-P-B-O nanocages as efficient electrocatalysts for oxygen evolution reaction. *ACS Nano* **2019**, 13, 12969-12979.

(142) Ji, X. Q.; Ren, X.; Hao, S.; Xie, F. Y.; Qu, F. L.; Du, G.; Asiri, A.; Sun, X. P. Remarkable enhancement of the alkaline oxygen evolution reaction activity of NiCo₂O₄ by an amorphous borate shell. *Inorg. Chem. Front.* **2017**, 4, 1546-1550.

(143) Gorlin, M.; Ferreira de Araujo, J.; Schmies, H.; Bernsmeier, D.; Dresp, S.; Gliech, M.; Jusys, Z.; Chernev, P.; Kraehnert, R.; Dau, H.; Strasser, P. Tracking catalyst redox states and reaction dynamics in Ni-Fe oxyhydroxide oxygen evolution reaction electrocatalysts: the role of catalyst support and electrolyte pH. *J. Am. Chem. Soc.* **2017**, 139, 2070-2082.

(144) Nsanzimana, J. M. V.; Gong, L. Q.; Dangol, R.; Reddu, V.; Jose, V.; Xia, B. Y.; Yan, Q. Y.; Lee, J. M.; Wang, X. Tailoring of metal boride morphology via anion for efficient water oxidation. *Adv. Energy Mater.* **2019**, 9, 1901503.

(145) Chen, H. Y.; Chen, J. X.; Ning, P.; Chen, X.; Liang, J. H.; Yao, X.; Chen, D.; Qin, L. S.; Huang, Y. X.; Wen, Z. H. 2D heterostructure of amorphous CoFeB coating black phosphorus nanosheets with optimal oxygen intermediate absorption for improved electrocatalytic water oxidation. *ACS Nano* **2021**, 15, 12418-12428.

(146) Mao, H.; Guo, X.; Fu, Y. L.; Yang, H. R.; Zhang, Y.; Zhang, R.; Song, X. M. Enhanced electrolytic oxygen evolution by the synergistic effects of trimetallic FeCoNi boride oxides immobilized on polypyrrole/reduced graphene oxide. *J. Mater. Chem. A* **2020**, 8, 1821-1828.

(147) Chua, X. J.; Luxa, J.; Eng, A. Y. S.; Tan, S. M.; Sofer, Z.; Pumera, M. Negative electrocatalytic effects of p-doping niobium and tantalum on MoS₂ and WS₂ for the hydrogen evolution reaction and oxygen reduction reaction. *ACS Catal.* **2016**, 6, 5724-5734.

(148) Haq, T.; Mansour, S. A.; Munir, A.; Haik, Y. Gold-supported gadolinium doped CoB amorphous sheet: a new benchmark electrocatalyst for water oxidation with high turnover frequency. *Adv. Funct. Mater.* **2020**, 30, 1910309.

(149) Kwon, J.; Han, H.; Jo, S.; Choi, S.; Chung, K. Y.; Ali, G.; Park, K.; Paik, U.; Song, T. Amorphous nickel-iron borophosphate for a robust and efficient oxygen evolution reaction. *Adv. Energy Mater.* **2021**, 11, 2100624.

(150) Sun, S.; Zhai, T.; Liang, C. L.; Savilov, S. V.; Xia, H. Boosted crystalline/amorphous Fe₂O_{3-δ} core/shell heterostructure for flexible solid-state pseudocapacitors in large scale. *Nano Energy* **2018**, 45, 390-397.

(151) Wu, L. B.; Yu, L.; Zhu, Q. C.; McElhenny, B.; Zhang, F. H.; Wu, C.

Z.; Xing, X. X.; Bao, J. M.; Chen, S.; Ren, Z. F. Boron-modified cobalt iron layered double hydroxides for high efficiency seawater oxidation. *Nano Energy* **2021**, 83, 105838.

(152) Zhang, K.; Zhang, G.; Qu, J. H.; Liu, H. J. Disorder the atomic structure of Co(II) oxide via B-doping: an efficient oxygen vacancy introduction approach for high oxygen evolution reaction electrocatalysts. *Small* **2018**, 14, 1802760.

(153) Cheng, Z. F.; Pi, Y. C.; Shao, Q.; Huang, X. Q. Boron-doped amorphous iridium oxide with ultrahigh mass activity for acidic oxygen evolution reaction. *Sci. China Mater.* **2021**, 64, 2958-2966.

(154) Zuo, Y. P.; Rao, D. W.; Ma, S. N.; Li, T. T.; Tsang, Y. H.; Kment, S.; Chai, Y. Valence engineering via dual-cation and boron doping in pyrite selenide for highly efficient oxygen evolution. *ACS Nano* **2019**, 13, 11469-11476.

(155) Jiang, Z. Q.; Jiang, Z. J.; Maiyalagan, T.; Manthiram, A. Cobalt oxide-coated N- and B-doped graphene hollow spheres as bifunctional electrocatalysts for oxygen reduction and oxygen evolution reactions. *J. Mater. Chem. A* **2016**, 4, 5877-5889.

(156) Glavin, N.; Muratore, C.; Jespersen, M.; Hu, J.; Hagerty, P.; Hilton, A. M.; Blake, A. T.; Grabowski, C. A.; Durstock, M.; McConney, M.; Hilgert, D.; Fisher, T. S.; Voevodin, A. Amorphous boron nitride: a universal, ultrathin dielectric for 2D nanoelectronics. *Adv. Funct. Mater.* **2016**, 26, 2640-2647.

(157) Liu, H.; Zhang, X. H.; Li, Y. X.; Li, X.; Dong, C. K.; Wu, D. Y.; Tang, C. C.; Chou, S. L.; Fang, F.; Du, X. W. Conductive boron nitride as promising catalyst support for the oxygen evolution reaction. *Adv. Energy Mater.* **2020**, 10, 1902521.

(158) Liu, X. X.; Wang, Y. H.; Chen, L. B.; Chen, P. P.; Jia, S. P.; Zhang, Y.; Zhou, S. Y.; Zang, J. B. Co₂B and Co nanoparticles immobilized on the N-B-doped carbon derived from nano-B₄C for efficient catalysis of oxygen evolution, hydrogen evolution, and oxygen reduction reactions. *ACS Appl. Mater. Interfaces* **2018**, 10, 37067-37078.

(159) Zhao, W. N.; Xu, T.; Li, T.; Wang, Y. K.; Liu, H.; Feng, J. Z.; Ding, S. J.; Li, Z. T.; Wu, M. B. Amorphous iron(III)-borate nanolattices as multifunctional electrodes for self-driven overall water splitting and rechargeable zinc-air battery. *Small* **2018**, 14, 1802829.

(160) Tian, R. F.; Zhao, S. J.; Li, J. K.; Chen, Z. B.; Peng, W. F.; He, Y.; Zhang, L. L.; Yan, S.; Wu, L. L.; Ahuja, R.; Gou, H. Y. Pressure-promoted highly-ordered Fe-doped-Ni₂B for effective oxygen evolution reaction and overall water splitting. *J. Mater. Chem. A* **2021**, 9, 6469-6475.

(161) Saad, A.; Gao, Y.; Owusu, K. A.; Liu, W.; Wu, Y. Y.; Ramiere, A.; Guo, H. C.; Tsiakaras, P.; Cai, X. K. Ternary Mo₂NiB₂ as a superior bifunctional electrocatalyst for overall water splitting. *Small* **2022**, 18, 2104303.

(162) Xu, Y. L.; Wang, C.; Huang, Y. H.; Fu, J. Recent advances in electrocatalysts for neutral and large-current-density water electrolysis. *Nano Energy* **2021**, 80, 105545.

(163) Liu, H. X.; Li, X. Y.; Chen, L. L.; Zhu, X. D.; Dong, P.; Chee, M. O. L.; Ye, M. X.; Guo, Y. H.; Shen, J. F. Monolithic Ni-Mo-B bifunctional electrode for large current water splitting. *Adv. Funct. Mater.* **2021**, 32, 2107308.

(164) Wu, Z. X.; Nie, D. Z.; Song, M.; Jiao, T. T.; Fu, G. T.; Liu, X. E. Facile synthesis of Co-Fe-B-P nanochains as an efficient bifunctional electrocatalyst for overall water-splitting. *Nanoscale* **2019**, 11, 7506-7512.

(165) Qiang, C. C.; Zhang, L.; He, H. L.; Liu, Y. Y.; Zhao, Y. Y.; Sheng, T.; Liu, S. J.; Wu, X. L.; Fang, Z. Efficient electrocatalytic water splitting by

bimetallic cobalt iron boride nanoparticles with controlled electronic structure. *J. Colloid Interface Sci.* **2021**, 604, 650-659.

(166) Li, Y. J.; Huang, B. L.; Sun, Y. J.; Luo, M. C.; Yang, Y.; Qin, Y. N.; Wang, L.; Li, C. J.; Lv, F.; Zhang, W. Y.; Guo, S. J. Multimetal borides nanochains as efficient electrocatalysts for overall water splitting. *Small* **2019**, 15, 1804212.

(167) Hu, Q.; Li, G. M.; Han, Z.; Wang, Z. Y.; Huang, X. W.; Chai, X. Y.; Zhang, Q. L.; Liu, J. H.; He, C. X. General synthesis of ultrathin metal borate nanomeshes enabled by 3D bark-like N-doped carbon for electrocatalysis. *Adv. Energy Mater.* **2019**, 9, 1901130.

(168) Cheng, Y.; Pang, K. L.; Xu, X. H.; Yuan, P. F.; Zhang, Z. G.; Wu, X.; Zheng, L. R.; Zhang, J. N.; Song, R. Borate crosslinking synthesis of structure tailored carbon-based bifunctional electrocatalysts directly from guar gum hydrogels for efficient overall water splitting. *Carbon* **2020**, 157, 153-163.

(169) Anjum, M. A. R.; Lee, M. H.; Lee, J. S. Boron- and nitrogen-codoped molybdenum carbide nanoparticles imbedded in a BCN network as a bifunctional electrocatalyst for hydrogen and oxygen evolution reactions. *ACS Catal.* **2018**, 8, 8296-8305.

(170) Xu, H. B.; Fei, B.; Cai, G. H.; Ha, Y.; Liu, J.; Jia, H. X.; Zhang, J. C.; Liu, M.; Wu, R. B. Boronization-induced ultrathin 2D nanosheets with abundant crystalline-amorphous phase boundary supported on nickel foam toward efficient water splitting. *Adv. Energy Mater.* **2019**, 10, 1902714.

(171) Yuan, H. F.; Wang, S. M.; Ma, Z. Z.; Kundu, M.; Tang, B.; Li, J. P.; Wang, X. G. Oxygen vacancies engineered self-supported B doped Co₃O₄ nanowires as an efficient multifunctional catalyst for electrochemical water splitting and hydrolysis of sodium borohydride. *Chem. Eng J.* **2021**, 404, 126474.

(172) Shi, D.; Chang, B.; Ai, Z. Z.; Jiang, H. H.; Chen, F. Z.; Shao, Y. G.;

Shen, J. X.; Wu, Y. Z.; Hao, X. P. Boron carbonitride with tunable B/N Lewis acid/base sites for enhanced electrocatalytic overall water splitting. *Nanoscale* **2021**, 13, 2849-2854.

(173) Chodvadiya, D.; Som, N. N.; Jha, P. K.; Chakraborty, B. Enhancement in the catalytic activity of two-dimensional α -CN by B, Si and P doping for hydrogen evolution and oxygen evolution reactions. *Int. J. Hydrogen Energy* **2021**, 46, 22478-22498.

(174) Zhang, H. X.; Liu, M.; Bu, X. H.; Zhang, J. Zeolitic BIF crystal directly producing noble-metal nanoparticles in its pores for catalysis. *Sci. Rep.* **2014**, 4, 3923.

(175) Liu, M. R.; Hong, Q. L.; Li, Q. H.; Du, Y. H.; Zhang, H. X.; Chen, S. M.; Zhou, T. H.; Zhang, J. Cobalt boron imidazolate framework derived cobalt nanoparticles encapsulated in B/N codoped nanocarbon as efficient bifunctional electrocatalysts for overall water splitting. *Adv. Funct. Mater.* **2018**, 28, 1801136.

(176) Zheng, Y.; Jiao Y.; Zhu, Y. H.; Cai, Q. R.; Vasileff, A.; Li, L. H.; Han, Y.; Chen, Y.; Qiao, S. Z. Molecule-level g-C₃N₄ coordinated transition metals as a new class of electrocatalysts for oxygen electrode reactions. *J. Am. Chem. Soc.* **2017**, 139, 3336-3339.

(177) Tang, S. B.; Zhou, X. H.; Liu, T. Y.; Zhang, S. Y.; Yang, T. T.; Luo, Y.; Sharman, E.; Jiang, J. Single nickel atom supported on hybridized graphene-boron nitride nanosheet as a highly active bi-functional electrocatalyst for hydrogen and oxygen evolution reactions. *J. Mater. Chem. A* **2019**, 7, 26261-26265.

Received: May 10, 2022

Accepted: May 19, 2022

Published online: May 26, 2022

Published: September 22, 2022



Feng-Ge Wang received her B.Eng. degree in Chemical Engineering and Process from Weifang University in 2020. She is currently a master's student in the research group of Associate Professors Dong Bin and Liu Bin at China University of Petroleum (East China). Her research interests focus on nanostructures for electrocatalysis.



Xin Liu received her B.Eng. degree in Chemical Engineering and Technology from Qingdao University of Science and Technology in 2021. She is currently a master's student in chemical engineering at China University of Petroleum (East China). Her research interest covers electrocatalytic nanostructures.



Qian-Xi Lv received his B.S. degree in Chemistry from China University of Petroleum (East China) in 2022. He is currently a M.S. student in Prof. Bin Dong's group at China University of Petroleum (East China). His research direction is electrolytic water catalyst.



Dr. **Bin Liu** received his B.Eng. degree in Chemical Engineering and Process from China University of Petroleum (East China) in 2007, and Ph.D. degree in Chemical Engineering and Technology from China University of Petroleum (East China) in 2012. He is currently an associate professor at University of Petroleum (East China). His research interests include green petroleum refining process, clean oil hydrogenation catalyst and process, biomass efficient catalytic hydrogenation conversion, new energy catalytic conversion and waste green resource utilization.



Prof. **Yong-Ming Chai** received his Ph.D. from China University of Petroleum (East China) in 2008. Now he is a professor in State Key Laboratory of Heavy Oil Processing, College of Chemistry and Chemical Engineering, China University of Petroleum (East China). He was doing research as a visiting scholar in Marquette University from 2015.03 to 2016.03. His research interests are catalyst of hydrosulfurization process of heavy oil and transition metal-based electrocatalysts.



Dr. **Bin Dong** received his B.S. and Ph.D. from Lanzhou University in 2002 and 2008, respectively. He was doing research as a visiting scholar in Marquette University from 2014.03 to 2015.03. Now Dr. Dong is an Associate Professor in College of Chemistry and Chemical Engineering, China University of Petroleum (East China). His research interests mainly focus on the transition metal-based functional materials for energy conversion and storage including electrocatalysis and photoelectrocatalysis for small molecules.